SOURCE, EMPLACEMENT, AND EVOLUTION OF THE MORGAN CREEK PLUTON, SIERRA NEVADA BATHOLITH, CALIFORNIA, USA

by

John Philip Porter

A dissertation submitted to the faculty of
The University of Utah
in partial fulfillment of the requirements for the degree of

Doctor of Philosophy

in

Geology

Department of Geology and Geophysics

The University of Utah

December 2013

The University of Utah Graduate School

STATEMENT OF DISSERTATION APPROVAL

The dissertation of **John Philip Porter**

has been approved by the following supervisory committee members:

Erich U. Petersen	, Chair	**14 Oct. 2013** Date Approved
John M. Bartley	, Member	**22 Oct. 2013** Date Approved
John R. Bowman	, Member	**21 Oct. 2013** Date Approved
Barbara P. Nash	, Member	**22 Oct. 2013** Date Approved
Eric H. Christiansen	, Member	**14 Oct. 2013** Date Approved

and by **John M. Bartley**, Chair of

the Department of **Geology and Geophysics**

and by David B. Kieda, Dean of The Graduate School.

ABSTRACT

The similar timescales and field relationships in magmatic systems suggest common processes, whether the system is mineralized or has associated volcanism. Though often overlooked because of alteration and their relatively small size, the magmatic-hydrothermal environment may prove key to a holistic model of magmatic systems. Seven age distributions from the Morgan Creek pluton were determined by LA MC-ICP-MS U-Pb zircon analysis and the ages of six molybdenite samples from the adjacent Pine Creek tungsten skarn were determined by Re-Os molybdenite analysis to examine the timing, duration, and evolution of a mineralized magmatic system. The molybdenite ages range from 91.0 to 107.2 Ma. Ages for three of the six samples are identical within error (±0.5 Ma) at ~94 Ma. Ages of 91.0 and ~94 Ma may represent distinct mineralizing events, whereas the oldest two ages from disseminated molybdenite in the skarn may indicate disturbance of the Re-Os system. The U-Pb data show dominant populations at ~96-98 and ~94 Ma. The main facies of the Morgan Creek pluton, comprising over 95% of the pluton, can be divided into three groups based on mafic mineral abundance and whole rock major and trace element geochemistry. Major element geochemistry is very similar to that of plutons in nearby intrusive suites. However, trace element geochemistry (Ba, Rb, Sr, Zr, and REE) suggest a distinct genesis from typical intrusive suite magmas. Trace element models suggest the magmas that formed the Morgan Creek pluton were derived from partial melting of upper

crustal rocks. The Morgan Creek pluton was emplaced either as a single batch of magma, or through multiple rapid pulses that led to a single magma body. Fractional crystallization of a relatively homogenous volume of magma led to the chemical variations seen within the pluton. The age and compositional data show that the Morgan Creek pluton is not a part of the Lake Edison Granodiorite, as was previously interpreted. Instead, the Morgan Creek pluton represents an early stage of the John Muir Intrusive Suite, possibly correlative with the Basin Mountain pluton which is commonly interpreted to be part of the Lake Edison Granodiorite.

TABLE OF CONTENTS

LIST OF TABLES

ACKNOWLEDGEMENTS

Well, here I am. Nine years after starting my first classes as a Ph.D. student at the University of Nevada, Reno, I finally get to give my formal thanks to the people and organizations that have helped me finish this dissertation. A lot has happened in these past nine years and many people have contributed, directly and less directly.

Most of all, I want to thank my wife, Erica, and my son, Rainier, for their patience and help throughout the long haul. I could not have asked for a better field partner or copy editor. They endured my absence, my stress, and my complaints. Rainier, age 5, also deserves credit for his suggestions of how to improve the text. He even offered what he called "A real dis-ss-er-tai-shin" to help me through a tough bit of writing (". . .whenever a superhero interacts with a rock from his or her planet it gets the flue, the power weakens , e.t.c."). The best part of being at this point, the science written up and polished to a dull sheen, is that, for the first time in years, I can spend guilt-free time with my family. It feels good.

My research committee, Erich Petersen (chair), John Bartley, John Bowman, Barb Nash, and Eric Christiansen, provided invaluable feedback and encouragement throughout the whole process.

Erich not only provided feedback and encouragement through the many years, but he trusted me enough to allow me to follow my own interests. Erich also exposed me to new rocks and new people from Utah to Chile. Though not directly related to my

research, Erich provided a great example of a professor who cared about his students, those he was mentoring as an advisor, and those in his classroom.

John Bartley and Eric Christiansen also deserve special mention. They each provided me with hours of conversation about porphyries and plutons. These conversations and gallons or red ink on early manuscripts helped me present my ideas in a more coherent way and steered me away from the wrong paths, however inviting they seemed at the time.

Greg and Mallary Carling, Jordan Gillespie, and Mike Stearns all provided good help and good company in the field. Gerry Austin, Kim Schroeder, Stan Nelson, and the rest of the geology staff at Kennecott Utah Copper provided support and were very understanding of the unusual schedule that this research sometimes demanded.

The research was financially supported by student grants from the Hugh McKinstry Student Research Fund of the Society of Economic Geologists and the Geological Society of America. Doug Hayes and Pete Belec allowed me access to the Pine Creek minesite and showed me around the old mill, one of the highlights of my field season. Frances Alvarado with the Forest Service helped me work through some permitting issues. The staff at the White Mountain Research Station made it a welcoming place to stay when I wasn't camping on the shores of Lower Morgan Lake.

To all on this list and the many others who helped me get here: thank you.

CHAPTER 1

INTRODUCTION

Recent work published in both the plutonic and economic geology literature has focused on the timescales and mechanisms for emplacement of magma in the upper crust. The timescales and mechanisms for pluton emplacement are important for the structural or tectonic geologist to develop better models for the formation and evolution of rocks in magmatic arcs. Robust models for pluton emplacement are also important to answer questions about pluton emplacement in the upper crust, including the long-standing "space problem" (e.g., Bowen, 1948). To the ore geologist, understanding the timescales and modes of emplacement of plutons in the upper crust is critical to understand the processes that give rise to the economic deposits that supply a large portion of the world's metals (e.g., Seedorff et al., 2005; Sillitoe, 2010; Chiaradia, et al., 2013).

Mounting field evidence suggests that many, if not most, plutons were emplaced incrementally, by small batches of magma, rather than rapidly as one large batch of magma that solidified from the outside in (e.g., Weibe and Collins, 1998; Mahan et al., 2003; Stearns, 2009). In many cases, different stages of intrusion can be mapped, demonstrating the composite nature of some intrusions. Geochronological studies show that the timescales of emplacement of large plutons is too long to sustain a single body of magma (e.g., Brown and McClelland, 2000; McNulty et al., 2000; Coleman et al., 2004;

Miller et al., 2007; Davis et al., 2012). This thinking, in large part displaced the previous models of pluton ascent by stoping and diapirism with a model that involves magma transport and emplacement through dikes and sills (e.g., Brown and McClelland, 2000; Mahan et al., 2003; Glazner et al,. 2004; Bartley et al., 2008). In some cases, there is evidence that plutons were emplaced through multiple mechanisms (e.g., Pignotta et al., 2010).

Shallow composite plutons associated with magmatic-hydrothermal systems are common, especially in porphyry deposits, the most important source for global Cu and Mo production (Sillitoe, 2010). In porphyry deposits, the composite intrusions are chiefly composed of pre- and syn-mineral intrusive rocks that are part of the same magmatic system (Seedorff et al., 2005; Sillitoe, 2010). The porphyry environment provides a link between the deeper parts of the plutonic system and the volcanic system.

The shallow composite plutons that host magmatic-hydrothermal systems are only the high-level expressions of much larger magmatic systems. The formation and emplacement of the deep plutons related to magmatic-hydrothermal systems has not received much attention because of lack of exposure. However, in some cases, tilting has exposed some of the deeper parts of the magmatic system. The best-known of these is the Yerington batholith which has been tilted nearly 90 degrees, exposing the upper ~6 km of the crust (Dilles, 1987). The exposure shows evidence of incremental emplacement in the plutons that make up the batholith. Some Arizona porphyry systems have also been tilted and exposed in similar manner, but in addition to tilting, many of those systems have also been dismembered (Stavast, 2006; Stavast et al., 2008; Maher, 2008).

A recent examination of the geometry and crystallization history of a subplutonic magma system was based largely on aeromagnetic data and deep drilling in and around the Bingham Canyon porphyry Cu-Mo-Au deposit (Steinberger et al., 2013). Space for the shallow Bingham stock, host of the world-class deposit, may have been created through Basin and Range extensional faulting (Kloppenburg et al., 2010). The deeper magma reservoir may have been emplaced incrementally, but mineralization required extraction of water, sulfur, and metals from hundreds of km^3 of magma over a short time, requiring a coherent magma chamber at some point in the evolution of the deeper batholith (Steinberger et al., 2013).

Many of the studies revealing the complicated nature of pluton emplacement have been carried out in the Sierra Nevada batholith, shaping ideas about the formation of large igneous suites (e.g., Bateman and Chappell, 1979; Kistler et al.,1986; Bateman, 1992; Coleman et al., 2004; Memeti et al., 2010). Perhaps the best-studied intrusive suite in the Sierra Nevada batholith is the Cretaceous Tuolumne Intrusive Suite. The suite is composed primarily of granodiorite and is spatially and temporally zoned, with the youngest, interior plutons being the most felsic (Bateman and Chappell, 1979). Early work interpreted this zonation to be the result of the fractional crystallization of a single body of magma (Bateman and Chappell, 1979). The work on the very well-exposed suite informed later work and advanced a model whereby large igneous complexes were emplaced.

Reports of incremental emplacement of small plutons are less common in the literature. Mahan et al. (2003) and Stearns (2009) reported on the incremental construction of the dike-fed McDoogle pluton in the southern John Muir Intrusive Suite,

south of the Tuolumne Intrusive Suite. In the western Sierra Nevada batholith, the Jackass Lakes pluton has been shown to be formed incrementally, possibly through multiple mechanisms (McNulty et al., 1996; Pignotta et al., 2010).

The primary focus of this dissertation is the Morgan Creek pluton, also in the John Muir Intrusive Suite. The Morgan Creek pluton is a small (~1.5 by 8 km) pluton on the eastern edge of the central John Muir Intrusive Suite that is related to the Pine Creek W-Mo(-Cu) skarn (Newberry, 1982). The Pine Creek skarn is the largest of many tungsten deposits associated with the granitic rocks of the Sierra Nevada batholith (Bateman, 1953, 1965, 1992; Newberry, 1980, 1982). The Morgan Creek pluton was chosen for its restricted size and relationship to the skarn, which has associated molybdenum mineralization amenable to dating by the Re-Os system (Stein et al., 2001). This dissertation addresses some of the advances in the understanding of pluton emplacement and how it relates to intrusions associated with mineralization.

The second chapter, *Incremental Emplacement in Plutonic and Magmatic-hydrothermal Systems*, reviews the literature on the timescales of both mineralized and unmineralized plutons. The similar timescales of emplacement summarized in Chapter 2 suggests that the same processes are happening at all levels of magmatic systems. A corollary is that there is no fundamental difference between the magmatic systems that generate unmineralized and mineralized plutons. The difference between mineralized and unmineralized plutons must lie elsewhere.

The age profiles of magmatic-hydrothermal systems provide a more complete picture of the processes involved in the generation and emplacement of magmatic systems. Not only can the age and timescale of granitoid emplacement be determined in

magmatic-hydrothermal systems, but Re-Os and K-Ar series dating of hydrothermal minerals can provide insight into the duration of postmagmatic thermal anomalies. The timing and duration of hydrothermal activity is important to understanding mineralized systems, but the postmagmatic minerals commonly dated in magmatic-hydrothermal systems also add to the overall understanding of magmatic systems.

The Morgan Creek pluton and the associated Pine Creek tungsten skarn were both dated, using U-Pb zircon and Re-Os molybdenite dating techniques, respectively to determine the existence and extent of protracted magmatism and pluton emplacement in a small Sierran pluton. The results were published in the proceedings of the 2010 Geological Society of Nevada symposium (Porter et al., 2011), and are reprinted in Chapter 3, *Timing of the Pine Creek Tungsten Skarn and the Causative Morgan Creek Pluton, California: Implications for Ore Genesis and Regional Geology*. Zircons from the pluton and molybdenite from the mineralized skarn were separated and dated. Laser ablation ICP-MS U-Pb zircon dates for samples from the Morgan Creek pluton show a wide spread of ages. The spread in ages did not permit a geologically meaningful determination of the average crystallization age for zircons formed in the Morgan Creek pluton, but did show multiple Late Cretaceous age populations and some scattered Jurassic ages of inherited zircons. Three of the six Re-Os molybdenite dates were within error of each other and overlap with the main ~94 Ma population in the U-Pb data. From these data, the age of the Morgan Creek pluton and the associated mineralization in the Pine Creek tungsten skarn is interpreted to be ~94 Ma, in agreement with previously published low-precision U-Pb zircon data (Stern et al., 1981).

The spread in both sets of age data is somewhat puzzling. Both the U-Pb and Re-Os data show age populations at ~107, ~94, and ~91 Ma. The ~94 and ~91 Ma populations likely reflect the age of crystallization and emplacement of the Morgan Creek pluton and Pb-loss, respectively. The ~107 age does not correlate with any other known plutonism in the vicinity and may reflect inheritance from a concealed pluton at depth. It is also possible that the older population, along with the ~97 Ma population in the U-Pb data are the result of bad analyses. Cretaceous U-Pb ages may have been contaminated with inherited Jurassic cores. This probably did happen for some of the analyses, but the consistency in ages forming the populations makes this scenario seem unlikely.

The spread in Re-Os ages is more difficult to explain. The Re-Os system is well-studied and usually interpreted to be robust when used to date molybdenite mineralization (e.g., Stein et al., 2001). Molybdenites from the Pine Creek skarn have previously unreported common Os, but accounting for the common Os does not reconcile the ages. Based on the geochonological data, multiple pulses of mineralization over ~16 million years is permissible from the age data, although it is very unlikely.

The fourth chapter, *Magmatic Evolution and Upper Crustal Source of the Morgan Creek Pluton, an Early Member of the John Muir Intrusive Suite, Sierra Nevada Batholith, California*, characterizes the Morgan Creek pluton and discusses its place within the John Muir Intrusive Suite. Mineralogically, it shows that the Morgan Creek pluton is a true granite, both modally and chemically. Previous work (Cray, 1981) had shown two compositional facies, a small siliceous facies in the northern part of the pluton and a low color index granite comprising the main facies. Cray (1981) reported textural variations in the main facies, but did not identify any chemical groupings within the main

facies. The third chapter presents petrography, QEMSCAN automated mineralogy, magnetic susceptibility, and major and trace element geochemical data that shows that the Morgan Creek pluton has at least three distinct rock types in the main facies.

Mineralogically, the rocks of the Morgan Creek pluton are granites and are more felsic towards the interior of the pluton. Biotite is the dominant mafic mineral, but hornblende is present in all analyzed samples. Titanite is a prominent trace mineral in much of the pluton, but in the most felsic rocks, it is essentially absent, and ilmenite is present. Magnetite is common in unaltered Morgan Creek rocks.

Magnetic susceptibility measurements in the Morgan Creek pluton are low and correlate with magnetite content. Along the eastern edge of the pluton, where it is in contact with metasedimenary rocks, magnetic susceptibility values are anomalously low and magnetite is absent. The magnetic susceptibility and petrography suggest that this anomalous zone was the result of previously unreported hydrothermal alteration affecting the rock within ~300 m of the eastern contact.

Major element geochemistry of the Morgan Creek pluton is very similar to rocks of the John Muir, Tuolumne and Whitney Intrusive Suites; however, the trace element geochemistry of the Morgan Creek pluton is distinct from that of all other rocks of the intrusive suites. Trace element modeling (Rb, Sr, Ba, Zr) suggests that the composition of the Morgan Creek granites is consistent with having been formed by partial melting of upper crustal rocks, probably similar to an average granodiorite from the intrusive suites. The Lamarck Granodiorite, a younger member of the John Muir Intrusive Suite, shows elevated Ba, like the Morgan Creek, suggesting the transition from melting upper crustal rocks to melting the lower crustal sources typical of Sierran granitoids was gradual.

Jurassic granitoids of the early Sierra Nevada arc (e.g., Barth et al., 2011) may have been the source for the Morgan Creek magma.

Chemical and mineralogical zoning in the Morgan Creek pluton are consistent with fractional crystallization of a relatively homogeneous magma. Similar compositional and textural variations on a comparable scale have been reported in the Tuolumne Intrusive Suit (Memeti et al., 2010; Coleman et al., 2012). The main facies of the pluton may have been emplaced in multiple pulses if they were emplaced rapidly enough that the pluton was relatively homogenous at the onset of crystallization.

The geochronology and geochemistry of the Morgan Creek pluton show that it is not correlative with the main part of the Lake Edison Granodiorite, as it is currently interpreted in the literature (Bateman, 1992). Instead, it may be correlative with the Basin Mountain pluton, currently mapped as the southeastern extent of the Lake Edison Granodiorite. Older maps showed the Morgan Creek and Basin Mountain plutons as correlative units, distinct from the Lake Edison Granodiorite (Bateman, 1965; Cray, 1981). The data presented in Chapters 3 and 4 suggest that the ideas that led to those maps may need to be revisited.

References

Barth, A.P., Walker, J.D., Wooden, J.L., Riggs, N.R., and Schweickert, R.A., 2011, Birth of the Sierra Nevada magmatic arc: Early Mesozoic plutonism and volcanism in the east-central Sierra Nevada of California: Geosphere, v. 7, p. 877-897.

Bartley, J.M., Coleman, D.S., and Glazner, A.F., 2008, Incremental pluton emplacement by magmatic crack-seal: Transactions of the Royal Society of Edinburgh: Earth Sciences, v. 97, p. 383-396.

Bateman, P., 1953, Geology of the Tungstar and Hanging Valley tungsten skarns: USGS Open File Report 53-11, 10 p.

Bateman, P.C., 1965, Geology and tungsten mineralization of the Bishop district, California: USGS Professional Paper 470, 208 p.

Bateman, P.C., 1992, Plutonism in the central part of the Sierra Nevada batholith, California: USGS Professional Paper 1483, 186 p.

Bateman, P.C. and Chappell, B.W., 1979, Crystallization, fractionation, and solidification of the Tuolumne Intrusive Series, Yosemite National Park, California: GSA Bulletin, v.90, p. 465-482.

Bowen, N.L., 1948, The granite problem and the method of multiple prejudices: *in* Giluly, J., et al., (eds.), Origins of Granite, Geological Society of America Memoirs, 28, p. 79-90.

Brown, E.H. and McClelland, W.C., 2000, Pluton emplacement by sheeting and vertical ballooning in part of the southeast Coast Plutonic Complex, British Columbia: GSA Bulletin, v. 112, p. 708-719.

Chiaradia, M., Schaltegger, U., Spikings, R., Wotzlaw, J.F., and Ovtcharova, O., 2013, How accurately can we date the duration of magmatic-hydrothermal events in porphyry systems?: Economic Geology, v. 108, p. 565-584.

Coleman, D.S., Gray, W., and Glazner, A.F., 2004, Rethinking the emplacement and evolution of zoned plutons: Geochronologic evidence for incremental assembly of the Tuolumne Intrusive Suite, California: Geology, v. 32, p. 433-436.

Coleman, D.S., Bartley, J.M., Glazner, A.F., and Pardue, M.J., 2012, Is chemical zonation in plutonic rocks driven by changes in source magma composition or shallow crustal differentiation: Geospherre, v. 8 p. 1568-1587.

Cray, 1981, The geochemistry and petrology of the Morgan Creek pluton, Inyo County, California: Unpublished PhD thesis, University of California, Davis, 454 p.

Davis, J.W., Coleman, D.S., Gracely, J.T., Gaschnig, R., and Stearnes, M., 2012, Magma accumulation rates and thermal histories of plutons of the Sierra Nevada batholith, CA: Contributions to Mineralogy and Petrology, v. 163, p. 449-465.

Dilles, J.H., 1987, Petrology of the Yerington batholith, Nevada: Evidence for evolution of porphyry copper ore fluids: Economic Geology, v. 82, p. 1750-1789.

Glazner, A.F., Bartley, J.M., Coleman, D.S., Gray, W., and Taylor, R.Z., 2004, Are plutons assembled over millions of years by amalgamation from small magma chambers?: GSA Today, v. 14, p. 4-11.

Kistler, R.W., Chappell, B.W., Peck, D.L., and Bateman, P.C., 1986, Isotopic variation in the Tuolumne Intrusive Suite, central Sierra Nevada, California: Contributions to Mineralogy and Petrology, v. 94, p. 205-220.

Kloppenburg, A., Grocott, J., and Hutchinson, D., 2010, Structural setting and synplutonic fault kinematics of a Cordilleran Cu-Au-Mo porphyry mineralization system, Bingham mining district, Utah: Economic Geology, v. 105, p. 743-761.

Mahan, K.H., Bartley, J.M., Coleman, D.S., Glazner, A.F., and Carl, B.S., 2003, Sheeted intrusion of the synkinetic McDoogle pluton, Sierra Nevada, California: GSA Bulletin, v. 115, p. 1570-1582.

Maher, D.J., 2008, Reconstruction of middle Tertiary extension and Laramide porphyry copper sysetms, east-central Arizona: Unpublished Ph.D. dissertation, University of Arizona, 328 p.

McNulty, B., Tobisch, O., Cruden, A. and Gilder, S., 2000, Multistage emplacement of the Mount Givens pluton, central Sierra Nevada batholith, California: Geological Society of America Bulletin, v. 112, p. 119-135

Memeti, V., Paterson, S., Matzel, J., Mundil, R., and Okaya, D., 2010, Magmatic lobes as "snapshots" of magma chamber growth and evolution in large, composite batholiths: An example from the Tuolumne intrusion, Sierra Nevada, California: GSA Bulletin, v. 122, p. 1912-1931.

Miller, J.S., Matzel, J.E.P., Miller, C.F., Burgess, S.D., and Miller, R.B., 2007, Zircon growth and recycling during the assembly of large, composite arc plutons: Journal of Volcanology and Geothermal Research, v. 167, p. 282-299.

Newberry, R.J., 1980, The geology and chemistry of skarn formation and tungsten deposition in the central Sierra Nevada, California: Unpublished Ph.D. dissertation, Stanford, University, 325 p.

Newberry, R.J., 1982, Tungsten-bearing skarns of the Sierra Nevada. I. The Pine Creek mine, California: Economic Geology, v. 77, p. 823-844.

Pignotta, G.S., Paterson, S.R., Coyne, C.C., Anderson, J.L., and Onezime, J., 2010, Processes involved during incremental growth of the Jackass Lakes pluton, central Sierra Nevada batholith: Geosphere, v. 6, p. 130-159.

Porter, J.P., Bartley, J., Petersen, E., and Barra, F., 2011, Timing of the Pine Creek tungsten skarn and the causative Morgan Creek pluton, California: Implications for ore genesis and regional geology: *in* R. Steininger and B. Pennell, eds. Great Basin Evolution and Metallogeny: Geological Society of Nevada Symposium Proceedings, p. 397-417.

Seedorff, E., Dilles, J.H., Proffett, J.M., Einaudi, M.T., Zurcher, L., Stavast, W.J.A., Johnson, D.A., and Barton, M.D., 2005, Porphyry deposits: Characteristics and origin of hypogene features: *in* Hedenquist, J.H., Thompson, J.F.H., Goldfarb, R.J., and Richards, J.P., eds., Economic Geology 100th Anniversary Volume, p. 251-298.

Sillitoe, R.H., 2010, Porphyry copper systems: Economic Geology, v. 105, p. 3-41.

Stavast, W.J.A., 2006, Three-dimensional evolution of magmatic hydrothermal systems, Schultze Granite and Ruby Star Granodiorite, Arizona: Unpublished Ph.D. dissertation, University of Arizona, 203 p.

Stavast, W.J.A., Butler, R.F., Seedorff, E., Barton, MD., and Ferguson, C.A., 2008, Tertiary tilting and dismemberment of the Laramide arc and related hydrothermal systems, Sierrita Mountains, Arizona: Economic Geology, v. 103, p. 429-636.

Steinberger, I., Hinks, D., Dreisner, T., and Heinrich, C., 2013, Source plutons driving porphyry copper ore formation: Combining geomagnetic data, thermal constraints, and chemical mass balance to quantify the magma chamber beneath the Bingham Canyon deposit: Economic Geology, v. 108, p. 605-640.

Stearns, M.A., 2009, Anatomy and assembly of the McDoogle pluton near Sawmill Lake, central Sierra Nevada, California: Unpublished MS thesis, University of Utah, 109 p.

Stern, T.W., Bateman, P. C., Morgan, B.A., Newell, M.F. and Peck, D.L., 1981, Isotopic U-Pb ages of zircon from the granitoids of the central Sierra Nevada, California: USGS Professional Paper No. 1185, 17 p.

Stein, H., Markey, R., Morgan, J., Hannah, J. and Schersten, A., 2001, The remarkable Re-Os chronometer in molybdenite: How and why it works: Terra Nova, v. 13, p. 479-486.

Weibe, R.A. and Collins, W.J., 1998, Depositional features and stratigraphic sections in granitic plutons: Implications for the emplacement and crystallization of granitic magmas: Journal of Structural Geology, v. 20, p. 1273-1289.

CHAPTER 2

PROTRACTED, INCREMENTAL EMPLACEMENT IN PLUTONIC AND MAGMATIC-HYDROTHERMAL SYSTEMS

Abstract

Field and geochronological evidence suggest that incremental and often protracted emplacement is common in mineralized and unmineralized magmatic systems. The similar timescales and field relationships observed in mineralized and unmineralized systems suggest common processes of magma formation and emplacement. Mineralized magmatic systems require that a volume of melt tens to hundreds of km^3 in volume be generated and stored at depth prior to the main mineralizing event. The magma chamber (a coherent volume of melt ± crystals) that supplies the mineralized system is generated late in the lifespan of a magmatic system and is most likely the result of an increase in the rate of magma input to the system, but thermal preparation may also play a role. A four stage model for the formation of intrusive magmatic systems in the mid- to upper-crust accounts for both mineralized and unmineralized systems. In stage 1, magma is intruded into cool wall rocks, preserving internal contacts. Stage 2 sees the initial formation of volumes of melt-rich magma at depth, as well as the development of a cupola that focuses

hydrothermal activity. Magmatic activity ceases at stage 2 in unmineralized (plutonic) systems. During stage 3 the deep high-melt fraction magma chambers crystallize. Metal-rich volatiles released during crystallization follow the structural pathways of earlier dikes to the cupola, where the metals are deposited when they encounter favorable PT conditions. Minor magmatic activity continues for some time, represented by stage 4 in the model. Just as mineralized systems are an extension of the upper plutonic environment, they underlay the volcanic environment and provide a link between the two extremes of magmatic systems. Though often overlooked because of alteration and, perhaps, their relatively small size, the magmatic-hydrothermal environment may prove key to a holistic understanding of magmatic systems.

Introduction

Work on the styles and mechanisms for pluton emplacement over the past two decades has resulted in a shift in the understanding of how magma moves and is emplaced in the upper-crust. Whereas past models called on stoping or diapirism as important mechanisms driving ascent and emplacement of magmas in the mid- to upper-crust (e.g., Miller and Paterson, 1999 and references therein), recent work suggests that dike-fed magma chambers (coherent volumes of mixed melt ± crystals) may be the norm (Clemens and Mawer, 1992; Petford et al., 2000; Cruden and McCaffrey, 2001; Vigneresse, 2004).

Most studies of pluton emplacement have focused on relatively fresh, unmineralized plutons that were emplaced in the mid- to upper-crust (e.g., Donegal plutons, plutons in the Sierra Nevada batholith, adn the Coast Plutonic Comples; Pitcher and Berger, 1972; Paterson and Vernon, 1995; Brown and McClelland, 2000; Mahan et

al., 2003; Coleman et al., 2004; Miller et al., 2007; Pignotta et al., 2010). A family of well-studied intrusions that have received little attention from workers studying pluton emplacement is the diverse group that form and host magmatic-hydrothermal systems. The best-studied group of magmatic-hydrothermal systems is the porphyry-type systems that are large deposits hosted in composite intrusions (Seedorff et al., 2005; Sillitoe, 2010).

The intrusions associated with magmatic-hydrothermal systems have been overlooked largely because the hydrothermal fluids that act to concentrate metals also alter large volumes of rock (e.g., Meyer and Hemley, 1967; Seedorff et al., 2005; Sillitoe, 2010). This alteration obscures the geochemical signatures of magma genesis, making the determination of the original magmatic composition challenging. Despite the challenges of working in magmatic-hydrothermal systems, they deserve consideration with the rest of the magmatic system because the shallow host intrusions often represent the upper exposures of larger plutonic systems at depth (Seedorff et al., 2005; Steinberger et al., 2013). Because of their economic significance, they are well-studied, and exploration and mining of the systems provide excellent three dimensional exposure in many deposits (e.g., Bingham, Utah; Kloppenburg et al., 2010; Porter et al., 2012; Steinberger et al., 2013).

This paper touches on aspects of the entire magmatic system, from the lower crustal source to volcanic products but focuses on the plutonic and hypabyssal environments. As used herein, magma refers to a mix of crystal and melt. I use melt referring to molten rock with very low crystal fraction, less than ~10%. Magma may be mobile at low to moderate crystal fraction (<40-60%; Annen, 2009), but mobility is not a

requisite for magma, as used below. This contribution aims to bridge the gap between the complementary work in the pluton emplacement and ore deposit fields. I summarize and compare field and geochronologic data from plutonic and magmatic-hydrothermal systems. These observations are incorporated into a comprehensive general model of the formation and evolution of mineralized or unmineralized magmatic systems.

Evidence for incremental emplacement in plutonic and magmatic-hydrothermal systems

Field evidence in nonmineralized plutons

Field evidence suggests that many plutons form by the repeated injection of small pulses of magma (Cruden and McCaffrey, 2001; Glazner et al. 2004; Bartley et al., 2008). Field evidence for incremental pluton emplacement includes sharp internal contacts, with or without compositional change, dike and enclave swarms, and composite intrusions composed of a number of distinct but genetically related intrusive bodies. In large plutons or plutonic suites, field evidence for incremental emplacement is often obscured by later pulses of magma and other magmatic processes that can homogenize the pluton (Bartley et al., 2008).

Evidence for incremental emplacement commonly suggests that plutons formed by the repeated injection of subparallel dikes or sills (e.g., Tikoff and Teyssier, 1992; Tikoff et al., 1999; Petford et al., 2000; Vigneresse, 2004). An example of the former is the McDoogle pluton in the eastern Sierra Nevada batholith. The three distinct phases of the pluton show sharp internal contacts and wall-rock screens that strike subparallel to the pluton walls (Fig. 2.1A; Mahan et al., 2003; Stearns, 2009). Some plutons in the Coast Plutonic Complex of British Columbia formed as a stack of subparallel horizontal sills, a

similar, if rotated scenario to the McDoogle (Fig. 2.1B; Brown and McClelland, 2000). Tonalite sills on the edges of the pluton are interleaved with wall rock schists. Magmatic foliation within the plutons dips towards the center of the equant intrusions, suggesting that the center of the pluton was depressed as the stack of sills grew (Brown and McClelland, 2000).

The Jackass Lakes pluton on the western side of the Sierra Nevada shows a more complicated picture of incremental emplacement. The pluton was initially interpreted to have formed incrementally by successive pulses brought in by dikes (Fig. 2.1C; McNulty et al., 1996). Abrupt changes in magmatic fabric, often without any apparent change in modal or chemical composition, also provide evidence for incremental emplacement in the Jackass Lakes pluton (Pignotta et al., 2010); similar relationships are preserved in the McDoogle pluton (Mahan et al., 2003; Stearns, 2009). Enclave swarms and distinct, mappable rock units throughout the pluton show that the construction of the Jackass Lakes pluton was, indeed, incremental, but several mechanisms were involved in forming the mapped pluton (Pignotta et al., 2010).

Geochronologic evidence for protracted, incremental emplacement

Large, detailed geochronologic data sets strongly suggest that many plutons were emplaced not only incrementally, but over protracted periods. The Tuolumne Intrusive Suite in California showed an emplacement history for the suite that lasted about 10 Myr (Fig. 2.2; Coleman et al., 2004). Individual plutons within the suite were emplaced over periods approaching 4 Myr. The protracted emplacement of the plutons that make up the intrusive suite precludes its formation by the cooling of a single large volume of melt

(Glazner et al., 2004). The John Muir Intrusive Suite south of the Tuolumne is similar in size and compositional range, and shows similar age relationships (Fig. 2.2; Davis et al., 2012).

Like the larger Tuolumne and John Muir Intrusive Suites (>12000 km^2; Bateman, 1992; Davis et al,. 2012), the Mount Stewart Batholith (~700 km^2; Miller et al., 2007) and Tenpeaks pluton (>200 km^2) in the Cascade arc both show evidence for emplacement on timescales much longer than the expected cooling rate of comparably sized bodies of magma (Fig. 2.2; Matzel et al., 2006). U-Pb ages for the deep (20-25 km) Tenpeaks pluton span ~2.5 Myr, whereas the shallower (~7-10 km) Mount Stewart Batholith has zircon ages that cover a ~5.5 Myr spread (Fig. 2.2). Both intrusions show complicated relationships between different age domains, with age differences across gradational contacts between compositionally similar rocks as common as sharp contacts between rocks of different compositions.

Even in plutons lacking the density of age data presented for the Tuolumne and John Muir Intrusive Suites and Mount Stewart Batholith, U-Pb data suggest protracted pluton formation. Two dates on the Jackass Lakes pluton, cited above as an example of a pluton with good field evidence of incremental emplacement (McNulty et al., 1996; Wiebe, 2000; Pignotta et al., 2010) record zircon crystallization over at least 0.4 Myr and possibly >1 Myr (McNulty et al., 1996). Although not nearly as long as some of the larger plutons mentioned above, this is still longer than the expected lifespan of a conductively cooled intrusion the size of the Jackass Lakes pluton.

The Mount Givens Granodiorite is a large Cretaceous Sierran pluton with U-Pb dates that range from 92.8 to 87.9 Ma, consistent with protracted incremental

emplacement (Stern et al., 1981; Tobisch et al., 1995). The analytical errors (>2%) of these dates are much greater than what now can be achieved by ID-TIMS (~0.1%; e.g., Mattinson, 2005), but the age differences are statistically significant. Field evidence in the Mount Givens Granodiorite is consistent with incremental emplacement.

Less precise SHRIMP and LA-ICP-MS data can also resolve protracted emplacement. Although weighted averages often underestimate errors or overestimate the precision leading to geologically meaningless ages (von Quadt et al., 2011; Chiaradia et al., 2013), the distribution of individual analyses may be consistent with protracted emplacement. Complicated SHRIMP U-Pb distributions from the Spirit Mountain batholith in southern Nevada show that it was emplaced over about 2 Myr (Fig. 2.2; Walker et al., 2007)

Field evidence for incremental emplacement in magmatic-hydrothermal systems

Most magmatic-hydrothermal systems are hosted in the upper few km of the crust. Consequently, they are generally smaller than the midcrustal systems discussed above. Many, if not most, magmatic-hydrothermal systems are either hosted in or associated with composite plutons that are formed incrementally.

Perhaps the most dramatic examples of multiple intrusive and accompanying mineralizing events are Climax-type porphyry Mo systems, Cu-poor systems associated with high-silica rhyolite intrusions (White et al., 1981). At the Climax deposit itself, three ore zones have been recognized, each associated with separate porphyritic high-silica rhyolite stocks (Wallace et al., 1968; White et al., 1981). At Henderson, Colorado, twelve porphyry stocks in three intrusive centers host a high-grade mineralized core (Fig. 2.3A;

Carten et al., 1988; Seedorff and Einaudi, 2004). In both of these examples, each intrusive pulse brought with it some mineralization, and the superposition and repeated injection of ore-forming fluids provided the requisite Mo grade for economic mining.

The superposition of intrusive and associated hydrothermal events is also important in other types of magmatic-hydrothermal systems, although less so than in Climax-type porphyry Mo systems. Composite intrusions in porphyry-related systems exist both at the deposit (~1-2 km) and district (~2-10 km) scales.

The Bingham Stock in Utah is a composite intrusion that hosts the giant Bingham Canyon porphyry Cu-Mo-Au deposit (Fig. 2.3B; Redmond and Einaudi, 2010; Porter et al., 2012). The pluton comprises one equigranular intrusion and three major porphyritic dike units. Recent work on the Bingham porphyry Cu-Mo-Au deposit showed a permissible reconstruction of the deposit wherein the Bingham Stock was emplaced as a number of small pulses of magma in a dynamically evolving structural framework (Kloppenburg et al., 2010).

The Ertsberg district in Indonesia hosts the giant Grasberg porphyry Cu-Au deposit and several other zones of skarn and stockwork mineralization. The main intrusive centers in the young district (Fig. 2.3C; Pollard et al., 2005) are both composite. The Grasberg Intrusive Complex is a narrow diatreme complex comprising three intrusive phases. The adjacent and slightly older Ertsberg intrusive complex is composed of the main equigranular diorite and a series of porphyry dikes which contributed to stockwork and skarn mineralization (Gibbins, 2006). These plutons are the shallow manifestations of larger magma bodies at depth (McMahon, 1994; Porter and Titley, 2005). The dike swarms that host mineralization in deposits such as the Ertsberg

Stockwork Zone (Freihauf et al., 2005, Gibbins, 2006) and the Anne Mason system at Yerington, Nevada (Dilles, 1987) show a similar morphology to plutons made from dikes such as the McDoogle pluton (Mahan et al., 2003).

Some mineralized systems in the Great Basin have been tilted, exposing the deeper parts of the magmatic system that led to mineralization, and suggest the incremental emplacement of the upper parts of the system are also reflected at depth. The Jurassic Yerington batholith in western Nevada has been tilted about 90 degrees to the west providing a cross section through the upper 6 km of the system (Dilles, 1987). Evidence for incremental emplacement in the early stages of the batholith includes sharp contacts between rocks of similar composition, implying multiple pulses of compositionally similar material making up the bulk of the pluton. Sharp internal contacts are absent in later plutonic phases of the batholith (Dilles, 1987).

The Ruby Star Granodiorite, host of the Mission, Twin Buttes and Sierrita-Esperanza porphyry Cu-Mo systems in southern Arizona, has been tilted and dismembered by Tertiary extension. The deeper parts of this system show internal contacts, with and without major compositional changes (Stavast, 2006). The reported internal structure of the batholith is not as clear as it is at Yerington, but the evidence for multiple pulses of intrusive activity remains.

Lifespan of magmatic-hydrothermal systems

Abundant geochronologic data for the timing and lifespan of hydrothermal systems are available in the literature because of the importance of timing in exploration; the type and style of magmatic-hydrothermal systems are commonly grouped in time and space (e.g., Andean Cu province; Sillitoe and Perelló, 2005). Geochronologic data sets

for magmatic-hydrothermal systems commonly cover both the igneous rocks and the alteration and mineralization associated with the release of magmatic fluids. Besides U-Pb zircon data that pinpoint the crystallization ages of igneous rocks in magmatic-hydrothermal systems, the K-Ar and Re-Os systems are most commonly used to study the timing and evolution of hydrothermal systems. Using data from all three parts of the system, it is possible to determine the duration of magma emplacement, mineralization, and post-mineralization magmatic activity and cooling.

Intrusive rocks from the Quellaveco porphyry Cu-Mo deposit span about 5 Myr based on TIMS and LA-ICP-MS U-Pb zircon dates (Fig. 2.2; Sillitoe and Mortensen, 2010). Mineralizing porphyry intrusions lagged behind the intrusive rocks that host mineralization by about 1 Myr. Mineralization accompanying the intrusion of the dikes was active intermittently over 2.5-4 Myr.

The Bagdad porphyry Cu-Mo deposit is a low-grade porphyry deposit in northwestern Arizona. The only published age for the igneous rocks in the deposit is a K-Ar biotite age of 72.6 ± 2.6 Ma (Damon and Mauger, 1966). Re-Os ages for three samples from the Bagdad deposit were interpreted to represent two periods of Mo mineralization, the first at about 75.8 Ma and the second at about 71.8 Ma (Fig. 2.2; Barra et al., 2003). Mineralization at Bagdad thus occurred over a period of at least 4 Myr, but the data are insufficient to determine whether mineralization was episodic or continuous during this period.

A more complete picture of the duration and evolution of magmatic systems comes from using multiple dating techniques. U-Pb zircon and Re-Os molybdenite data from the Nacozari porphyry Cu-Mo district in northern Mexico show that the magmatic

system comprising several discrete intrusions associated with the La Caridad Cu-Mo deposit was active for at least 4 Myr, with a single pulse of mineralization introduced near the end of magmatism (Fig. 2.2; Valencia et al., 2005). Including nearby andesitic volcanism, the life span of the magmatic system, exceeds 10 Myr. Two overlapping Re-Os molybdenite analyses suggest that mineralization lasted less than 1 Myr.

Although large datasets for magmatic-hydrothermal systems are becoming more common, few cover the complete history of a combined magmatic-hydrothermal system. Three detailed datasets are summarized below.

The Bajo de la Alumbrera system in northwestern Argentina is hosted in the Farallón Negro Volcanic Complex (Halter et al., 2004). The andesitic volcanic rocks of the complex are intruded by a number of shallow plutons and plugs of wide-ranging composition (Halter et al., 2004). The shallow plutons and porphyritic plugs are responsible for the mineralization in the area. Volcanic activity started around 9.5 Ma and lasted until around 7 Ma (Halter et al., 2004). Intrusive activity in the district overlapped in time with volcanism, starting around 8.5 Ma (Halter et al., 2004; Harris et al., 2004) and persisting for about a million years after volcanism ceased (Halter et al., 2004; Harris et al., 2004; von Quadt et al., 2011).

The protracted igneous history in the district was punctuated by episodic mineralization. Multiple pulses of mineralization associated with different porphyry intrusions contributed to the mineral inventory, with two pulses depositing more than 80% of the metals in the system (Proffett, 2003). High precision TIMS U-Pb dates show the two pulses were emplaced in quick succession around 7.2 Ma (von Quadt et al., 2011). U-Th/He thermochronology on the deposit suggests a very fast initial cooling

history after the end of magmatic and hydrothermal activity, followed by slower cooling through the closure temperatures of the lower-temperature dating techniques (Harris et al., 2008), suggesting continued magma input at depth.

The Rio Blanco-Los Bronces deposit is another giant system in the Chilean Andes that shows evidence for protracted magmatism and mineralization. High precision U-Pb zircon dates show that the magmatic system initiated around 12 Ma with the emplacement of the granodiorite of the San Francisco batholith, which hosts the porphyry intrusions associated with the deposit (Fig. 2.2; Deckart et al., 2005; Toro et al,. 2012). The mineralizing intrusions were emplaced between 6.32 and 4.92 Ma. The main stage of mineralization occurred around 5.23 Ma; minor mineralization preceded the main stage by about 1 Myr. $^{40}Ar/^{39}Ar$ dating of secondary biotite supports the Re-Os data and suggests mineralization may have continued for 1 Myr, which suggests magmatic input continued for almost 1 Myr after mineralization (Figs. 2.2, 2.4; Deckart et al., 2005; Toro et al., 2012).

El Teniente is a nested mineralized system comparable in size and style to the giant Rio Blanco/Los Bronces system (Cooke et al., 2005; Vry et al., 2010). A large SHRIMP U-Pb zircon, Ar/Ar and Re-Os molybdenite data set has been collected for this deposit (Figs. 2.2, 2.4; Maksaev et al., 2004). The geochronology shows that the igneous rocks formed over approximately 2 Myr between ~6.5 and 4.5 Ma during at least three distinct pulses of igneous activity. Unlike in other systems discussed above, each pulse of intrusive activity brought with it some accompanying (Cu-)Mo mineralization, although the bulk of the mineralization was brought in with the penultimate mineralizing episode around 5 Ma (Cannell et al., 2005). All but the last pulse correlates with one of the pulses

of intrusive activity identified by the U-Pb data. Most of the $^{40}Ar/^{39}Ar$ data cluster between 5 and 4.5 Ma, indicating the system as a whole cooled below the closure temperature of biotite over about 0.5 Myr (Figs. 2.2, 2.4; Maksaev et al., 2004)

Discussion

Lifespans of magmatic and hydrothermal systems

The data summarized above clearly indicate similar timescales for mineralized and unmineralized magmatic systems (Fig. 2.2). Incremental and often protracted pluton emplacement is common and is characteristic of magmatic activity at all depths and scales. It further supports the interpretation that magmatic-hydrothermal systems are merely the upper-crustal manifestations of fairly normal large igneous systems that extend to depth (Richards, 2003; Sillitoe, 2010).

Hydrothermal activity can span millions of years, but mineralization does not generally span the duration of a magmatic system, (Figs. 2.2, 2.4). However, as with magma input in the plutonic environment, the durations of individual mineralizing pulses of mineralization are very short. Numerical models show that shallow stocks the size of those that host porphyry systems (several km^3) cool on the order of tens of thousands of years (e.g., Cathles, 1997). Theoretical work suggests the Butte and Bajo de la Alumbrera systems may have formed in less than 1000 years (Cathles and Shannon, 2007), and dating and thermal modeling at Bingham Canyon shows the igneous and hydrothermal activity in the host Bingham Stock spanned less than 0.3 Myr, although the source pluton was active over a longer period (von Quadt et al., 2011; Steinberger et al,. 2013).

In most systems the bulk of mineralization and hydrothermal activity takes place in only a few short-lived pulses. The bulk of Cu mineralization at Bingham (Redmond

and Einaudi, 2010; Porter et al., 2012) and El Teniente (Cannell et al., 2005) occurred in one hydrothermal episode. At Bajo de la Alumbrera, an estimated 80% of the 4 Mt defined copper reserves was deposited in two large pulses, with the remaining 20% spread over three smaller pulses (Fig. 2.4; Proffett, 2003).

Implications of magmatic-hydrothermal systems for the formation of magma chambers

Metals that are concentrated in porphyry and other magmatic-hydrothermal mineral systems are deposited from primary fluids that exsolve directly from a crystallizing melt (Ulrich and Heinrich, 2002). Because the majority of the metals are deposited in one or two large pulses, this requires that there be a large body of melt available to supply the magmatic-hydrothermal system. How much melt is required?

Based on a hypothetical system starting with a "typical" calc-alkaline melt, about 50 km^3 of magma are required to supply copper to a modest porphyry system (6 Mt contained Cu; Cline and Bodnar, 1991). Field evidence for a mineralized system with a similar amount of contained Cu suggests about 65 km^3 of magma were required (Dilles, 1987; Cline and Bodnar, 1991). Sulfur budget calculations of the Ertsberg Stockwork Zone and associated skarn deposits which contain some 8 Mt Cu, require that some 50-70 km^3 of magma contribute to those deposits (Porter and Titley, 2005).

Larger deposits require larger volumes of magma. Based on the mass balance of ore metals McMahon (1994) calculated that between 105 and 195 km^3 of magma are required to supply the Cu for the Grasberg alone (28 Mt contained Cu; Cooke et al., 2005). Using a different approach and assuming the Grasberg system shares the same deep source as mineralization associated with the adjacent Ertsberg intrusive complex (36

Mt total contained Cu; Cooke et al., 2005; Friehauf et al., 2005), between 235 and 315 km^3 of magma are required to supply the system (Porter and Titley, 2005). The Butte system, a similarly-sized porphyry Cu deposit as the Grasberg (>30 Mt contained Cu; Field et al., 2005) deposit requires 300-400 km^3 of magma (data from Field et al., 2005; Cathles and Shannon, 2007).

The volume of melt required to form even large magmatic-hydrothermal ore systems does not equate to very large plutons. The McDoogle pluton is one of the smallest plutons in the John Muir intrusive suite, with an outcrop area of about 24 km^2. Assuming the pluton has a reasonable thickness of 5 km (Petford et al., 2000), its 120 km^3 would be sufficient to supply metals and fluids to a large porphyry system. The Jackass Lakes pluton discussed above has a surface outcrop of approximately 13 x 17 km (Pignotta et al., 2010). At 5 km thick it represents approximately 1100 km^3 of crystallized melt. Each major Cretaceous nested intrusive suite in the Sierra Nevada comprises several thousand km^3 of plutonic rock (Bateman, 1992; Davis, 2010). Individual plutons in the suites may exceed 5000 km^3 (e.g., Lamarck Granodiorite; Davis, 2010).

Modest to large plutons may be critical to generating a sufficient melt volume to form large porphyry deposits in protracted magma systems. At average magma fluxes for plutonic systems of 10^{-3} or 10^{-4} km^3/yr (Crisp, 1984; Coleman et al., 2004; Matzel et al., 2006), individual pulses of magma crystallize before the next pulse is emplaced (Annen, 2009). Even if the wall rocks are heated by successive pulses of magma, hot wall rocks alone are not enough to sustain a large volume of high melt fraction magma (Annen, 2009; Davis, 2010). However, increased emplacement rate may lead to pluton-scale

volumes of magma containing >40-60% melt (magma chambers) being generated and sustained (Annen, 2009).

Numerical models show that a magma flux around 3 x 10^{-3} km^3/yr is able to form and sustain a magma chamber, which is necessary to prevent premature exsolution of potentially mineralizing fluids. Given an appropriate chamber geometry and magma flux, up to 35% of the volume of the pluton may comprise a melt-rich magma (>40-60% melt; Annen, 2009). If conditions allow for 30% of the entire pluton volume to be a mobile magma, then the 300-400 km^3 of melt necessary to supply giant magmatic-hydrothermal systems, like those that formed Butte and Grasberg, could be constructed in a pluton with a total volume of as little as 1000-1300 km^3, on the order of the size of the Jackass Lakes pluton discussed above (Pignotta et al., 2010).

Plutonic-hydrothermal system model

A model is offered below for the plutonic-hydrothermal system that considers the short duration of individual mineralizing events, the multimillion year timescales of mineralized systems, and the timescales of magmatic systems. Although volcanism is an important part of magmatic systems, the model below deals only with the intrusive environment. This model highlights ties between existing models for the formation of plutons and magmatic-hydrothermal systems.

Stage 1: Pluton construction

In the first stage magma is transferred from the lower crust into a relatively cool portion of the mid- to upper-crust. Early in stage 1 the magmatic system is closed, with magma being transferred only from the lower- to upper-crust and not the surface. Late in

stage 1 a volcanic system may be established above the plutonic environment, opening the system and allowing some of the magma to pass up through the plutonic environment to the surface.

Intrusion into cold wall rocks and/or a low magma flux prevent the establishment of a sufficient volume of high melt fraction magma at this early stage. Individual pulses of magma become frozen at the emplacement level before the next arrives; evidence of incremental emplacement such as internal contacts, is preserved (Fig. 2.5; McDoogle Pluton and Ruby Star Granite; Mahan et al., 2003; Stavast, 2006; Stearns, 2009). These smaller pulses of magma will release their volatile component, but not enough fluid will be present to form large volumes of mineralization. Stage 1 lasts up to a few million years and builds plutons that may eventually be exposed at the surface (i.e., Jackass Lakes pluton; McNulty et al., 1996; Pignotta et al., 2010).

Stage 2: Batholith construction and establishment of a magma chamber

As magmatic activity continues, the temperature of the wall rocks increases and magmatic flux varies. In this stage a coherent volume of magma (magma chamber) is established. Increased magmatic flux creates the appropriate conditions for the magma chamber which is necessary to supply magmatic-hydrothermal systems (Ulrich and Heinrich, 2002).

Although a large, coherent volume that contains a high melt fraction (40-60% melt; Annen, 2009) may form, the crystal fraction of the magma could vary widely. Melt content in the magma chamber may be very low, consistent with geophysical data from subvolcanic reservoirs (e.g., Waite and Moran, 2009). In a mineralizing system, enough melt must be present and accessible that the tens to hundreds of km^3 of melt can release

their volatiles in a very short time, as little as hundreds of years (Cathles and Shannon, 2007). A high melt fraction magma may convect and transport smaller batches of magmatic fluid to the top of the magma chamber, prolonging the period of exsolution (Shinohara et al., 1995).

In the subvolcanic portion of the system, the cupola that will host mineralization is developed at this stage (Fig. 2.5). The hypabyssal stocks that host mineralization lag behind the establishment of a volcanic edifice (e.g., Bajo de la Alumbrera and Bingham; Halter et al., 2004; von Quadt et al., 2011). A cupola serves to focus mineralizing fluids and generally forms in transtensional oversteps (Tosdal and Richards, 2001; Richards, 2003; Cloos and Sapiie, 2005). Although the cupola generally forms quickly, there is evidence of incremental emplacement at these shallow depths, too (Kloppenburg et al., 2010).

Internal contacts are absent in plutons formed during this stage. Early batches of magma have time between pulses to cool below the solidus and preserve internal contacts. Increased magma flux, coupled with warmer wall rocks keep large parts of the system above the solidus, preventing the preservation of internal contacts. Stage 2 lasts up to several million years. In most large plutonic systems, the bulk of the magma is emplaced during this stage.

Stage 3: Volatile release and mineralization

With the thermal preparation of stages 1 and 2, the formation of magma chambers to supply the mineralized deposit, and the preparation of a cupola to focus mineralization, the groundwork for hydrothermal alteration and mineralization is in place. The main stage of mineralization generally coincides with the emplacement of porphyry dikes and

usually occurs near the end of the magmatic system (Fig. 2.5; Seedorff et al., 2005; Sillitoe, 2010).

Volumetrically, the dikes represent a small portion of the overall magma system; they act as conduits for mineralizing fluids, rather than a source of mineralizing fluids (Fig. 2.5; Sillitoe, 2010). The dikes act as conduits for magmatic volatiles released from the deep magma chamber during or shortly after dike emplacement. Fluid pressures build at depth until they overcome lithostatic pressure and generate a fracture network that allows the fluids to permeate to the mineralizing zone. Fluids ascend and metals are deposited where PT conditions are favorable (e.g., Gruen et al., 2010; Landtwing et al., 2010).

During the latter part of stage 1 and early in stage 2, the magmatic system is largely open; magma ascends from the lower crustal source and some is extruded at the surface. An explosive eruption like the 1991 Pinatubo eruption can lead to the rapid release of enough volatiles to form an entire porphyry system (Gerlach et al., 1996). Such eruptions, with their large volatile releases, suggest more than one magma chamber may be formed over the life of a magmatic system. Mineralization generally occurs late in fertile magmatic systems. To avoid volatile release into the atmosphere, the system must be closed before the transition from stage 2 to stage 3. What, then, causes the system to close in the latter stages of the magmatic system, allowing for the storage and focused subsurface release of mineralizing volatiles?

An evolving structural framework plays a large role. Many porphyry systems form during transitions of the regional stress regime, usually caused by changes in subduction geometry, rate, or both (Tosdal and Richards, 2001). Accompanying the shift

in convergent rates or subduction geometry, a change in style or productivity of volcanism and intrusive activity may be expected. Tosdal and Richards (2001) attributed this to the change from a stress environment wherein magmatic overpressure that leads to explosive eruptions gives over to more passive buoyant ascent.

The duration of stage 3 is shorter than previous stages. The full mineralizing sequence may take place over more than a million years (Fig. 2.5), but each mineralizing event is very short (Cathles and Shannon, 2007).

Stage 4: Postmineralization igneous activity

Late to postmineralization dikes are common in many magmatic-hydrothermal systems. The main pulse of mineralization is related to the crystallization of a volume of magma, and the late stage dikes may either be remnants of that large system or they may represent later pulses of magma introduced to the system after the main stage of mineralization (Fig. 2.5). Postmineral volcanism is also common in many mineralized magmatic systems (e.g., Bingham; Deino and Keith, 1997).

These dikes reveal little about the size of magma reservoir at depth, but they offer clues as to the longevity of magmatic systems. In most systems, hypabyssal magmatism ceases soon after mineralization (e.g., Bingham; von Quadt et al., 2011). These late dikes represent the waning stages of a pluton-forming magmatic event in the upper part of the system.

The magmatic-hydrothermal environment as a plutonic-volcanic link

There is a clear spatial, and often compositional, relationship between volcanic rocks and some plutons (e.g., Colorado River extensional corridor and San Juan Volcanic Field; Metcalf, 2004; Lipman, 2007). The link between volcanic activity and the intrusive systems that generate magmatic-hydrothermal mineralization is well established (e.g., Yerington, Bingham, Bajo de la Alumbrera and Yanacocha; Dilles and Wright, 1988; Waite et al., 1997; Halter et al., 2004; Longo et. al., 2010). The timescales of volcanic systems are similar to the timescales of unmineralized and mineralized intrusive systems. For example, Grunder et al. (2006) presented evidence that over 300 km^3 of magma of the Aucanquilcha volcanic complex, was erupted over more than 11 Myr. The Altiplano volcanic system was active over more than 9 Myr (de Silva and Gosnold, 2007). Rocks in the Yanacocha Volcanic Field discussed above show both protracted volcanic and mineralizing hydrothermal activity (Longo et al., 2010), as does the Bodie volcanic field in eastern California (John et al., 2012).

Conclusions

The magmatic-hydrothermal environment, long overlooked by many workers may be the missing link between the plutonic and volcanic environments. Magmatic-hydrothermal systems provide a direct link between the volcanic and plutonic systems. They are connected to unerupted batholithic scale magma chambers at depth and coeval or younger volcanic rocks are found in close proximity to hydrothermal deposits (Seedorff et al., 2005; Sillitoe, 2010). The common timescales and the link between the volcanic and plutonic systems that magmatic-hydrothermal systems represent strongly

suggest common mechanisms across all three environments and call for a more holistic approach to the study of magmatic systems. For a complete understanding, plutonic, magmatic-hydrothermal, and volcanic environments must be considered together to generate the most correct models for the evolution and emplacement of magmatic systems.

Whereas the processes that form unmineralized plutonic and mineralized magmatic-hydrothermal systems have been recognized as being similar (e.g., Dilles, 1987; Tosdal and Richards, 2001; Richards, 2003), field and geochronologic data suggest that the magmatic systems involved in both environments commonly grow incrementally and are active over protracted periods. One outcome of the common processes is that, at least in some systems, hundreds of km^3 of high-melt fraction magma must have been present at some point in the evolution of the magmatic system. These volumes of mobile magma generally form late in the evolution of a magmatic system, either owing to some combination of an increase in magma flux or a smaller temperature gradient between batches of emplaced magma and the country rocks.

Reevaluation of available geochonologic data may be in order to determine whether some of the spread in ages may be explained by the presence of magma chambers. Geochronologic data showing protracted emplacement of shallow plutons may in part be dating the formation and emplacement of the deep sources for shallow magmas (e.g., Bajo de la Alumbrera; Harris et al., 2008; von Quadt et al., 2011).

Whatever the apparent similarities between the timescales of magmatic-hydrothermal and unmineralized plutonic environments, shallow stocks represent a key part in the overall picture. The subvolcanic environment they represent is an

underutilized source of information that may help answer some of the basic questions of the evolution of the upper-crust.

Figure 2.1. Simplified geologic maps of three plutons that show evidence for incremental emplacement. All three maps are at the same scale. A. The McDoogle pluton in the John Muir Intrusive Suite of the Sierra Nevada is composed of two distinct compositional phases that are in sharp contact with each other. On the margins of the pluton dikes of McDoogle rocks are interleaved with wallrocks (map modified from Stearns, 2009). B. The Breckenridge pluton of the Coast Plutonic Complex in British Columbia shows evidence for formation by the stacking of magma sheets. Sheet contacts can be mapped in the northern part of the pluton, and sheets are interleaved with surrounding schists on the margins of the pluton (map modified from Brown and McClelland, 2000). C. The Jackass Lakes pluton in the western Sierra Nevada shows evidence for formation by multiple pulses of magma. Internal contacts and dikes of Jackass Lakes granodiorite in the wall rock are evidence of the incremental emplacement of the pluton (modified from Pignotta et al., 2010).

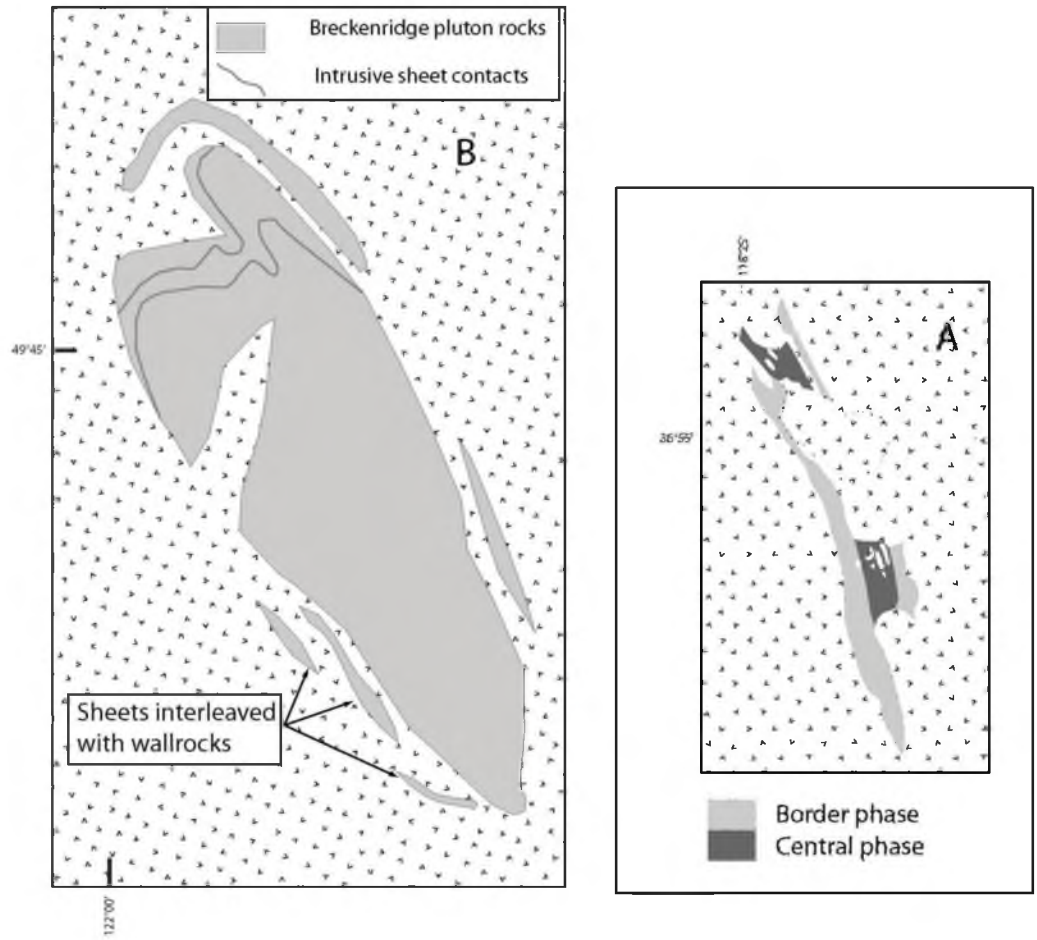
Breckenridge pluton rocks
Intrusive sheet contacts
B
Sheets interleaved with wallrocks
49°45'
122°00'
A
118°25'
38°55'
Border phase
Central phase

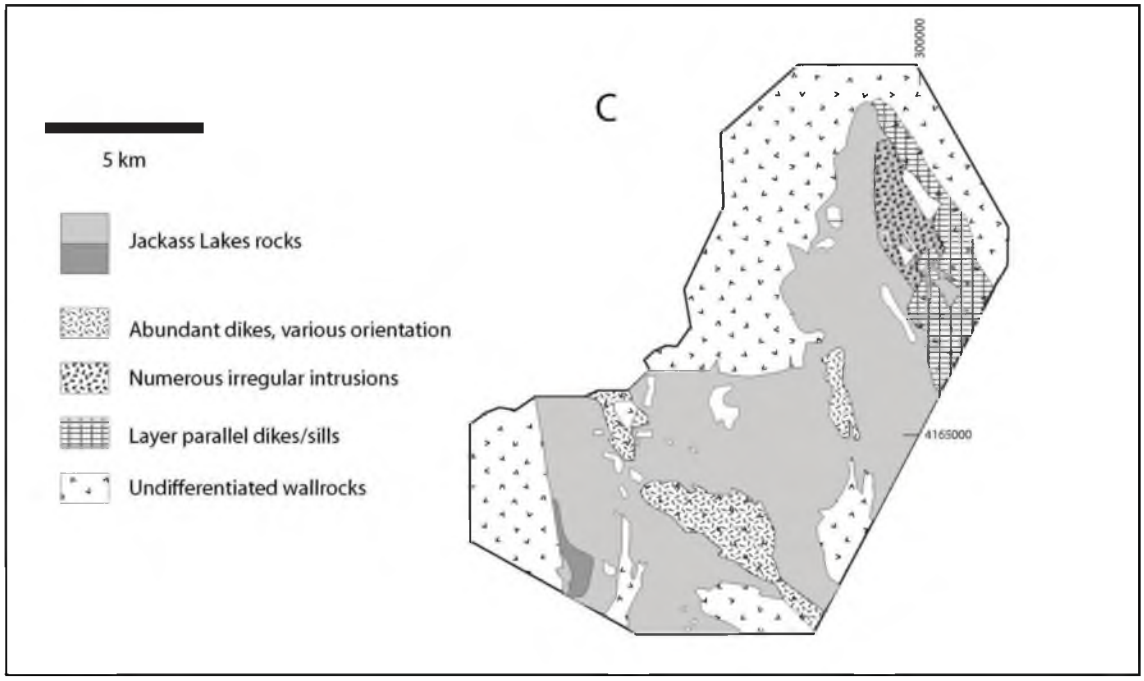
5 km
Jackass Lakes rocks
Abundant dikes, various orientation
Numerous irregular intrusions
Layer parallel dikes/sills
Undifferentiated wallrocks
C
300000
4165000

Figure 2.2. Summary of age data for the magmatic systems discussed in the text. Data for all systems is normalized with the youngest date set at zero. Data sources: 1. Walker et al., 2007; 2. Matzel et al., 2006; 3. Davis et al., 2012; 4. Coleman et al., 2004; 5. Maksaev et al., 2004; 6. Harris et al., 2004, 2008; 7. Deckart et al., 2005; 8. Pollard et al., 2005; Gibbins, 2006; 9. Valencia et al., 2005; 10. Barra et al., 2003; 11. Sillitoe and Mortenson, 2010; 12. Longo et al., 2010; 13. Grunder et al., 2006.

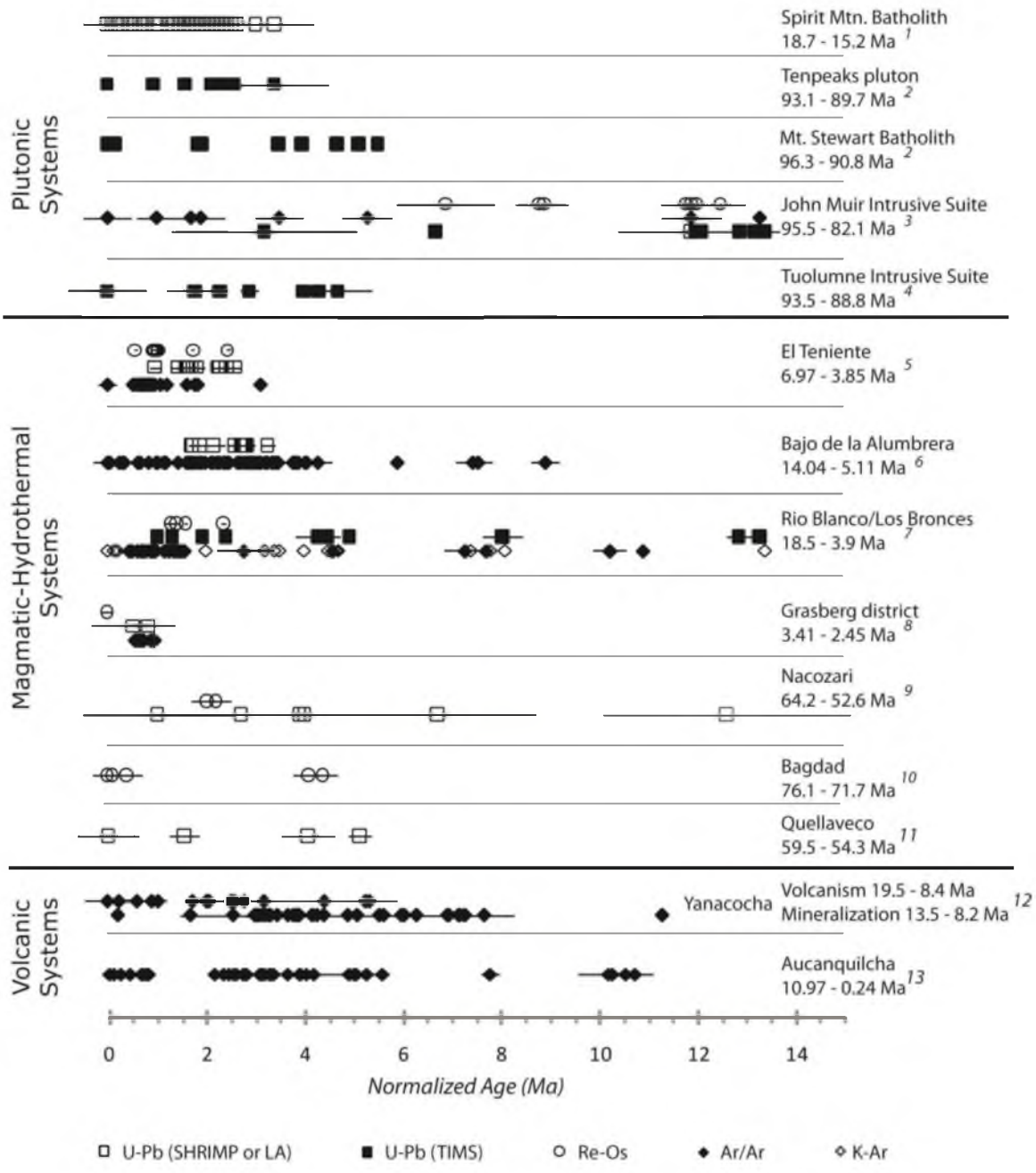
Plutonic Systems
Spirit Mtn. Batholith
18.7 - 15.2 Ma 1
Tenpeaks pluton
93.1 - 89.7 Ma 2
Mt. Stewart Batholith
96.3 - 90.8 Ma 2
John Muir Intrusive Suite
95.5 - 82.1 Ma 3
Tuolumne Intrusive Suite
93.5 - 88.8 Ma 4
Magmatic-Hydrothermal Systems
El Teniente
6.97 - 3.85 Ma 5
Bajo de la Alumbrera
14.04 - 5.11 Ma 6
Rio Blanco/Los Bronces
18.5 - 3.9 Ma 7
Grasberg district
3.41 - 2.45 Ma 8
Nacozari
64.2 - 52.6 Ma 9
Bagdad
76.1 - 71.7 Ma 10
Quellaveco
59.5 - 54.3 Ma 11
Volcanic Systems
Yanacocha
Volcanism 19.5 - 8.4 Ma
Mineralization 13.5 - 8.2 Ma 12
Aucanquilcha
10.97 - 0.24 Ma 13
0
2
4
6
8
10
12
14
Normalized Age (Ma)
U-Pb (SHRIMP or LA)
U-Pb (TIMS)
Re-Os
Ar/Ar
K-Ar

Figure 2.3. Simplified maps of three plutons associated with mineralized systems. All three plutons are at the same scale and in contrast to the legends in Figure 2.1, lighter gray indicates younger intrusions on all three maps. A. Twelve overlapping rhyolitic intrusions formed and host the Henderson porphyry Mo deposit. Sharp contacts exist between intrusive pulses, and each brought with it a pulse of Mo mineralization, the overlap of which brought grades up to economic values (modified from Seedorff and Einaudi, 2004). B. The Grasberg intrusive complex hosts the giant Grasberg porphyry Cu-Au deposit. Sharp contacts exist between the individual units, but mineralization occurred in one large pulse (modified from Pollard et al., 2005). C. The Bingham stock hosts the Bingham porphyry Cu-Mo-Au deposit and is formed by five distinct rock types that were emplaced over a short period (modified from Porter et al., 2012).

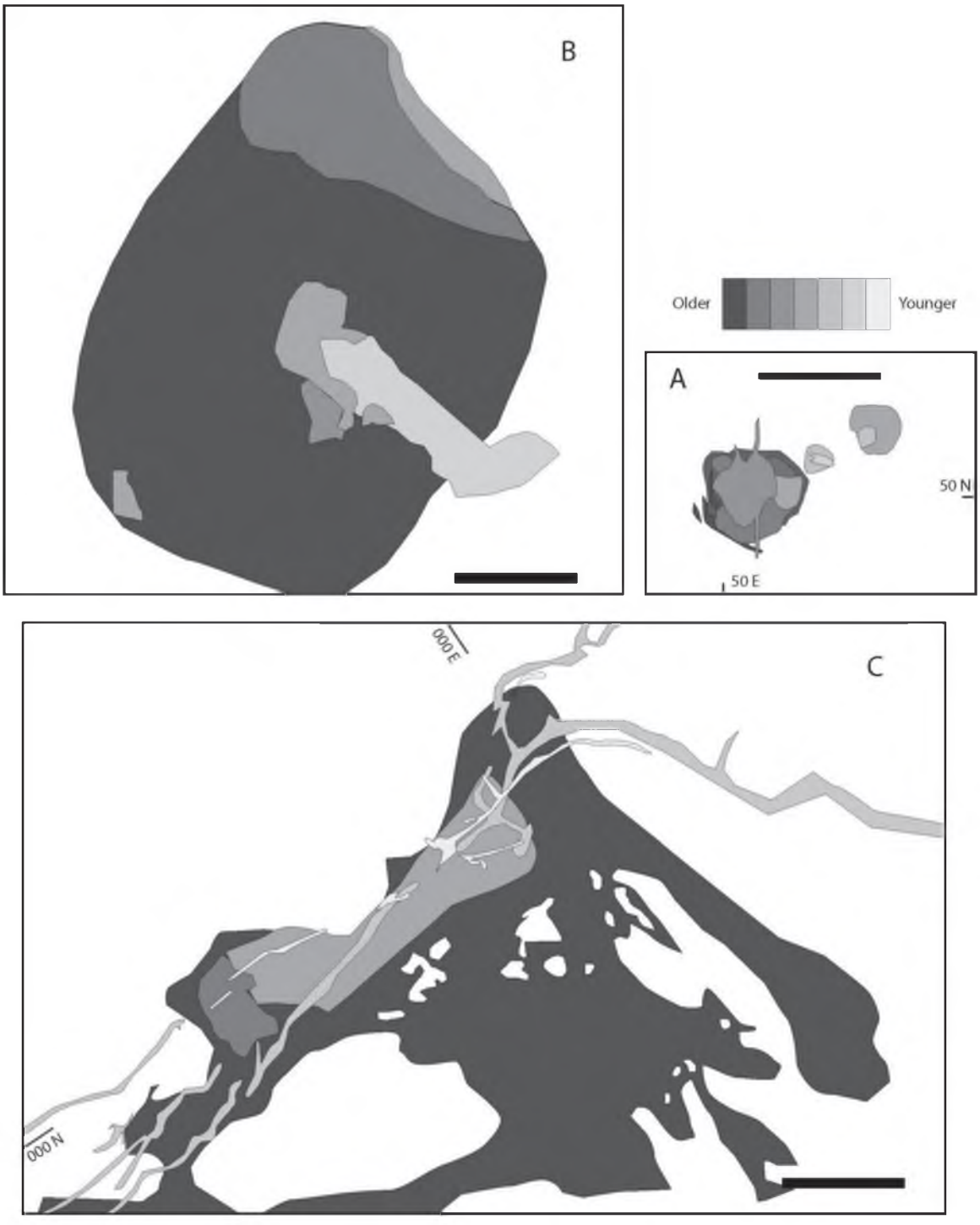
B
Older
Younger
A
50 N
50 E
C
000 E
000 N

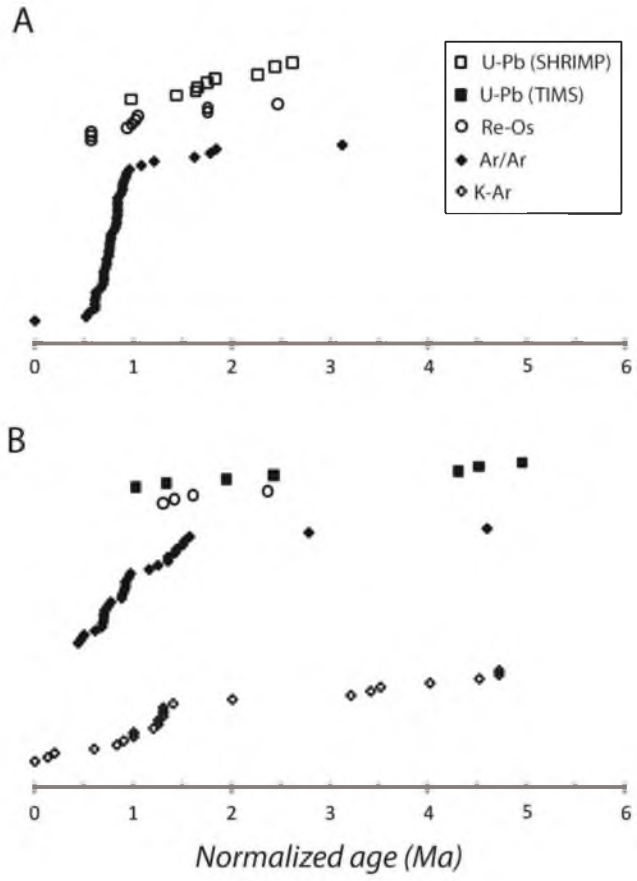

Figure 2.4. A comparison of normalized ages (youngest age = 0 Myr) for El Teniente (A) and the last 6 Myr of the Rio Blanco/Los Bronces (B) magmatic-hydrothermal systems. Each point represents a single analysis, excluding the analytical uncertainty. The figure shows that both systems show protracted magmatism and mineralization. Pulses of magmatism (U-Pb ages) are punctuated by mineralizing episodes (Re-Os ages). The K-Ar and Ar/Ar data sets both show that heat was emplaced into parts of the system after the end of mineralization. The magmatic system at El Teniente ceased soon after the last episode of mineralization, but the Rio Blanco/Los Bronces system shows a slower end to the system, with the last K-Ar age almost 1.5 Myr after the end of mineralization. Data from Maksaev et al., 2004 and Deckart et al., 2005.

Figure 2.5. Schematic model showing the stages of development of a magmatic system comprising both plutonic and magmatic-hydrothermal systems. A. Stage 1: Development of plutonic rocks with internal contacts, represented by light gray lines, and other evidence of incremental emplacement preserved. B. Stage 2: Development of later stage batholithic rocks and preparation of a cupola that will later host mineralization. Reservoirs of high-melt volume magma are developed during this stage. C. Stage 3: Crystallization of the large magma reservoirs occurs, possibly accompanied by the underplating of mafic alkaline magmas (e.g., Maughan et al., 2002). Metal rich magmatic volatiles are released and follow the same structural path as coeval porphyry intrusions. Some melt reservoirs may be preserved. D. Stage 4: Late or postmineral dikes, representing the waning stages of magmatism are emplaced and cut most mineralization. See text for further discussion.

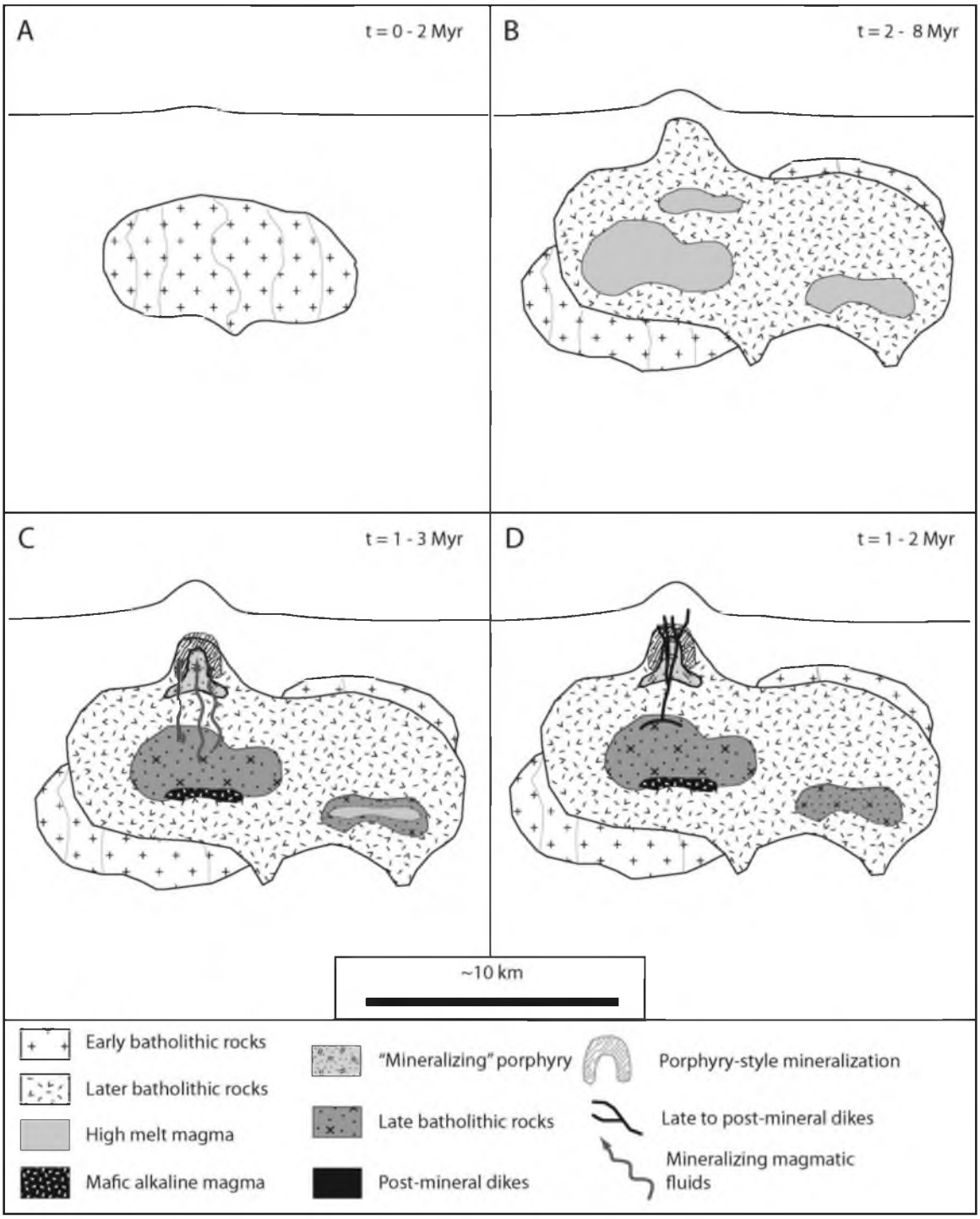
A
t = 0 - 2 Myr
B
t = 2 - 8 Myr
C
t = 1 - 3 Myr
D
t = 1 - 2 Myr
~10 km
Early batholithic rocks
Later batholithic rocks
High melt magma
Mafic alkaline magma
"Mineralizing" porphyry
Late batholithic rocks
Post-mineral dikes
Porphyry-style mineralization
Late to post-mineral dikes
Mineralizing magmatic fluids

References

Annen, C., 2009, From plutons to magma chamber: Thermal constraints on the accumulation of eruptible silicic magma chambers in the upper crust: Earth and Planetary Science Letters, v. 284, p. 409-416.

Barra, F., Ruiz, J., Mathur, R., and Titley, S., 2003, A Re-Os study of sulfide minerals from the Bagdad porphyry Cu-Mo deposit, northern Arizona, USA: Mineralium Deposita, v. 38, 585-596.

Bartley, J.M., Coleman, D.S., and Glazner, A.F., 2008, Incremental pluton emplacement by magmatic crack-seal: Transactions of the Royal Society of Edinburgh: Earth Sciences, v. 97, p. 383-396.

Bateman, P.C., 1992, Plutonism in the Central Part of the Sierra Nevada Batholith, California: USGS Professional Paper 1483, 186 p.

Brown, E.H. and McClelland, W.C., 2000, Pluton emplacement by sheeting and vertical ballooning in part of the southeast Coast Plutonic Complex, British Columbia: GSA Bulletin, v. 112, p. 708-719.

Cannell, J., Cooke, D.R., Walshe, J.L., and Stein, H., 2005, Geology, Mineralization, alteration, and structural evolution of El Teniente porphyry Cu-Mo deposit: Economic Geology, *v.* 100, p. 979-1004.

Carten, R.B., Geraghty, E.P., Walker, B.M., and Shannon, J., 1988, Cyclic development of igneous features and their relationship to high-temperature hydrothermal features in the Henderson porphyry molybdenum deposit, Colorado: Economic Geology, v. 83, p. 266-296.

Cathles, L.M., 1997, An analysis of the cooling of intrusives by ground-water convection which includes boiling: Economic Geology, v. 72, p. 804-826.

Cathles, L.M., and Shannon, R., 2007, How potassium silicate alteration suggests the formation of porphyry ore deposits begins with the nearly explosive but barren expulsion of large volumes of magmatic water: Earth and Planetary Science Letters, v. 262, p. 92-108.

Chiaradia, M., Schaltegger, U., Spikings, R., Wotzlaw, J.F., and Ovtcharova, O., 2013, How accurately can we date the duration of magmatic-hydrothermal events in porphyry systems?: Economic Geology, v. 108, p. 565-584.

Clemens, J. D., and Mawer, C. K., 1992, Granitic magma transport by fracture propagation, 1992: Tectonophysics, v. 204, p. 339-360.

Cline, J.S. and Bodnar, R.J., 1991, Can economic porphyry copper mineralization be generated by a typical calc-alkaline melt?: Journal of Geophysical Research, v. 96, p. 8113-8126.

Cloos, M. and Sapiie, B., 2005, Porphyry copper deposits: Strike-slip faulting and throttling cupolas: Geological Society of America Abstracts with Programs, v. 37, p. 97.

Coleman, D.S., Gray, W., and Glazner, A.F., 2004, Rethinking the emplacement and evolution of zoned plutons: Geochronologic evidence for incremental assembly of the Tuolumne Intrusive Suite, California: Geology, v. 32, p. 433-436.

Cooke, D.R., Hollings, P., and Walshe, J.L., 2005, Giant porphyry deposits: Characteristics, distribution, and tectonic controls: Economic Geology, v. 100, p. 801-818.

Crisp, J.A.,1984, Rates of magma emplacement and volcanic output: Journal of Volcanology and Geothermal Research, v. 20, p. 177-211.

Cruden, A.R. and McCaffrey, K.J.W., 2001, Growth of plutons by floor subsidence: Implications for rates of emplacement, intrusion spacing and melt-extraction mechanisms: Physics and Chemistry of the Earth (A), v. 26, p. 303-315.

Davis, J.W., 2010, Thermochronology and cooling histories of plutons, implications for incremental pluton assembly: Unpublished PhD dissertation, University of North Carolina, 119 p.

Davis, J.W., Coleman, D.S., Gracely, J.T., Gaschnig, R., and Stearnes, M., 2012, Magma accumulation rates and thermal histories of plutons of the Sierra Nevada batholith, CA: Contributions to Mineralogy and Petrology, v. 163, p. 449-465.

Damon P.E. and Mauger R.L., 1966, Epierogeny-orogeny viewed from the Basin and Range Province: SME Transactions, v. 235, p. 99–112.

de Silva, S.L. and Gosnold, W., 2007, Episodic construction of batholiths: Insights from the spatiotemporal development of an ignimbrite flare-up: Journal of Volcanology and Geothermal Research, v. 167, p. 320-335.

Deckart, K., Clark, A.H., Aguilar, A., Vargas R., Bertens, A., Mortensen, J.K., and Fanning, M., 2005, Magmatic and hydrothermal chronology of the giant Rio Blanco porphyry copper deposit, central Chile: Implications of an integrated U-Pb and 40Ar/39Ar database: Economic Geology, v. 100, p. 905-934.

Deino, A., and Keith, J.D., 1997, Ages of volcanic and intrusive rocks in the Bingham mining district, Utah: Society of Economic Geologists Guidebook Series, v. 29, p. 91–100.

Dilles, J.H., 1987, Petrology of the Yerington batholith, Nevada: Evidence for evolutoin of porphyry copper ore fluids: Economic Geology, v. 82, p. 1750-1789.

Dilles, J.H., and Wright, J.W., 1988, The chronology of early Mesozoic arc magmatism in the Yerington district of western Nevada and its regional implications: GSA Bulletin, v. 100, p. 644-652.

Field, C.W., Zhang, L., Dilles, J.H., Rye, R.O., and Reed, M.H., 2005, Sulfur and oxygen isotopic record in sulfate and sulfide minerals of early, deep, pre-Main Stage porphyry Cu-Mo and late Main Stage base-metal deposits, Butte district, Montana: Chemical Geology, v. 215, p. 61-93.

Friehauf, K., Titley, S.R., and Gibbins, S., 2005, Porphyry-style mineralization in the Ertsberg Diorite, Gunung Bijih (Ertsberg/Grasberg) district, West Papua, Indonesia: *in* Porter, T.M., ed., Super Porphyry Copper & Gold Deposits, A Global Perspective, PGC Publishing, Adelaide, v. 2, p. 357-366.

Gerlach, T.M., Westrich, H.R., and Symmonds, R.B., 1996, Preeruption vapor in magma of the climactic Mount Pinatubo eruption: Source of the giant stratospheric sulfur dioxide cloud: *in* Newhall, C. and Punongbayan, R. eds., Fire and Mud: Eruptions and Lahars of Mount Pinatubo, Philippines, University of Washington Press, 415-433

Gibbins, S.L., 2006, The magmatic and hydrothermal evolution of the Ertsberg Intrusion in the Gunung Bijih (Ertsberg) mining district, West Papua, Indonesia: Unpublished PhD dissertation, University of Arizona, 384 p.

Glazner, A.F., Bartley, J.M., Coleman, D.S., Gray, W., and Taylor, R.Z., 2004, Are plutons assembled over millions of years by amalgamation from small magma chambers? GSA Today, v. 14, p. 4-11.

Gruen, G., Henrich, C.A., and Schroeder, K., 2010, Bingham Canyon porphyry Cu-Mo-Au deposit. II. Vein geometry and ore shell formation by pressure-driven rock extension: Economic Geology, v. 105, p. 69-90.

Grunder, A.L., Klemetti, E.W., Feely, T.C., and McKee, C.M., 2006, Eleven million years of arc volcanism and the Aucanquilcha Volcanic Cluster, northern Chilean Andes: Implications for the life span and emplacement of plutons: Transactions of the Royal Society of Edinburgh: Earth Sciences, v. 97, p. 415-436.

Halter, W.E., Bain, N., Becker, K., Heinrich, C.A., Landtwing, M., VonQuadt, A., Clark, A.H., Sasso, A.M., Bissig, T., and Tosdal, R.M., 2004, From andesitic volcanism to the formation of a porphyry Cu-Au mineralizing magma chamber: The Farallon Negro volcanic complex, northwestern Argentina: Journal of Volcanology and Geothermal Research, v. 136, p. 1-30.

Harris, A.C., Allen, C.M., Bryan, S.E., Campbell, I.H., Holcombe, R.J., and Palin, J.M., 2004, ELA-ICP-MS U-Pb zircon geochronology of regional volcanism hosting the Bajo de la Alumbrera Cu-Au deposit: Implications for porphyry-related mineralization: Mineralium Deposita, v. 39, p. 46-67.

Harris, A.C., Dunlap,W.J., Reiners, P.W., Allen, C.M., Cooke, D.R., White, N.C., Campbell, I.H., and Golding, S.D., 2008, Multimillion year thermal history of a porphyry copper deposit: Application of U-Pb, 40Ar/39Ar and (U-Th)/He chronometers, Bajo de la Alumbrera copper-gold deposit, Argentina: Mineralium Deposita, v. 43, p. 295-314.

John, D.A., duBray, E.A., Blakely, R.J., Fleck, R.J., Vikre, P. G., Box, S.E., and Moring, B.C., 2012, Miocene magmatism in the Bodie Hills volcanic field, California and Nevada: A long-lived eruptive center in the southern segment of the ancestral Cascades arc: Geosphere, v. 8, p. 44-97.

Kloppenburg, A., Grocott, J., and Hutchinson, D., 2010, Structural setting and synplutonic fault kinematics of a Cordilleran Cu-Au-Mo porphyry mineralization system, Bingham mining district, Utah: Economic Geology, v. 105, p. 743-761.

Landtwing, M.R., Furrer, C., Pettke, T., Guillong, M., and Heinrich, C.A., 2010, The Bingham Canyon porphyry Cu-Mo-Au deposit: III. Zoned copper-gold ore deposition by magmatic vapor expansion: Economic Geology, v. 105, p. 91–118.

Lipman, P.W, 2007, Incremental assembly and prolonged consolidation of Cordilleran magma chambers: Evidence from the Southern Rocky Mountain volcanic field: Geosphere: v. 3, p. 42-70.

Longo, A.A., Dilles, J.H., Grunder, A.I., and Duncan, R., 2010, Evolution of calc-alkaline volcanism and associated hydrothermal gold deposits at Yanacocha, Peru: Economic Geology, v. 105, p. 1191-1241.

Mahan, K.H., Bartley, J.M., Coleman, D.S., Glazner, A.F., and Carl, B.S., 2003, Sheeted intrusion of the synkinetic McDoogle pluton, Sierra Nevada, California: GSA Bulletin, v. 115, p. 1570-1582.

Maksaev, V., Munizaga, F., McWilliams, M., Fanning, M., Mathru, R., Ruiz, J., and Zentilli, M., 2004, New chronology for El Teniente, Chilean Andes, from U-Pb, 40Ar/39Ar, Re-Os, and fission-track dating: Implications for the evolution of a supergiant porphyry Cu-Mo deposit: *in* Sillitoe, R.H., Perello, J., and Vidal, C.E., eds., Andean Metallogeny: New Discoveries, Concepts and Updates: SEG Special Publication 10, p. 15-54.

Mattinson, J., 2005, Zircon U–Pb chemical abrasion ("CA-TIMS") method: Combined annealing and multi-step partial dissolution analysis for improved precision and accuracy of zircon ages: Chemical Geology v. 220, p. 47–66.

Matzel, J.E.P., Bowring, S.A., and Miller, R.B., 2006, Time scales of pluton construction at differing crustal levels: Examples from the Mount Stuart and Tenpeak intrusions, North Cascades, Washington: GSA Bulletin, v. 118, p. 1412-1430.

Maughan, D.T., Keith, J.K., Christiansen, E.H., Pulsipher, T., Hattori, K., and Evans, N.J., 2002, Contributions from mafic alkaline magmas to the Bingham porphyry Cu–Au–Mo deposit, Utah, USA: Mineralium Deposita, v., 37, p. 14-37.

McMahon, T.P., 1994, Pliocene intrusions in the Gunung Bijih, (Ertsberg) mining district, Irian Jaya, Indonesia: Major- and trace-element chemistry: International Geology Review, v. 36, p. 925-946.

McNulty, B.A., Tong, W., and Tobisch, O.T., 1996, Assembly of a dike-fed magma chamber: The Jackass Lakes pluton, central Sierra Nevada, California: GSA Bulletin, v. 108, p. 926-940.

Metcalf, R.V., 2004, Volcanic-plutonic links, plutons as magma chambers and crust-mantle interaction: A lithospheric scale view of magma systems: Transactions of the Royal Society of Edinburgh: Earth Sciences, v. 95, p. 357-374.

Meyer, C. and Hemley, J.J., 1967, Wall rock alteration: *in* Barnes, H.L., ed., Geochemistry of Hydrothermal Ore Deposits, 1st Edition, p. 166-231.

Miller, J.S., Matzel, J.E.P., Miller, C.F., Burgess, S.D., and Miller, R.B., 2007, Zircon growth and recycling during the assembly of large, composite arc plutons: Journal of Volcanology and Geothermal Research, v. 167, p. 282-299.

Miller, R.B. and Paterson, S.R., 1999, In defense of magmatic diapirs: Journal of Structural Geology, v. 21, p. 1161-1173.

Paterson, S.R. and Vernon, R.H., 1995, Bursting the bubble of balooning plutons: A return to nested diapirs emplaced by multiple processes: GSA Bulletin, v. 107, p. 1356-1380.

Petford, N., Cruden, A.R., McCaffery, K.J.W., and Vigneresse, J.L., 2000, Granite magma formation, transport and emplacement in the Earth's crust: Nature, v. 408, p. 669-673.

Pignotta, G.S., Paterson, S.R., Coyne, C.C., Anderson, J.L., and Onezime, J., 2010, Processes involved during incremental growth of the Jackass Lakes pluton, central Sierra Nevada batholith: Geosphere, v. 6, p. 130-159.

Pitcher, W.S., and Berger, A.R., 1972, The geology of Donegal: A study of granite emplacement and unroofing, Regional geology series: New York, Wiley-Interscience, 435 p.

Pollard, P.J., Taylor, R.G., and Peters, L., 2005, Ages of intrusion, alteration, and mineralization at the Grasberg Cu-Au deposit, Papua, Indonesia: Economic Geology, v. 100, p. 1005-1020.

Porter, J.P. and Titley, S.R., 2005, Sulfur content of the Ertsberg magma of West Papua Indonesia and sulfur budget of associated ore deposits, deduced from apatite sulfur compositions: Geological Society of America Abstracts with Programs, v. 37, n. 7, p. 164.

Porter, J.P., Schroeder, K., and Austin, G., 2012, Geology of the Bingham Canyon porphyry Cu-Mo-Au deposit, Utah, *in* Hedenquist, J.W., Harris, M., and Camus, F., eds, Geology and Genesis of Major Copper Deposits and Districts of the World: A Tribute to Richard H. Sillitoe: SEG Special Publication 16, p. 147-166.

Proffett, J.M., 2003, Geology of the Bajo de la Alumbrera porphyry copper-gold deposit, Argentina: Economic Geology, v. 98, p. 1535-1574.

Richards, J.P., 2003, Tectono-magmatic precursors for porphyry Cu-(Mo-Au) deposit formation: Economic Geology, v. 98, p. 1515-1533.

Redmond, P.B. and Einaudi, M.T., 2010, the Bingham Canyon porphyry Cu-Mo-Au deposit. I. Sequence of intrusions, vein formation and sulfide deposition: Economic Geology, v. 105, p. 43-68.

Seedorff, E., Dilles, J.H., Proffett, J.M., Einaudi, M.T., Zurcher, L., Stavast, W.J.A., Johnson, D.A., and Barton, M.D., 2005, Porphyry deposits: Characteristics and origin of hypogene features: *in* Hedenquist, J.H., Thompson, J.F.H., Goldfarb, R.J., and Richards, J.P., eds., Economic Geology 100th Anniversary Volume, p. 251-298.

Seedorff, E. and Einaudi, M.T,. 2004, Henderson porphyry molybdenum system, Colorado: I. Sequence and abundance of hydrothermal mineral assemblages, flow paths of evolving fluids, and evolutionary style: Economic Geology, v. 99, p. 3-37.

Shinohara, H., Kazahaya, K., and Lowenstern, J.B., 1995, Volatile transport in a convecting magma column: Implications for porphyry Mo mineralization: Geology, v. 23, p. 1091-1094.

Sillitoe, R.H., 2010, Porphyry copper systems: Economic Geology, v. 105, p. 3-41.

Sillitoe, R.H. and Mortensen, J.D., 2010, Longevity of porphyry copper formation at Quellaveco, Peru: Economic Geology, v. 105, p. 1157-1162.

Sillitoe, R.H. and Perelló, J., 2005, Andean copper province: Tectonomagmatic settings, deposit types, metallogeny, exploration, and discovery: *in* Hedenquist, J.H., Thompson, J.F.H., Goldfarb, R.J., and Richards, J.P., eds., Economic Geology 100th Anniversary Volume, p. 251-298

Stavast, W.J.A., 2006, Three-dimensional evolution of magmatic hydrothermal systems, Schultze Granite and Ruby Star Granodiorite, Arizona: Unpublished Ph.D. dissertation, University of Arizona, 203 p.

Stern, T.W., Bateman, P. C., Morgan, B.A., Newell, M.F. and Peck, D.L., 1981, Isotopic U-Pb ages of zircon from the granitoids of the central Sierra Nevada, California: USGS Professional Paper No. 1185, 17 p.

Stearns, M.A., 2009, Anatomy and assembly of the McDoogle pluton near Sawmill Lake, central Sierra Nevada, California: Unpublished MS thesis, University of Utah, 109 p.

Steinberger, I., Hinks, D., Dreisner, T., and Heinrich, C., 2013, Source plutons driving porphyry copper ore formation: Combining geomagnetic data, thermal constraints, and chemical mass balance to quantify the magma chamber beneath the Bingham Canyon deposit: Economic Geology, v. 108, p. 605-640.

Tikoff, B. and Teyssier, C., 1992, Crustal-scale, en echelon "P-shear" tensional bridges: A possible solution to the batholithic room problem: Geology, v. 20, p. 927-930.

Tikoff, B., de Saint Blanquat, M., and Teyssier, C., 1999, Translation and the resolution of the pluton space problem: Journal of Structural Geology, v. 21, p. 1109-1117.

Tobisch, O.T., Saleeby, J.B., Renne, P.R., McNulty, B.A., and Tong, W., 1995, Variations in deformation fields during development of a large volume magmatic arc, central Sierra Nevada, California: Geological Society of America Bulletin, v. 107, p. 148–166.

Toro , J.C., Ortúzar, J., Zamorano, J., Cuadra, P,. Hermosilla, J., and Spröhnle, C,. 2012, Protracted magmatic-hydrothermal history of the Rio Blanco-Los Bronces district, central Chile: Development of world's greatest known concentration of copper: *in* Hedenquist, J.W., Harris, M., and Camus, F., eds, Geology and Genesis of Major Copper Deposits and Districts of the World: A Tribute to Richard H. Sillitoe: SEG Special Publication 16, p. 105-126.

Tosdal, R.M. and Richards, J.P., 2001, Magmatic and structural controls on the development of porphyry C±Mo±Au deposits: *in* SEG Reviews in Economic Geology, v. 14, p. 157-181.

Ulrich, T. and Heinrich, C.A., 2002, Geology and alteration geochemistry of the porphyry Cu-Au deposit at Bajo de la Alumbrera, Argentina: Economic Geology, v. 97, p. 1865-1888.

Valencia, V.A., Ruiz, Z., Barra, F., Geherls, G., Ducea, M., Titley, S.R., and Ochoa-Landin, L., 2005, U-Pb zircon and Re-Os molybdenite geochronology from La Caridad porphyry copper deposit: Insights for the duration of magmatism and mineralization in the Nacozari district, Sonora, Mexico: Mineralium Deposita, v. 40, 175-191.

Vigneresse, J.L., 2004, A new paradigm for granite generation: Transactions of the Royal Society of Edinburgh: Earth Sciences, v. 95, p. 11-22.

von Quadt, A., Erni, M., Martinek, K., Peytcheva, I., and Heinrich, C., 2011, Zircon crystallization and the life times of magmatic-hydrothermal ore systems: Geology, v. 39, p. 731-734.

Vry, V.H., Wilkinson, J.J., Seguel, J., and Millán, J., 2010, Multistage intrusion, brecciation, and veining at El Teniente, Chile: Evolution of a nested porphyry system: Economic Geology, v. 105, p. 119-153.

Waite, G.P. and Moran, S.C., 2009, V_p structure of Mount St. Helens, Washington, USA, imaged with local earthquake tomography: Journal of Volcanology and Geothermal Research, v. 182, p. 113-122.

Waite, K.A., Keith, J.D., Christiansen, E.H., Whitney, J.A., Hattori, K., Tingey, D.G., and Hook, C.J., 1997, Petrogenesis of the volcanic and intrusive rocks associated with the

Bingham Canyon Porphyry Cu-Au-Mo deposit, Utah: SEG Guidebook Series, v. 29, Geology and Ore Deposits of the Oquirrh and Wasatch Mountains, Utah, p. 69-90.

Walker, B.A., Miller, C.F., Claiborne, L.L., Wooden, J.L., and Miller, J., 2007, Geology and geochemistry of the Spirit Mountain batholith, southern Nevada: Implications for timescales and physical processes of batholith construction: Journal of Volcanology and Geothermal Research, v. 167, p. 239-262.

Wallace, S.R., Muncaster, N.K., Jonson, D.C., Mackenzie, W.B., Bookstrom, A.A., and Surface, V.E., 1968, Multiple intrusion and mineralization at Climax, Colorado: *in* Ore Deposits of the United States, 1933-1967: The Graton-Sales Volume, Ridge, J.D., ed., p. 605-640.

White, W.H., Bookstrom, A.A., Kamilli, R.J., Ganster, M.W., Smith, R.P., Ranta, D.E., and Steininger, R.C., 1981, Character and origin of Climax type molybdenum deposits: Economic Geology 75th Anniversary Volume, p. 270–316.

Wiebe, R., 2000, Pluton construction by sequential deposition from a multiply replenished chamber: Geological Society of America Abstracts with Programs, 2000, v. 32, p. 171.

CHAPTER 3

TIMING OF THE PINE CREEK TUNGSTEN SKARN AND THE CAUSATIVE MORGAN CREEK PLUTON, CALIFORNIA: IMPLICATIONS FOR ORE GENESIS AND REGIONAL GEOLOGY

Reformatted and reprinted with permission from the Geological Society of Nevada.
Originally published as

Porter, J.P., Bartley, J., Petersen, E., and Barra, F., 2010, Timing of the Pine Creek tungsten skarn and the causative Morgan Creek pluton, California: Implications for ore genesis and regional geology: *in* Steininger, R. and Pennell, B. eds. Great Basin Evolution and Metallogeny, Geological Society of Nevada: 2010 Symposium Proceedings, May14-22, 2010, p. 397-417.

Abstract

Eleven new Re-Os molybdenite ages from six samples from the Pine Creek tungsten skarn near Bishop, California, and seven new laser ablation multicollector inductively coupled plasma mass spectrometry (LA MC-ICP-MS) U-Pb zircon ages from the adjacent Morgan Creek pluton, have been determined in order to examine the timing and duration of the magmatic-hydrothermal system. The Re-Os analyses show ages of 91.0, ~94, 104.6, and 107.2 Ma, over an apparent 16 M.y. period of mineralization. Ages for three of the six samples are identical within error (±0.5 Ma) at ~94 Ma. Ages of 91.0 and ~94 Ma likely represent distinct mineralizing events, whereas the oldest two ages (104.6 and 107.2 Ma) from disseminated molybdenite in the skarn may indicate disturbance of the Re-Os system. Two of the three ages in the main 94 Ma group were from quartz pods or veins that could have sheltered the molybdenite from late fluid flow that might have disturbed the Re-Os isotopic system in the disseminated molybdenite.

The main group of molybdenite ages (~94 Ma) matches well with the dominant population of U-Pb zircon ages from the Morgan Creek pluton. The U-Pb data show two dominant populations at ~96-98 and ~94 Ma. The broad peak of ages from ~96-98 Ma probably represents inherited zircons from mafic rocks on the pluton's western contact. Crystallization of the Morgan Creek quartz monzonite likely started around 94 Ma, represented by the large zircon population, and ceased after a pulse of intrusive activity at about 91 Ma. The young zircon population also overlaps with the youngest Re-Os molybdenite age, further supporting igneous and hydrothermal activity spanning ~3 M.y. A small population of zircons in five of the seven samples yields ages between 100 and 110 Ma that resemble the older molybdenite ages. The match between anomalously old

Re-Os ages and U-Pb zircon age populations raises the possibility of older mineralizing magmatism (at depth?) in the Pine Creek system.

The combined Re-Os and U-Pb geochronology leads to two main findings. 1) The main pulse of mineralization to form the Pine Creek tungsten deposit occurred at ~94 Ma, with a later pulse at ~91 Ma. It is possible, though very unlikely, that mineralization began as much as 13 M.y. earlier. 2) The ~94 Ma U-Pb age of the plutonic rocks clearly demonstrates that the Morgan Creek pluton is not an isolated outlier of the Lake Edison Granodiorite, as previously inferred. The age places the Morgan Creek pluton among several early (95-93 Ma) components of the John Muir intrusive suite that generally are small (2-3 km width) concordant dike-like bodies that range in composition from diorite to leucogranite.

Introduction

Timing and duration are key to understanding igneous and hydrothermal processes. Advances in geochronology have reduced costs and improved precision and speed of geochronologic analyses. When multiple dating techniques are used, a more complete history of magmatic and hydrothermal systems can be deciphered. The use of more precise and more rapid techniques has led to larger datasets being used to unravel complex magmatic and magmatic-hydrothermal histories (e.g., Coleman et al., 2004; Maksaev et al., 2004).

Using larger datasets, large plutonic suites in the Sierra Nevada, as well as some individual plutons within these suites, have been shown to have more protracted histories than previously thought (Coleman et al., 2004; Gaschnig, 2005; Gracely, 2007; Miller et al., 2007). Likewise, detailed geochronology of ore deposits has shown many magmatic-

hydrothermal ore systems were constructed by superimposing magmatic-hydrothermal events over millions of years, and that the system may not return to ambient temperatures for hundreds of thousands to millions of years after the end of mineralization (e.g., El Teniente and Bajo de la Alumbrera; Maksaev et al., 2004; Harris et. al., 2008). Geochronology has also been crucial in refining plutonic relationships in the eastern Sierra Nevada. Early mapping relied solely on textural and compositional similarities to group rocks in plutonic suites (e.g., Bateman et al., 1965). Geochronology has since resolved a more complex magmatic history in the Sierran arc (e.g., Stern et al., 1981; Coleman et al., 2004; Gracely, 2007).

This work focuses on the timing and duration of the Pine Creek tungsten skarn and its causative intrusion, the Morgan Creek quartz monzonite. Re-Os molybdenite and LA MC-ICP-MS U-Pb zircon dates were obtained from multiple samples of the skarn and intrusion, respectively. The new dates are used to assess timing and duration of the combined magmatic-hydrothermal system. The possibility of protracted magmatism is assessed to the extent the data allow, and the system is placed in context within the surrounding John Muir Intrusive Suite.

Geologic setting

Regional setting

The Morgan Creek pluton is a relatively small (approximately 1.5 by 8 km) pluton on the eastern edge of the John Muir Intrusive Suite (Fig. 3.1). The John Muir Intrusive Suite comprises eight separate plutons that are temporally and compositionally related (Bateman, 1992; Gracely, 2007). The intrusive suite was emplaced as part of the Sierra Crest magmatic event that was responsible for over 4000 km^2 of exposed plutonic rocks

throughout the Sierra Nevada (Coleman and Glazner, 1997). Much of the magma that was intruded during the Sierra Crest magmatic event formed large plutonic suites that are restricted in age and generally trend compositionally from mafic to felsic (Bateman, 1992; Coleman and Glazner, 1997).

The John Muir Intrusive Suite was emplaced concurrently with the Tuolumne Intrusive Suite to the north; the two plutonic suites share many common characteristics (Bateman, 1992; Coleman and Glazner, 1997; Coleman et al., 2004). Emplacement of the John Muir Intrusive Suite overlaps the start of emplacement of the Whitney Intrusive Suite to the south (Hirt, 2007).

Rocks of the John Muir Intrusive Suite range widely in composition. Silica contents vary from below 50% in mafic rocks at the center of the Lamarck Granodiorite (Frost and Mahood, 1987) to greater than 75% SiO_2 in the siliceous facies of the Morgan Creek pluton (Cray, 1981; Bateman et al., 1984; J. Porter, unpublished data). Most of the rocks in the suite are intermediate to felsic in composition. Granodiorite and granite are the dominant modal compositions (Bateman, 1992). Most of the plutons that comprise the intrusive suite show mineralogical zoning and internal contacts (e.g., Bateman et al., 1965; Cray, 1981; Bateman, 1992; McNulty et al., 2000; Hathaway, 2002; Mahan et al., 2003; Gaschnig, 2005; Gracely, 2007).

Bateman (1992) included the Morgan Creek quartz monzonite in the John Muir Intrusive Suite. He interpreted the igneous mass to be an isolated part of the Lake Edison Granodiorite, cut off from the main body by the Mono Creek Granite.

Local geology

Intrusive wall rocks

The Morgan Creek quartz monzonite is bounded on the north and south by the Round Valley Peak Granite and Mono Creek Granite, respectively (Fig. 3.1; Cray, 1981; Bateman,1992). Both are younger intrusions of the John Muir Suite. Much of the western contact is against the Jurassic Chickenfoot Lake Granodiorite (172 ± 8 Ma; Rb/Sr analysis by R.W. Kistler, cited in Bateman, 1992).

Four mafic intrusions are also in contact with the Morgan Creek pluton. The plutons are identified as quartz diorite, although compositions range from mafic granodiorite to hornblende gabbro (Newberry, 1982). Previous geochronology defines two distinct periods of mafic intrusion in the mafic bodies bordering the Morgan Creek pluton. The quartz diorite exposed inside the Pine Creek Mine on the eastern edge of the pluton has been dated at ~168 Ma (Stern et al., 1981).

The mafic intrusions on the west side of the Morgan Creek quartz monzonite are both Cretaceous. U-Pb dating of the northwestern mafic body yielded a Cretaceous U-Pb zircon age of 95.3 ± 1.1 Ma (Gaschnig et al., 2006). The southwestern mafic body had been correlated with the eastern quartz diorite intrusion (Cray, 1981), but U-Pb dating suggests that this intrusion was emplaced at 97.5 ± 1.0 Ma, more or less concurrently with the northwestern mafic body (Frost and Mattinson, 1988). The northwestern body has not been dated.

Metasediments of the Pine Creek septum

The eastern edge of the pluton is in contact with the Pine Creek septum. The rocks of the septum are folded into a tight syncline and exposed rocks dip almost vertically

(Fig. 3.1). The septum is dominated by micaceous quartzite and biotite hornfels, with some Triassic volcaniclastic rocks present at the southern end. Approximately 300 m of limestone near the base of the sedimentary succession is exposed on the western limb of the syncline, where it is in contact with the Morgan Creek pluton for much of its strike length. Skarn mineralization in the Pine Creek deposit is hosted in these limestones.

The ages of rocks in the Pine Creek septum are poorly known because of the dominance of siliciclastic rocks and the metamorphism of the limestones. Similarities between rocks of the Pine Creek septum and those of the Mount Morrison roof pendant, some 15 km to the north-northwest, led Bateman (1992) to interpret them as part of the same sedimentary package. Thus, the rocks of the Pine Creek septum have been assigned a Pennsylvanian to Permian age based on fossils from the Mount Morrison roof pendant (Bateman, 1992).

Skarn mineralization of the Pine Creek deposit

Detailed descriptions of mineralization in the Pine Creek deposit have been given by Bateman (1945), Gray et al. (1968), and Newberry (1982). The salient features are outlined below and are shown schematically in Figure 3.2. Skarn terminology used follows Newberry (1982).

The metacarbonate rocks are described below from the least altered marble to skarn closest to the Morgan Creek quartz monzonite (inner zone; Newberry, 1982). The marble comprises fairly uniform 3-4 mm calcite crystals with small anhedral diopside (Gray et al., 1968; Newberry, 1982). Vesuvianite needles mark the beginning of the outer zone of the skarn. Wollastonite, scheelite and pyroxene are also present in the thin (0.01 – 0.5 m) outer zone.

Garnet increases toward the intrusion and is reported to have replaced vesuvianite (Newberry, 1982). The main zone (normal tactite of Gray et al., 1968) is the thickest of the skarn zones (0.01-10 m) and hosts the majority of the scheelite mineralization. It is defined as the zone where > 75% of the vesuvianite is replaced by garnet. The main zone skarn consists of grandite garnet, pyroxene, and scheelite. Minor calcite, vesuvianite, epidote, titanite, quartz and Cu-sulfides are present throughout the main zone skarn.

Approaching the intrusion, scheelite disappears and pyroxene is less abundant, marking the transition from the main zone to the inner zone. Garnet and quartz are more abundant in the inner zone, and epidote is locally present. Although tungsten mineralization drops off in the inner zone, it shows generally higher Mo grades. Pods of quartz-epidote skarn are locally present (Brown et al., 1985).

Skarn mineralization is found over more than 1 km vertically but is limited in lateral extent. The skarn is generally less than 25 m wide. Skarn mineralization blossoms up to 45 m at the present day surface (Bateman et al., 1965). Width decreases at depth in the system (see Newberry 1982). Skarn mineralization is widest where overhangs in the wall rock acted as structural traps for upwelling fluids (Gray et al., 1968).

The Morgan Creek quartz monzonite

The Morgan Creek quartz monzonite is the causative intrusion for the Pine Creek skarn. The pluton is in contact with the mineralized skarn and underground exposure shows local mineralization of the intrusive rocks (Newberry, 1982). The Pine Creek tungsten deposit has been well studied (Bateman, 1953; Gray et al., 1968; Newberry, 1982; Brown et al., 1985) but, with the exception of one dissertation on the intrusion (Cray, 1981), little work has focused on the Morgan Creek quartz monzonite. Cray

identified three mappable units within the pluton: a coarse-grained facies comprising the majority of the intrusion, two petrographically equivalent fine-grained facies and a siliceous facies.

The coarse- and fine-grained phases comprise what Cray (1981) termed the main facies of the Morgan Creek quartz monzonite because they are mineralogically similar. Modally, rocks of the main facies are granodiorite to granite (Cray, 1981; J. Porter, unpublished data). Plagioclase is generally more abundant than alkali feldspar in the main facies. Plagioclase and alkali feldspar grains are generally similar in size, 2-4 mm in the more abundant coarse-grained phase and 1-2 mm in the fine-grained facies. Rocks of the main facies are generally equigranular to seriate. Alkali feldspar phenocrysts are locally present and reach lengths up to 1 cm.

Biotite is the most abundant mafic mineral in the pluton at 4 to 8 modal % (Cray, 1981). Hornblende is present through most of the intrusion in biotite-hornblende clots up to 6 mm across in the coarse-grained phase; most mafic clots in the coarse- and fine-grained facies are 2-4 mm. There are local, continuous zones where hornblende is rare to absent and mafic clots less abundant. Hornblende-rich mafic enclaves are present but uncommon throughout the intrusion. Enclaves are much more common in the areas with clots of hornblende. Magnetite, titanite, apatite and zircon are accessory minerals present throughout the Morgan Creek pluton (Cray, 1981; J. Porter, unpublished data). Allanite has also been reported as a rare accessory mineral (Cray, 1981).

The siliceous facies crops out in the northern part of the pluton, in sharp contact with surrounding main-facies rocks. Although sharp internal contacts have been observed within other parts of the Morgan Creek quartz monzonite (Newberry, 1982; J. Porter,

unpublished data), they are rare and were not found between the coarse- and fine-grained facies of the pluton, nor were sharp contacts found between the hornblende-bearing clotted rocks and biotite-only zones. The mineralogy of the siliceous facies broadly resembles that of the main facies, but biotite is less abundant (~2-3%) and hornblende is very rare (Cray, 1981).

Previous geochronology

Previous geochronology for the Morgan Creek quartz monzonite and surrounding rocks is summarized in Table 3.1. The rocks of the John Muir Intrusive Suite are fairly well dated, by isotope-dilution thermal-ionization mass spectrometry (ID-TIMS) of zircons using the U-Pb system (Table 3.1). Intrusive rocks in the suite range in age from 95 to 87 Ma. The oldest body in the suite as defined by Gracely (2007) is the Inconsolable Quartz Monzonite at 95.4 ± 0.3 Ma. A date from the Mono Creek Granite of 87.0 ± 0.1 Ma (Table 3.1; Gaschnig, 2005) indicates that the suite continued to grow for at least 8 M.y.

Within the John Muir Intrusive Suite, U-Pb zircon data from the large, composite Lamarck Granodiorite suggests a multimillion year emplacement. Gracely (2007) reported ages ranging from 94.2 to 91.9 Ma. The McDoogle pluton in the southern John Muir Intrusive Suite is similar in size and geometry to the Morgan Creek quartz monzonite. Field evidence favors incremental emplacement by diking (Mahan et al., 2003; Stearms et al., 2007), and high-precision geochronology suggests the emplacement occurred rapidly around 95 Ma (Table 3.1; Stearns et al., 2008). The Mount Givens Granodiorite is sometimes included as the westernmost member of the John Muir Intrusive Suite (e.g., Bateman, 1992). Limited geochronology for the Mount Givens

Granodiorite is consistent with protracted emplacement between 87.9 and 92.8 Ma (Stern et al., 1981; Tobisch et al., 1993).

The age of the Morgan Creek quartz monzonite is not as well-defined as those of other units of the John Muir Intrusive Suite. Stern et al. (1981) reported one slightly discordant TIMS U-Pb age of 93.2 ± 1.8 Ma from the Morgan Creek quartz monzonite collected from the 1500 level of the Pine Creek Mine. Gaschnig (personal communication, 2007) analyzed zircons from a sample taken from the northwest portion of the pluton. Although analytical problems did not allow for precise dating of the intrusion, his results were consistent with the published date of Stern et al. (1981).

Limited Ar-Ar dating of the Pine Creek skarn and nearby plutonic rocks show the Pine Creek deposit to be the apparent center of a large thermal anomaly that persisted after the cessation of the majority of magmatism in the immediate area (Newberry and Layer, 1998). Ages within the thermal anomaly range from 73-80 Ma, whereas ages outside the anomaly are more consistent with U-Pb zircon crystallization ages of most plutons in the John Muir Intrusive Suite (85-95 Ma; Newberry and Layer, 1998).

Methods

U-Pb geochronology

Approximately 2-5 kg of each sample were collected (see Fig. 3.1 for locations), crushed, and zircons were separated using heavy liquids and magnetic susceptibility. Zircons were mounted in epoxy and polished. Scanning electron microscope-cathode luminescence (SEM-CL) images were obtained to determine crystal zoning.

U-Pb geochronology of single zircons was conducted by laser ablation multicollector inductively coupled plasma mass spectrometry (LA MC-ICP-MS) at the

University of Arizona LaserChron Center. Analytical procedures followed those outlined in Gehrels et al. (2008). A 35 μm spot size was used for all analyses.

Most zircon grains were analyzed at the tip of the crystal to determine crystallization ages, but in some few cases analyses were also performed at the core of crystals to determine the presence of inheritance. Full analytical data for the concordant analyses are reported in the appendix.

Uncertainties shown in the data tables are at the 1σ level and include only measurement errors. The systematic error, which includes contributions from the standard calibration, age of the calibration standard, composition of common Pb, and U decay constants, is generally ~1-2% 2σ (V. Valencia, written communication, 2009).

Age distribution in the samples was evaluated using age probability plots constructed using the Isoplot program (Ludwig, 2008). These plots display the cumulative probability of ages in each sample, normalized to the number of analyses in the sample. The area under the curve is normalized, allowing comparison of distributions between samples with different numbers of analyses.

Re-Os geochronology

Four samples were collected from ore bodies within the Pine Creek mine. Two more samples from associated deposits were also collected and analyzed, one from the Adamson and one from the Brownstone mine. Although operations at the latter two mines were distinct from the main Pine Creek operation, all ore deposition was part of the same mineralizing system (Newberry et al., 1982).

Re-Os geochronology was performed as described by Barra et al. (2003, 2005). Molybdenite was drilled or scraped from hand samples, and approximately 50 to 100 mg of pure molybdenite was handpicked for each analysis. After Re and Os were purified and separated, isotopic ratios were determined by TIMS on a VG 54 mass spectrometer. A constant of $1.666 \times 10^{-11}\ a^{-1}$ was used for the decay of ^{187}Re (Smoliar et al., 1996). All errors are reported conservatively at ± 0.5%, which includes error from spike calibration, analytical errors, and uncertainty in the decay constant (0.31%). Replicate analyses for five of the six samples were performed.

Results

U-Pb geochronology

Results of U-Pb analyses are given in the appendix. All ages discussed below are $^{206}Pb/^{238}U$ ages. Ages that are more than 10% discordant were not used in the relative age probability plots and are not discussed below. Three hundred ten of the 450 analyses (69%) are less than 10% discordant and are included in the probability plots and discussions below. Disturbed or contaminated systems may be responsible for pulling isotopic ratios from concordia, but the data are inadequate to determine whether Pb loss or contamination of younger zircon tips with older ages from inherited cores occurred. The mean total error in all concordant analyses is 1.5%. Ages of individual analyses will not be discussed below because of the complicated age distribution observed in samples from the felsic Morgan Creek quartz monzonite. Rather than consider individual analytical ages, or imprecise mean weighted ages for the samples, this discussion will use the approximate ages of populations. We consider prominent peaks in the relative probability age plots as populations; all samples show multiple age populations.

Zircons from the Morgan Creek quartz monzonite range in age from 85.3 to 215 Ma (Fig 3.3, Appendix). The majority of concordant ages are middle Cretaceous, ranging from 85.3 to 112.9 Ma (Figs. 3.3 and 3.4). Inherited Jurassic and Triassic age cores from 12 analyses in 5 samples yield ages ranging from 155.7 to 215.0 Ma. The Cretaceous ages fall into three major populations: ~91 Ma, ~94 Ma, and 95-98 Ma, with 94 and 97 Ma the dominant populations among the entire data set (Fig. 3.4). A small, but distinct population at ~107 Ma is also present.

Samples 07-MC-009, and 07-MC-067 were collected from near the western contact of the Morgan Creek quartz monzonite in the coarse-grained facies (Fig. 3.1). Sample 07-MC-009 shows a very strong population at 93.5 Ma; the sample also shows smaller populations at ~98.5 and ~103.5 and 107 Ma. Sample 07-MC-067 shows a similar dominant peak at ~94 Ma; the distribution in this sample is somewhat more spread out than that of 07-MC-009. A broad population shows ages between ~96 and 96.5 Ma. Smaller peaks are also present at ~98 and ~100 Ma. There is also a ~91.5 Ma shoulder on the ~94 Ma peak.

The other sample from the coarse-grained facies, 07-MC-053, was collected closer to the eastern contact of the intrusion in one of the less-mafic portions of the coarse-grained facies (Fig. 3.1). The age distribution of this sample shows less spread than the others, but two prominent populations are discernable, both correlating with populations in other samples. The younger of the two populations yields an age of ~94 Ma, and the older, ~96 Ma. Two analyses produce an older peak at ~101 Ma (Fig. 3.5).

Samples 07-MC-017 and 07-MC-018 were collected north of the summit of Mount Morgan in the northern fine-grained facies (Fig. 3.1). Probability density plots of

both samples show a dominant peak at ~96 Ma. Sample 07-MC-017 shows a dominant peak at 95.8 and the dominant peak of 07-MC-018 is at ~96 Ma. Like samples from the coarse-grained facies, these northern fine-grained facies samples show populations at ~94 (07-MC-017) and ~94.5 Ma (07-MC-018). The two samples also show minor populations at ~91.5, and at ~100 Ma (Fig. 3.5).

The age distribution of 07-MC-058, representing rocks of the southern fine-grained facies, is much more complicated than that of the western samples. The dominant population in this sample is at ~98.5 Ma, but the age distribution also shows populations at ~90, ~93.5, and ~95.5 Ma. Older ages, as old as ~109 Ma are also present in this sample (Fig. 3.5).

Sample 07-MC-039 was collected from the siliceous facies. Zircon ages from this sample show a very dominant zircon population at ~96 Ma. A younger population at ~94 Ma is present, but is not as prominent as the older age. Some shoulders on the main peak suggest populations at ~92 and ~100 Ma, and some analyses with ages >100 Ma are present, though perhaps not prominent enough to qualify as a population (Fig. 3.5).

Re-Os geochronology

Results of the Re-Os analyses are shown in Table 3.2. Molybdenites from the Pine Creek skarn have low Re contents; all but one of the analyses show less than 100 ppm total Re. For a high-Mo deposit, low Re concentrations in molybdenite are not uncommon (e.g., Selby and Creaser, 2001; Stein et al., 2001; Raith and Stein, 2006). Common Os, monitored by analyzing for ^{192}Os, was detected in four of the six samples. In all but one sample, the total common Os is less than 10% of the measured ^{187}Os; the

sample with highest proportional common Os, 07-MC-029, also contains the lowest Re content.

Isotopic ages for Pine Creek molybdenites range from 90.9 Ma to 107.3 Ma. Replicate analyses were performed for all samples except 07-MC-020A; all replicate ages were identical, within error, to the age determined from the first analysis. For samples with replicate analyses, the age reported below is the mean age of both analyses.

Three of the six samples yield identical ages within error: sample 07-MC-045, which was collected from a quartz-rich pod in the outcrop of the Adamson-Panaminas claims between Wheeler Crest and Mount Morgan (94.0 ± 0.5 Ma); sample 07-MC-046, which was collected from a quartz vein near the D-Level of the Pine Creek orebody (94.3 ± 0.5 Ma); and sample 07-MC-020A from pyroxene-garnet skarn from C-level surface workings (94.6 ± 0.5 Ma).

Three other ages are represented by one sample each. Sample 07-MC-029, main zone skarn mined from the 90 block of the Pine Creek mine, was collected from the last train of ore mined from the Pine Creek deposit in 1990 (P. Belec, personal communication, 2007). The mean Re-Os model age for this sample is 91.0 ± 0.5 Ma.

Two other samples yield older ages than the three-sample Re-Os age cluster noted above. Sample 07-MC-047, from the pyroxene-garnet skarns at D-level near the quartz vein sampled in 07-MC-046, shows a mean age of 104.7 ± 0.5 Ma from two analyses. Sample 07-MC-005A, a pyroxene-quartz inner zone skarn, was collected near the portal of the Brownstone mine on the south side of Pine Creek canyon and yields a mean age from two analyses of 107.3 ± 0.5 Ma.

Discussion

Timing of the Morgan Creek quartz monzonite and Pine Creek tungsten skarn

Age and duration of the Morgan Creek quartz monzonite

The Morgan Creek quartz monzonite shows multiple zircon age populations. The two dominant age populations from all analyses occur at ~96-98 Ma and ~94 Ma. (Fig. 3.4). One of these two populations is dominant in every sample (Fig. 3.5).

The population at ~94 Ma is interpreted to represent the start of crystallization of the Morgan Creek quartz monzonite. The U-Pb age population overlaps with the cluster of three Re-Os ages from the Pine Creek skarn at 94.3 Ma. This age is well within error of the published U-Pb zircon age of the pluton (Stern et al., 1981).

The consistent age population at around 91 Ma may represent continued crystallization of the pluton, or a second pulse of magmatic activity approximately 3 M.y. after the start of crystallization. Alternatively, the younger age population could represent a Pb-loss event at around 91 Ma. Intrusion of the Lake Edison Granodiorite or the Mono Creek Granite, ~90 and ~89 Ma, respectively (Gaschnig, 2005; Gaschnig et al., 2006; J. Davis personal communication, 2009), may have led to Pb loss in the Morgan Creek zircons. However, because of the consistency of the ~91 Ma population across multiple samples, Pb loss is unlikely (V. Valencia, written communication, 2009); therefore, we interpret this age population as a second period of crystallization in the Morgan Creek.

Inherited zircons – crustal "provenance" of the Morgan Creek quartz monzonite

All age populations older than ~94 Ma are interpreted to be inherited from older intrusions. Cool, high-silica magmas like those that formed the Morgan Creek quartz monzonite (68-73 wt% SiO_2, J. Porter, unpublished data) are unable to dissolve inherited zircons from older intrusions (Miller et al., 2003). Inherited grains generally fall into one of three age ranges: 155.7-215, 100-112, and 95-98 Ma.

The younger Jurassic-aged zircons (155.7 and 180.1 Ma) were likely inherited from the Chickenfoot Lake Granodiorite and the unnamed mafic intrusions on the eastern contact of the Morgan Creek quartz monzonite. The age of the Chickenfoot Lake Granodiorite is poorly constrained (172 ± 8 Ma; analysis by R.W. Kistler, cited in Bateman, 1992) and is identical, within error, to U-Pb zircon data from the eastern mafic intrusion (~168 Ma; Stern et al., 1981). The older Jurassic to Late Triassic ages (186.7-215.0 Ma) were probably inherited from the Tungsten Hills Quartz Monzonite on the west side of the Pine Creek septum that has been dated at ~202 Ma (Stern et al., 1981).

Some of the ages in the 100-112.9 Ma range likely represent contamination of younger rims with inherited, probably Jurassic, cores. There are, however, two small populations in the 100-112.9 range that stand out. A small peak at ~103.5 and another at ~107.6 Ma each comprise a few analyses, and both peaks are made up of analyses from multiple samples. Both populations overlap with Re-Os ages, 104.7 and 107.3 ± 0.5 Ma, from the adjacent skarn mineralization. The nearest rocks that have been identified to have formed around this age are the ~100-110 Ma metavolcanics and shallow plutons in the Oak Creek pendant, ~50 km to the south-southwest (Saleeby et al., 1990). Although

no other dating has identified rocks of this age nearer to Pine Creek, the overlap of the U-Pb and Re-Os ages suggest that a previously unidentified period of magmatism and hydrothermal activity may have occurred before the earliest known activity in the John Muir Intrusive Suite.

The dominant inherited population in the Morgan Creek quartz monzonite ranges from ~96-98 Ma. The mafic plutons on the northwest, and southwest contacts of the Morgan Creek quartz monzonite are this age (Frost and Mattinson, 1989; Gaschnig et al., 2006). The deep plumbing system that fed the mafic plutons is interpreted to be the source of these zircons. All other Cretaceous-aged intrusions in the area are younger than these mafic bodies.

In the broad 96-98 Ma peak there are two populations, representing the two mafic intrusions on the western contact of the Morgan Creek pluton. The dominant population in the Morgan Creek zircon samples is influenced by the closer of the mafic intrusions. Samples 07-MC-017, 07-MC-018, and 07-MC-039, from the northern part of the pluton, show large populations around 96 Ma, nearer the 95 Ma age of the diorite of Rock Lake than the 97.5 Ma age of the diorite of Pine Lake. Likewise, samples 07-MC-009, 07-MC-058, and 07-MC-067 show prominent peaks in the mid to late 90 Ma range (Figs. 3.4 and 3.5).

Age and duration of mineralization at the Pine Creek tungsten skarn

All three age groups from the Re-Os data overlap with populations in the U-Pb data (Fig. 3.5 and 3.6). We interpret the cluster of Re-Os ages at 94.3 Ma to represent the main stage of mineralization at the Pine Creek tungsten skarn. This age overlaps the

dominant ~94 Ma zircon population we interpret to be main pulse of magmatism in the adjacent Morgan Creek quartz monzonite, discussed above. The 91.0 ± 0.5 Ma age from sample 07-MC-029 may represent a later pulse of mineralization or remobilization and reprecipitation of the ~94 Ma molybdenite event, caused by the later magmatic-hydrothermal pulse at ~91 Ma.

The 104.7 and 107.3 Ma ages from the samples collected at the D level surface workings of the Pine Creek mine and Brownstone portal, respectively, fall within the age of the small zircon age populations at ~104 and ~107 Ma (Figs. 3.5 and 3.6). As discussed above, no plutonic rocks of this age have been identified at this latitude in the eastern Sierra Nevada. The overlap of the two data sets represents either mineralization caused by a previously unidentified 100-110 Ma period of igneous activity or disturbed isotopic systematics.

If the overlapping ages do not represent a true early mineralizing event it is likely the 100-110 zircon ages arise from contamination of younger rims by Jurassic cores. Re loss or incorporation of Os would be needed to yield Re-Os ages older than the true formation age.

Preferential Re loss is unlikely. One reason the molybdenite Re-Os geochronometer is a robust system is that molybdenite is very resistant to supergene alteration (Stein et al., 2001). Disturbed Re-Os systematics have been reported (McCandless et al., 1993); however, because Re is more compatible in molybdenite, Os would be more likely than Re to be removed by secondary processes. Molybdenite from the samples that yield the older ages showed no evidence of supergene alteration, despite having been collected at the surface.

An older, "inherited" component of ^{187}Os may have contributed to the apparent anomalous ages. Triassic-aged tungsten mineralization is associated with the Tungsten Hills Quartz Monzonite, several kilometers to the east of study area (Bateman et al., 1965, 1992). Molybdenite incorporates essentially no common Os upon crystallization; therefore, in most cases all measured Os is radiogenic and produced from the decay of ^{187}Re. However, three of the six samples analyzed here show the presence of relatively significant amounts of common Os, which in one case (sample MC-029) is around 20-30% of the total Os (Table 3.2). If the source for the common Os was enriched in ^{187}Os, this could lead to premineralization Re-Os ages. Although this scenario is possible, it is unlikely. This is the first report of the presence of high amounts of common Os in molybdenite.

Although it is possible that the ages are merely apparent ages resulting from disturbed isotopic systems, the correlation of the ages from independent isotopic systems suggests that these ages represent actual events; it is unlikely that both isotopic systems would be disturbed in such a way that the apparent ages overlap. It is, therefore, permissible that igneous and mineralizing hydrothermal activity occurred as early as 107 Ma and continued, intermittently, until 91 Ma. The data presented here are insufficient to conclude that these overlapping ages represent real igneous and hydrothermal events, or whether they are the product of disturbed isotopic systematics. Further mineralogical and chemical studies are currently in progress to determine the nature and implications of the unusual molybdenites.

Protracted plutonism and mineralization in the Pine Creek system

Most recent studies reporting protracted plutonic emplacement histories, have focused on large intrusions and intrusive suites (e.g., Coleman et al., 2004; Miller et al., 2007). Small plutons like the Morgan Creek have not been subjected to the sampling that the larger plutons have. High-precision dating techniques have been applied to determine the emplacement history of the composite McDoogle pluton, similar in size to the Morgan Creek. The data show construction of the McDoogle pluton took place in less than 300 k.y. (Stearns, 2008). A similar timescale has been reported for the early phases of the Lamarck pluton (Gracely, 2007).

Detailed geochronology has been conducted on several magmatic-hydrothermal mineralizing systems. The outcrop extent of such systems is generally smaller than of large plutonic systems shown to have multimillion year histories, but larger intrusive bodies likely underlie most of them (e.g., Burnham, 1979; Dilles, 1987). Many magmatic-hydrothermal systems show geochronologic evidence for protracted histories of intrusive and associated hydrothermal activity.

Among the most comprehensive data sets are those for the giant Bajo de la Alumbrera porphyry Cu-Au system and El Teniente porphyry Cu-Mo system. The Bajo de la Alumbrera system shows igneous activity, including volcanic and intrusive rocks, that persisted over 3.5 M.y., and the hydrothermal system may have been active for >3 M.y. (Sasso, 1997; Halter et al., 2004; Harris et al., 2004, 2008). U-Pb dating of El Teniente shows igneous activity over 1.6 Ma, with a similar protracted mineralization shown by Re-Os dating of molybdenite (Maksaev et al., 2004). In the El Teniente system

Re-Os data show that, although mineralization occurred over almost 2 M.y., the bulk of the Mo was deposited in one large pulse of mineralization near the end of the life of the system (Cannell et al., 2005).

Deposit histories rarely span more than a few million years, but igneous and hydrothermal activity in mineral districts can remain active over a much longer period. The Cadia Cu-Au district in New South Wales, Australia, has a very protracted history for the large district that spans ~20 M.y. (Wilson et al., 2007). Although this timescale is similar to that of the spread in the Pine Creek Re-Os ages, mineralization in the Cadia district comprises several distinct deposits spread over tens of kilometers. By comparison, the Pine Creek is a single spatially restricted deposit, apparently formed over a similar period. Discounting the >100 Ma ages as products of a disturbed isotopic system would leave the Pine Creek deposit with a ~3 M.y. duration, in line with life-spans observed in other single deposits. A magmatic-hydrothermal history spanning ~16 M.y. at Pine Creek appears unlikely, in light of comparisons between deposit and district durations.

We interpret the geochronologic data from the Pine Creek tungsten skarn and Morgan Creek quartz monzonite to record two main pulses of igneous and hydrothermal activity at ~94 and ~91 Ma. The main pulse of magmatism and mineralization occurred near 94 Ma, and a smaller pulse occurred at 91 Ma. A more protracted history, up to ~16 M.y., is permissible based solely on the geochronology presented here, though more data are needed to determine whether the 104 and 107 Ma U-Pb populations and Re-Os ages represent separate events predating the main pulse, or if they represent some post-formation disturbance or premineralization inheritance in the U-Pb and Re-Os systems.

The Morgan Creek quartz monzonite as a distinct pluton in the John Muir Intrusive Suite

Bateman (1965, 1992) interpreted the Morgan Creek quartz monzonite to be part of the Lake Edison Granodiorite. The new U-Pb zircon data presented here show that the Morgan Creek quartz monzonite is one of the earliest plutons in the John Muir Intrusive Suite, and that emplacement of the pluton predated that of the Lake Edison Granodiorite by about 4 M.y. (Fig. 3.6; Stern et al., 1981; Gaschnig, 2006; J. Davis, Pers. Communication, 2009). The age of the Morgan Creek quartz monzonite matches more closely with the ages of the early components of the John Muir Intrusive Suite, including the Lamarck Granodiorite, the McDoogle pluton, and the Inconsolable pluton (Gracely, 2007; Stearns et al., 2009; J. Davis, Pers. Communication, 2009).

Conclusions

The combined Re-Os and U-Pb geochronology leads to two main findings. The first is that the crystallization of the Morgan Creek quartz monzonite and the main pulse of mineralization to form the Pine Creek tungsten deposit occurred at ~94 Ma. Formation of the pluton ceased around 91 Ma, although the data presented here are insufficient to determine whether magmatism was continuous or intermittent between 94 and 91 Ma. A second, apparently smaller pulse of Mo(-W) mineralization occurred near the end of magmatism at 91 Ma. Both U-Pb and Re-Os datasets suggest a possible, if unlikely, duration of magmatism and mineralization that spanned ~16 M.y. Formation of the magmatic-hydrothermal system over ~3 M.y. is consistent with reported timescales of other magmatic and magmatic-hydrothermal systems (e.g., Coleman et al., 2004;

Maksaev et al., 2004). This study suggests that even small plutons and their associated ore-forming systems can show protracted activity spanning millions of years.

The second key finding of this study is that the ~94 Ma U-Pb age of the plutonic rocks clearly demonstrates that the Morgan Creek pluton is not an isolated outlier of the Lake Edison Granodiorite, as previously inferred. In addition, the age of the Morgan Creek pluton places it among several early (95-93 Ma) components of the John Muir Intrusive Suite that generally are small (2 – 3 km width) concordant dike-like bodies that range in composition from diorite to leucogranite.

In the southern John Muir Intrusive Suite the Inconsolable pluton is similar in age and composition to the mafic intrusions on the western contact of the Morgan Creek pluton (Hathaway, 2002; Gracely, 2007). The McDoogle pluton on the southern extreme of the intrusive suite is more mafic than the Morgan Creek, but is of similar age, size and geometry (Mahan et al., 2003; Stearns and Bartley, 2008; Stearns et al., 2008). The leucocratic early rocks of the Lamarck Granodiorite also form tabular bodies and were coeval with the Morgan Creek pluton (Gracely, 2007). These early tabular intrusions are present along the entire strike length of the John Muir Intrusive Suite, and further study of their significance in the formation of large plutonic suites would be worthwhile.

Acknowledgements

Funding for field and analytical work was provided by a Hugh McKinstry grant from the Society of Economic Geologists and a student research grant from the Geological Society of America. Victor Valencia and the staff of the Arizona Laserchron Center provided analytical support. Doug Hayes and Pete Belek facilitated access to the Pine Creek mine property and provided insight into the history of the mine.

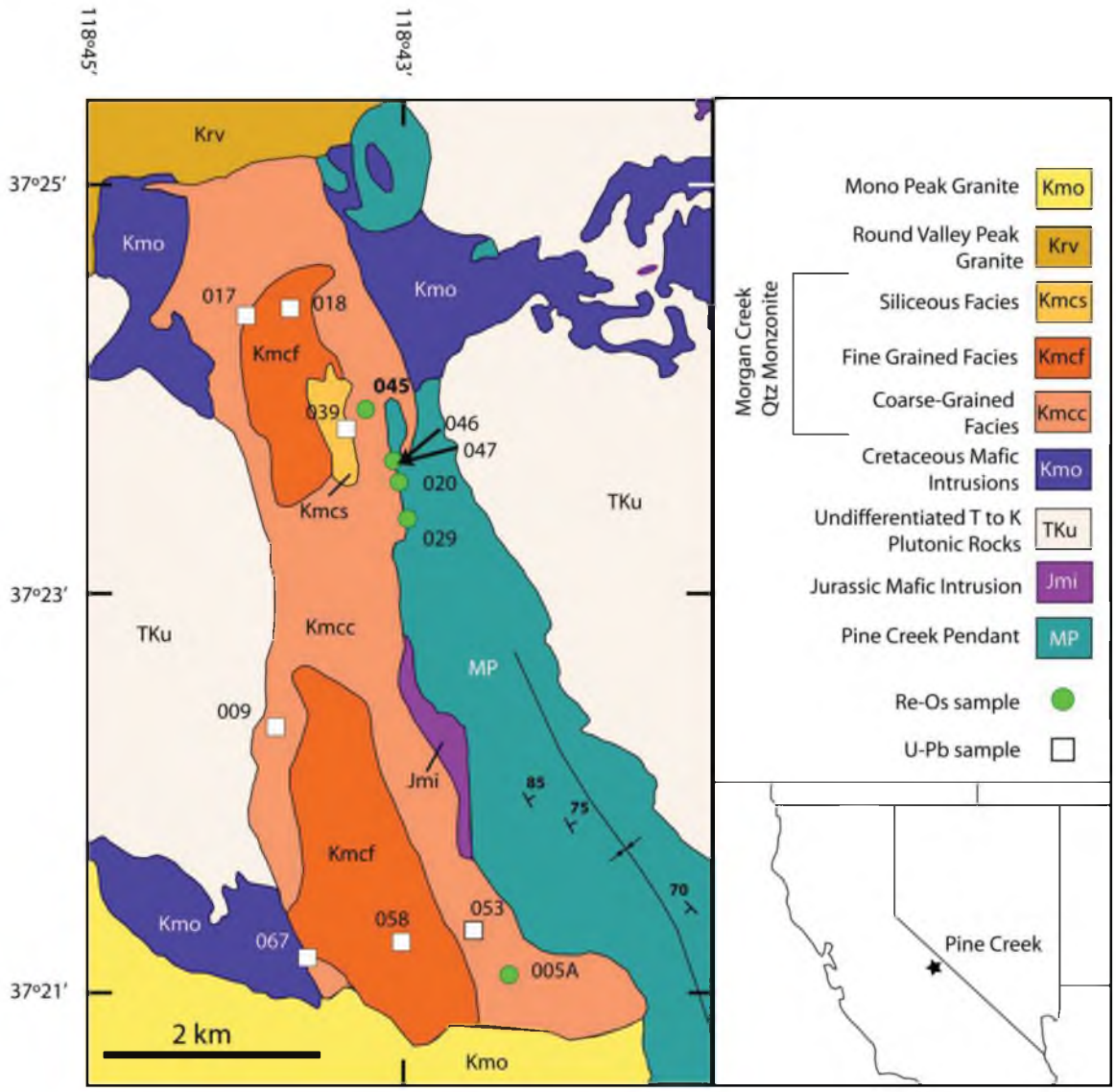

Figure 3.1. Simplified geologic map of the Morgan Creek pluton and surrounding area. The inset map shows the location of the Pine Creek district (after Bateman et al., 1965; Cray, 1981). U-Pb and Re-Os sample locations are also shown on the map.

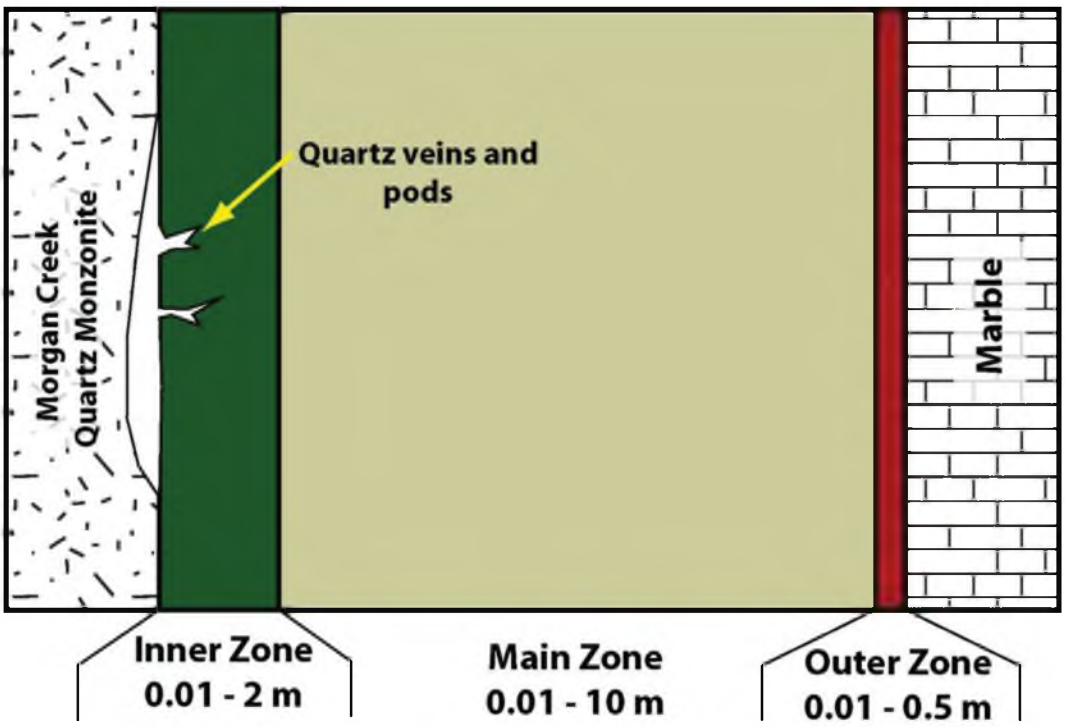

Figure 3.2. Schematic cross section of the mineralized Pine Creek skarn (after Newberry, 1982). Although most of the tungsten is located in the Main Zone skarns, Mo is hosted by the inner zone. Four of the six molybdenite samples were collected from pyroxene-garnet-skarns of the inner zone. One sample (07-MC-029) was collected from the Main Mone, and one (07-MC-046) was collected from a quartz-molybdenite vein near the quartz monzonite-skarn contact.

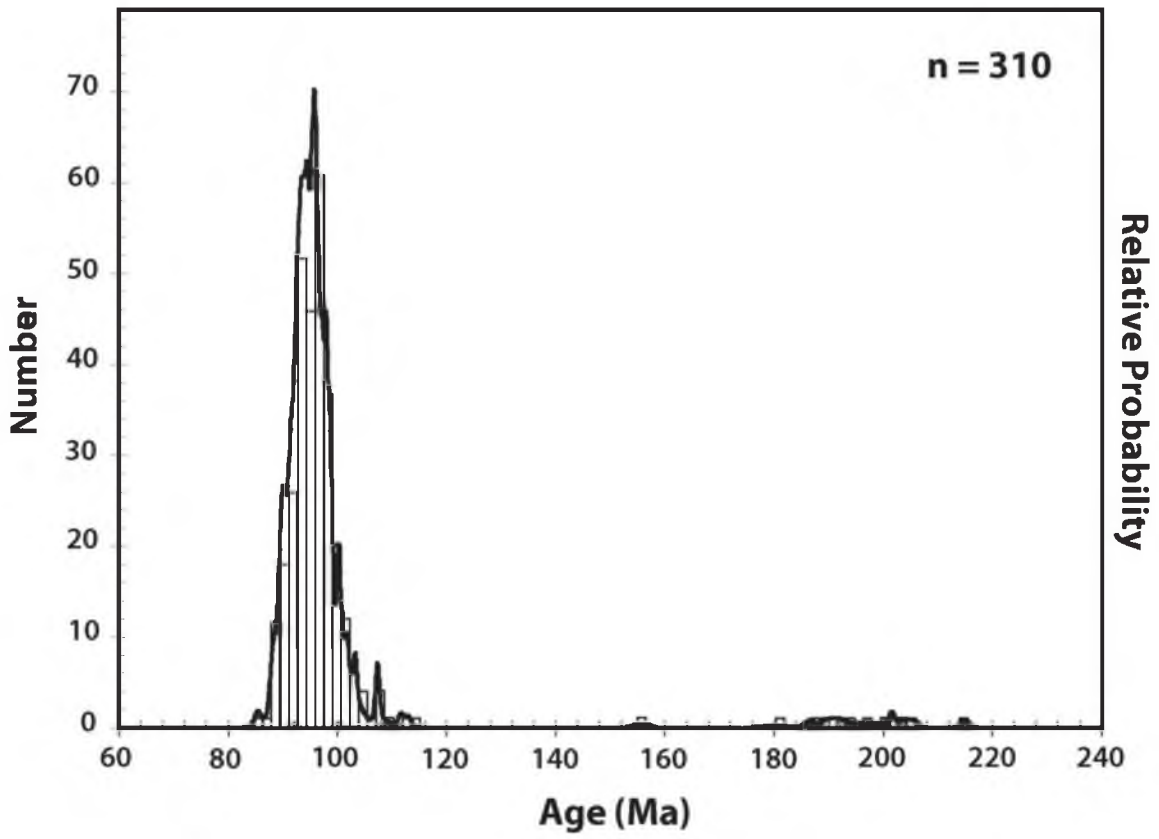

Figure 3.3. Histogram and relative probability plots for all Morgan Creek U-Pb samples, including inherited Jurassic/Cretaceous zircons.

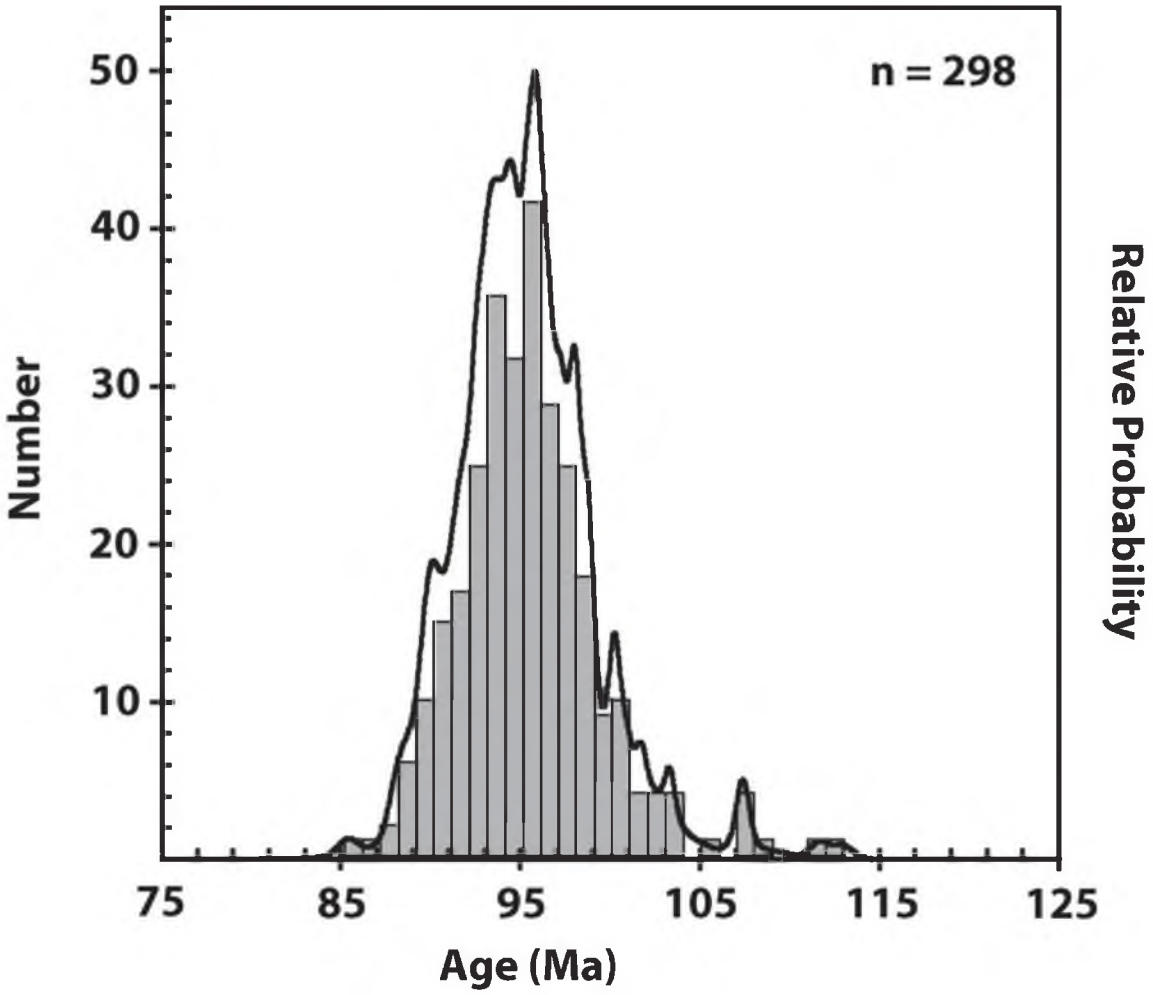

Figure 3.4. Histogram and relative probability plot for all Cretaceous Morgan Creek U-Pb analyses. The main population representing the beginning stages of crystallization is seen at ~94 Ma. The dominant population at ~96 ma represents inherited zircons from the mafic intrusions in contact with the Morgan Creek quartz monzonite. The ~91 Ma population found in some of the samples is present as a shoulder on the main peak.

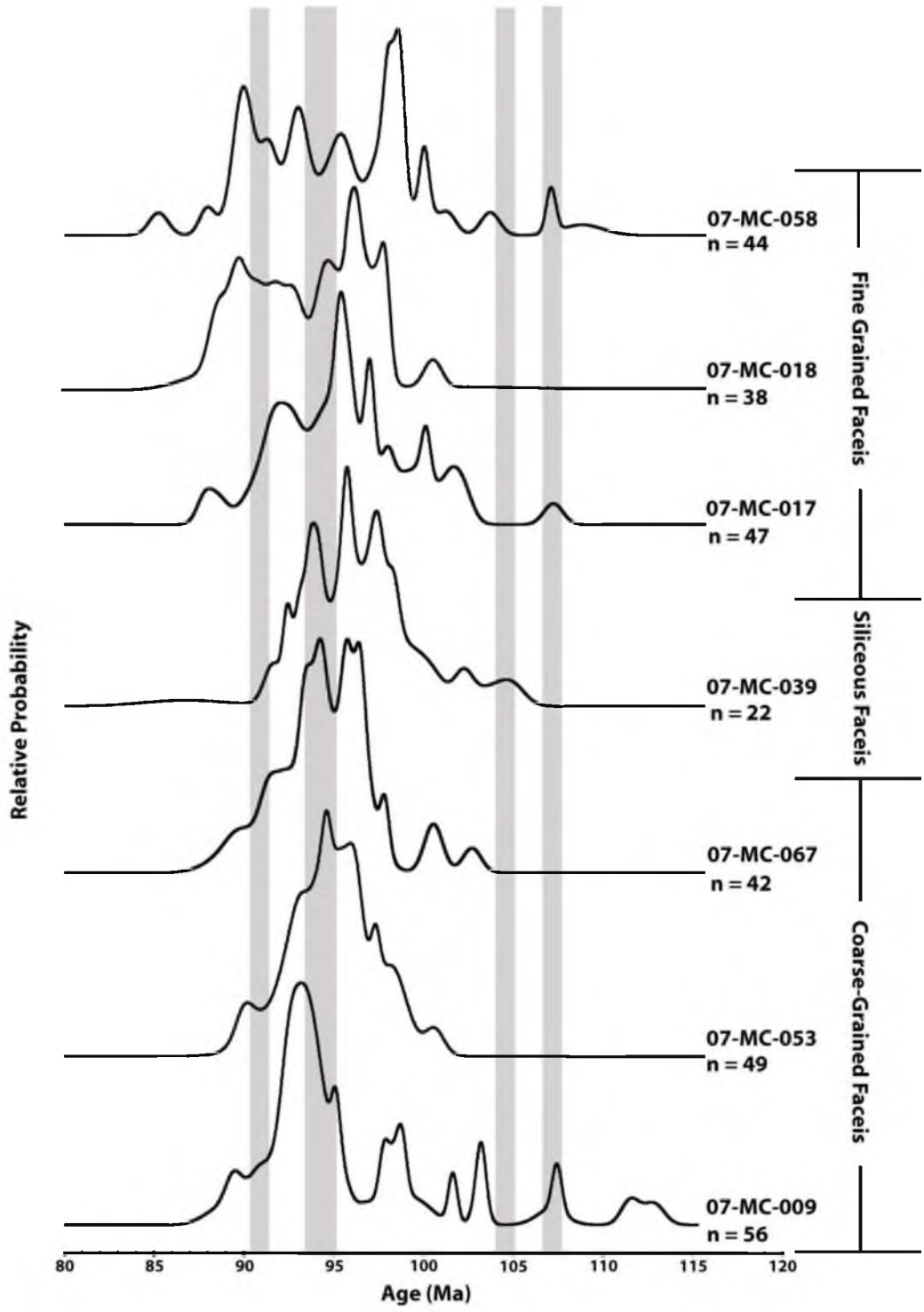

Figure 3.5. Relative probability plot of zircon analyses separated by sample. All age distributions are complicated, but all show populations that overlap with ranges of Re-Os ages, represented by the gray bars. Although U-Pb age populations do not overlap with Re-Os ages in every sample, all Re-Os ages are reflected in U-Pb zircon age populations.

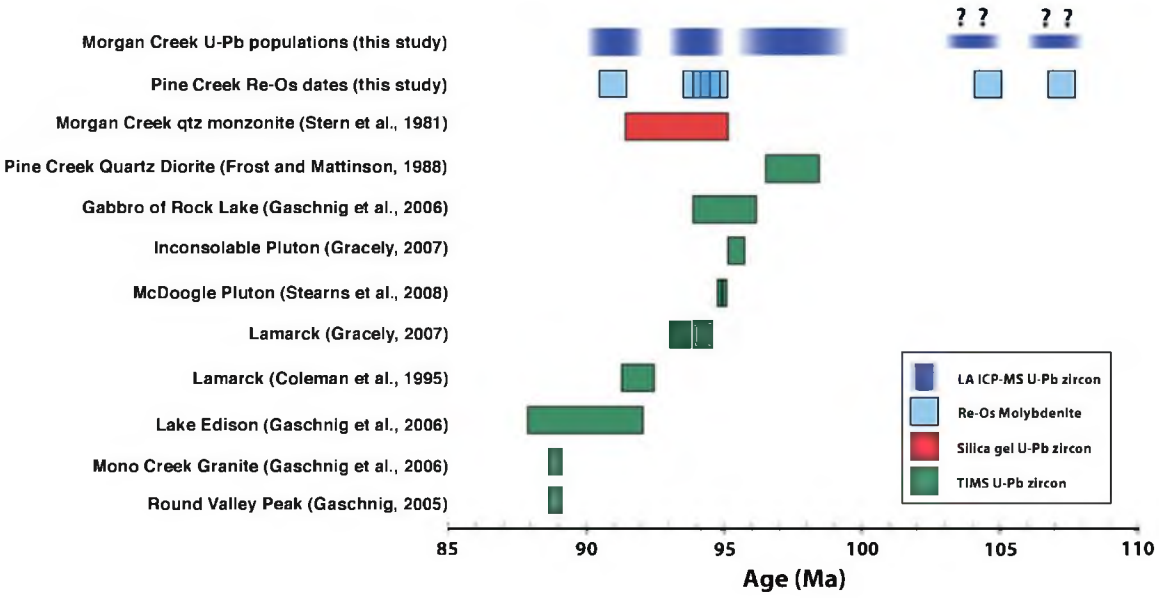

Figure 3.6. Age summary for the John Muir Intrusive Suite showing the relationship of the Morgan Creek-Pine Creek magmatic-hydrothermal system. Each box represents one reported isotopic age. The diffuse boundaries on the Morgan Creek U-Pb ages represent the uncertainty in the true age of the LA MC-ICP-MS zircon populations.

Table 3.1. Summary of U-Pb zircon ages of the John Muir Intrusive Suite

Unit	Age (Ma)	Reference
Pine Creek Quartz Diorite	97.5 ± 1.0	Frost and Mattinson, 1988
Inconsolable Quartz Monzonite	95.4 ± 0.3	Gracely, 2007
Rock Creek Gabbro	95.3 ± 1.1	Gaschnig et al., 2006
McDoogle Quartz Monzonite	94.8 ± 0.6, 95.0 ± 0.1	Mahan et al., 2003; Stearns et al., 2009
Morgan Creek quartz monzonite	93.2 ± 1.9	Stern et al., 1981
Lamarck Granodiorite		
klk4	94.2 ± 0.2	Gracely, 2007
klk1	94.1 ± 0.2	Gracely, 2007
klk3	93.8 ± 0.4	Gracely, 2007
klkm	93.8 ± 0.4	Gracely, 2007
klk	91.9 ± 0.6	Coleman et al., 1995
Lake Edison Granodiorite	90 ± 2.1	Gaschnig et al., 2006
Round Valley Peak Granodiorite	88.8 ± 0.2	Gaschnig, 2005
Mono Creek Granite	88.8 ± 0.2	Gaschnig et al., 2006

Table 3.2. Summary of Re-Os ages from the Pine Creek deposit

Sample No	Sample Location	Sample Wt. (mg)	Total Re (ppm)	^{187}Re (ppm)	^{187}Os (ppb)	Common Os (ppb)	Age	Error	Mean Age
MC-029-1	590 block - last ore car	47	4.60	2.88	4.37	1.26	91.0	0.5	91.0
MC-029-2	out of mine	48	5.31	3.32	5.04	3.59	90.9	0.5	
MC-005A-1	Adjacent to Brownstone	102	24.06	15.06	26.92	2.59	107.2	0.5	107.3
MC-005A-2	portal	77	31.95	20.00	35.78	2.11	107.3	0.5	
MC-045-1	Qtz-diopside skarn from	105	48.00	30.05	47.03	-	93.9	0.5	94.0
MC-045-2	Adamson portal	36	44.41	27.80	43.61	-	94.1	0.5	
MC-046-1	Qtz-moly vein from D-	51	45.04	28.19	44.18	-	94.0	0.5	94.3
MC-046-2	Level	104	53.09	33.23	52.43	-	94.6	0.5	
MC-047-1		102	72.31	45.27	79.18	4.27	104.9	0.5	104.7
MC-047-2	Skarn at D-Level	46	102.04	63.87	111.16	4.71	104.4	0.5	
C-Level	Skarn at C-Level open pit workings	69	21.43	13.41	21.16	0.59	94.6	0.5	94.6

References

Barra, F., Ruiz, J., Mathur, R. and Titley, S., 2003, A Re-Os study of sulfide minerals from the Bagdad porphyry Cu-Mo deposit, northern Arizona, USA: Mineralium Deposita, v. 38, p. 585-596.

Barra, F., Ruiz, J., Valencia, V., Ochoa-Landin, L., Chesley, J., and Zurcher, L., 2005, Laramide porphyry Cu-Mo mineralization in northern Mexico: Age constraints from Re-Os geochonology in molybdenite: Economic Geology, v. 100, p. 1605-161.

Bateman, P., 1953, Geology of the Tungstar and Hanging Valley tungsten skarns: USGS Open File Report 53-11, 10 p.

Bateman, P.C., 1992, Plutonism in the central part of the Sierra Nevada batholith, California: USGS Professional Paper No. 1483, 186 p.

Bateman, P.C., Pakiser, L.C., and Kane, M.F., 1965, Geology and Mineralization of the Bishop Tungsten District California: USGS Professional Paper No. 470, 208 p.

Bateman, P.C., Dodge, F. C. W. and Bruggman, P. E., 1984, Major oxide analyses, CIPW norms, modes, and bulk specific gravities of plutonic rocks from the Mariposa 1 x 2 degree sheet, central Sierra Nevada, California: Open File Report 84-162, 50 p.

Brown, P.E., Bowman, J.R., and Kelly, W.C., 1985, Petrologic and stable isotope constrains on the source and evolution of skarn-forming fluids at Pine Creek, California: Economic Geology, v. 80, p. 72-95.

Burnham, C.W., 1979, Magmas and hydrothermal fluids: *in* Barnes, H.L., ed., Geochemistry of Hydrothermal Ore Deposits, 2nd ed.: New York, John Wiley and Sons, p. 71–136.

Cannell, J., Cooke, D., Walshe, J., and Stein, H., 2005, Geology, mineralization, alteration, and structural evolution of El Teniente porphyry Cu-Mo deposit: Economic Geology, v. 100, p. 979-1004.

Coleman, D.S. and Glazner, A.F., 1997, The Sierra Crest magmatic even: Rapid formation of juvenile crust during the Late Cretaceous in California: International Geology Reviews, v. 39, p. 768-787.

Coleman, D.S., Gray, W. and Glazner, A.F., 2004, Rethinking the emplacement and evolution of zoned plutons: Geochronologic evidence for incremental assembly of the Tuolumne Intrusive Suite, California: Geology, v. 32, p., 433-436.

Cray, E.J., 1981, The geochemistry and petrology of the Morgan Creek pluton, Inyo County, California: Unpublished Ph.D. dissertation, University of California, Davis. 454 p.

Dilles, J., 1987, Petrology of the Yerington batholith, Nevada: Evidence for evolution of porphyry copper ore fluids: Economic Geology, v. 82, p. 1750-1789.

Frost, T.P. and Mahood, G.A., 1987, Field, chemical, and physical constraints on mafic-felsic magma interaction in the Lamarck Granodiorite, Sierra Nevada, California: Geological Society of America Bulletin, v. 99, p. 272-291.

Frost T.P. and Mattinson, J.M., 1988, Late Cretaceous U-Pb age of a mafic intrusion from the eastern Sierra Nevada, California: Isochron/West, v. 51, p. 15-18.

Gaschnig, R.M., 2005, Cause, timing, and significance of brittle deformation in Little Lakes Valley, eastern Sierra Nevada, California: Unpublished MS thesis, University of North Carolina at Chapel Hill, 85 p.

Gaschnig, R.M., Coleman, D.S. and Glazner, A.F., 2006, Twin of the Tuolumne: New geochronology from the Mono Pass Intrusive Suite: Abstracts with Programs - Geological Society of America, v. 38, p. 559.

Gracely, J.T., 2007, Rapid pluton emplacement via multiple discrete pulses, Lamarck Granodiorite, central Sierra Nevada Batholith, California: Unpublished MS thesis University of North Carolina at Chapel Hill, 82 p.

Gray, R.F., Victor, J.H., Bagan, R.J. and McKinley, H.L., 1968, Bishop tungsten district, California: *in* H. L. Ridge, J. D. (ed.) Ore Deposits of the United States, 1933-1967: The Graton-Sales Volume The American Institute of Mining, Metallurgical, and Petroleum Engineers, Inc., v. 2, p. 1531-1554.

Halter, W., Bain, N., Becker, K., Heinrich, C., Landtwing, M., VonQuadt, A., Clark, A., Sasso, A., Bissig, T., and Tosdal, R., 2004, From andesitic volcanism to the formation of a porphyry Cu-Au mineralizing magma chamber: The Farallon Negro volcanic complex, northwestern Argentina: Journal of Volcanology and Geothermal Research, v. 136, p. 1-30.

Harris, A., Dunlap, W., Reiners, P., Allen, C., Cooke, D., White, N., Campbell, I. and Golding, S., 2008, Multimillion year thermal history of a porphyry copper deposit: Application of U-Pb, $^{40}Ar/^{39}Ar$ and (U-Th)/He chronometers, Bajo de la Alumbrera copper-gold deposit, Argentina: Mineralium Deposita, v. 44, p. 1-20.

Hathaway, G. M., 2002, Geology of the Inconsolable Range, East-Central Sierra Nevada, Kings Canyon National Park and John Muir Wilderness, California: Magmatic Emplacement and the Dynamic Evolution of Composite Intrusions: PhD Dissertation, University of California, Los Angeles, 474 p.

Hirt, W., 2007, Petrology of the Mount Whitney Intrusive Suite eastern Sierra Nevada California: Implications for the emplacement and differentiation of composite felsic intrusions: Gelogical Society of America Bulletin, v. 119, p. 1185-1200.

Ludwig, K., 2003, User's Manual for Isoplot 3.6, A Geochronological Toolkit for Microsoft Excel: Berkeley Geochronology Center Special Publication, v. 4, 77 p.

Mahan, K.H, Bartley, J.M., Coleman, D.S., Glazner, A.F., and Carl, B.S., 2003, Sheeted intrusion of the synkinematic McDoogle pluton, Sierra Nevada, California: Geological Society of America Bulletin, v. 115, p. 1570-1582.

Maksaev, V., Munizaga, F., McWilliams, M., Fanninf, M., Mathur, R., Ruiz, J., and Zentilli, M., 2004, New chronology for El Teniente, Chilean Andes, from U-Pb, Ar/Ar, Re-Os and fission-track dating: Implications for the evolution of a supergiant porphyry Cu-Mo deposit: *in* Sillitoe, R., Perello, J. and Vidal, C. eds. Society of Economic Geologists Special Publication 11: Andean Metallogeny: New Discoveries, Concepts and Updated, p. 15-54.

McCandless, T.E., Ruiz, J., and Campbell, A.R., 1993, Re distribution in molybdenite from hypogene and supergene environments: Implications for Re-Os geochronometry: Geochimica et Cosmochimica Acta, v. 57, p. 889-905.

McNulty, B., Tobisch, O., Cruden, A. and Gilder, S., 2000, Multistage emplacement of the Mount Givens pluton, central Sierra Nevada batholith, California: Geological Society of America Bulletin, v. 112, p. 119-135

Miller, J.S., Matzel, J.E.P., Miller, C.F., Burgess, S.D., and Miller, R.B., 2007, Zircon growth and recycling during the assembly of large, composite arc plutons: Journal of Volcanology and Geothermal Research v. 167, p. 282 – 299.

Newberry, R., 1982, Tungsten-bearing skarns of the Sierra Nevada. I. The Pine Creek mine, California: Economic Geology, v. 77, p. 823-844.

Newberry, R.J., and Layer, P.W., 1998, The Pine Creek W-Mo-Cu-Bi-Au skarn, California: Multiple skarns associated with a thermal, chemical, and isotopic anomaly in the central Sierra Nevada: Geological Association of Canada/Mineralogical Association of Canada Joint Annual Meeting – Abstracts with Programs, v. 23, p. 87.

Raith, J. and Stein, H., 2006, Variscan ore formation and metamorphism at the Felbertal scheelite deposit (Austria): Constraining tungsten mineralisation from Re-Os dating of molybdenite: Contributions to Mineralogy and Petrology, v. 152, p. 505-521.

Saleeby, J.B., Kistler, R.W., Longiaru, S.J., Moore, J. G., Nokleberg, W.J., 1990, Middle Cretaceous silicic metavolcanic rocks in the Kings Canyon area, central Sierra Nevada, California, in Anderson, J. Lawford, ed., The nature & origin of Cordilleran magmatism: Geological Society of America Memoir, v. 174, p. 251-270.

Sasso, A.M., 1997, Geological evolution and metallogenetic relationships of the Farallón Negro Volcanic Complex, NW Argentina: Unpublished Ph.D. Dissertation, Kingston, Queens University, 842 p.

Selby, D. and Creaser, R., 2001, Re-Os geochronology and systematics in molybdenite from the Endako porphyry molybdenum deposit, British Columbia, Canada: Economic Geology, v. 96, p. 197-204.

Smoliar, M.I., Walker, R.J., and Morgan, J.W., 1996, Re-Os ages of group IIA, IIIA, IVA and IVB iron meteorites: Science, v. 271, p. 1099–1102.

Stearns, M. and Bartley, J.M., 2008, Assembly of the incrementally emplaced McDoogle pluton, central Sierra Nevada, CA: Geological Society of America - Abstracts with Programs, v. 40, p. 92.

Stearns, M., Bartley, J.M., and Coleman, D.S., 2008, Rapid emplacement of the McDoogle pluton into the Sawmill Lakes shear zone, Sierra Nevada, California: Geological Society of America – Abstracts with Programs, v. 40, p.188.

Stein, H., Markey, R., Morgan, J., Hannah, J. and Schersten, A, 2001, The remarkable Re-Os chronometer in molybdenite: How and why it works: Terra Nova, v. 13, p. 479-486.

Stern, T.W., Bateman, P. C., Morgan, B.A., Newell, M.F. and Peck, D.L., 1981, Isotopic U-Pb ages of zircon from the granitoids of the central Sierra Nevada, California: USGS Professional Paper No. 1185, 17 p.

Tobisch, O.T., Renne, P.R., and Saleeby, J. B.,1993, Deformation resulting from regional extension during pluton ascent and emplacement, central Sierra Nevada California: Journal of Structural Geology, v. 15, p. 609–628.

Valencia, V., Ruiz, J., Barra, F., Geherls, G., Ducea, M., Titley, S. and Ochoa-Landin, L., 2005, U-Pb zircon and Re-Os molybdenite geochronology from La Caridad porphyry copper deposit: Insights for the duration of magmatism and mineralization in the Nacozari district, Sonora, Mexico: Mineralium Deposita, v. 40, p. 175-191.

Wilson, A., Cooke, D., Stein, H., Fanning, C., Holliday, J., and Tedder, I., 2007, U-Pb and Re-Os geochronologic evidence for two alkalic porphyry ore-forming events in the Cadia district, new South Wales, Australia: Economic Geology, v. 102, p. 3-26.

CHAPTER 4

MAGMATIC EVOLUTION AND UPPER CRUSTAL SOURCE OF THE MORGAN CREEK PLUTON, AN EARLY MEMBER OF THE JOHN MUIR INTRUSIVE SUITE, SIERRA NEVADA BATHOLITH, CALIFORNIA

Abstract

The Morgan Creek pluton is a small, granitic (*sensu stricto)* pluton on the eastern edge of the Cretaceous John Muir Intrusive Suite. Two compositional domains are present in the pluton, the main and siliceous facies. The main facies comprises ~95 percent of the exposed pluton and can be further subdivided on the basis of texture and composition. The coarse-grained subfacies has an average crystal size of ~2 mm, twice the average crystal size of the weakly porphyritic fine-grained subfacies. All rocks in the pluton are classified as granites based on modal mineralogy and geochemistry. The main facies can be divided into three groups based on mafic mineral abundance and whole rock major and trace element geochemistry. Rocks with the highest total mafic mineral abundance, averaging 7.56 percent, are found exclusively in the coarse-grained rocks and rocks with the lowest mafic mineral content, 3.52 percent, are concentrated in the interior of the pluton in the fine-grained subfacies. A group of rocks with intermediate mafic

mineral abundance, 5.09 percent, is found in both the coarse- and fine-grained rocks. Titanite is common and ilmenite is absent in all but the most evolved rocks, suggesting open system behavior which lowered the fO_2 of the magma in the interior of the pluton. Magnetite is present in all unaltered Morgan Creek granite, and all rocks in the pluton are magnetite-series granites. However, magnetic susceptibility of rocks in the main facies is relatively low, with an average value for unaltered rocks of 8.42×10^{-3} SI units. A zone of near-zero magnetic susceptibility is present along the eastern margin of the pluton where it is in contact with metasedimentary rocks. Major element geochemistry is very similar to that of plutons in nearby intrusive suites. However, trace element geochemistry (Ba, Rb, Sr, Zr, and REE) suggests a distinct genesis from typical intrusive suite magmas. Trace element models using partition coefficients consistent with partial melting of upper crustal, K-feldspar and biotite-bearing rocks, suggest the magmas that formed the Morgan Creek pluton were derived from partial melting of upper crustal rocks. The Morgan Creek pluton was emplaced either as a single batch of magma, or through multiple rapid pulses that led to a single magma body. Fractional crystallization of a relatively homogenous volume of magma led to the chemical variations seen within the pluton. The textural and compositional variations in the Morgan Creek pluton share many similarities to lobes of the Tuolumne Intrusive Suite and of magmatic cycles described in the Half Dome Granodiorite within that suite. The compositional data support geochronological data to show that the Morgan Creek pluton is not a part of the Lake Edison Granodiorite, as was previously interpreted. Instead, the Morgan Creek pluton represents an early stage of the John Muir Intrusive Suite, possibly correlative with the

Basin Mountain pluton which is also commonly interpreted to be part of the Lake Edison Granodiorite.

Introduction

Large intrusive suites are a hallmark of the Sierra Nevada batholith. The suites typically comprise thousands of km^3 of intrusive rocks that are spatially, temporally, and genetically related (Bateman, 1992). Each intrusive suite is composed of multiple plutons, mappable, compositionally related units of rocks that are bounded by compositionally and/or texturally distinct rocks. Rocks in plutons have been emplaced over a restricted time scale; plutons are generally formed on the order of thousands to a few million years (Coleman et al., 2004; Davis et al., 2012).

Isotopic data show a mixed source for the magmas that make up the intrusive suites. Plutons in the western Sierra Nevada batholith have a more primitive isotopic signature than those to the east (Kistler and Peterman, 1973, Solomon and Taylor, 1989; Chen and Tilton, 1991). Within individual suites isotopic compositions commonly show a mixture of primitive and continental sources (Kistler et al., 1986; Lackey et al., 2012; Nelson et al., 2013). Within an individual suite, magma source can change over time; the well-studied Tuolumne Intrusive Suite was formed as a mixture of primitive and granitic melts, with the role of the primitive magma reduced in late stages of the suite (Kistler et al., 1986). Although isotopic compositions vary through space and time, major and trace element compositions of the suites tend to be similar along the length of the Sierra Nevada batholith (Bateman, 1992). Triassic and younger plutons in the western and northern Sierra Nevada have very similar bulk-chemical compositions to the Cretaceous

intrusive suites in the central Sierra Nevada batholith, despite having more isotopically primitive magma sources (Barth et al., 2011; Cecil, et al., 2012).

Three of the best-studied suites were emplaced in the Late Cretaceous period in the east-central Sierra Nevada: the Tuolumne, John Muir, and Whitney Intrusive Suites (Fig. 4.1; Bateman, 1992; Coleman and Glazner, 1998). Each of these suites was emplaced over several million years and generally became more silicic through time (Bateman, 1992; Coleman et al., 2004; Hirt, 2007; Davis et al., 2012). The John Muir Intrusive Suite is similar in many ways to the nearby Tuolumne and Whitney Intrusive Suites, located to the north, and south, respectively (Fig. 4.1). All three suites tend toward more silicic compositions through time, and the three intrusive suites were emplaced near the same time (Bateman, 1992; Coleman et al., 2004; Hirt, 2007; Davis et al., 2012). In contrast to its northern and southern cousins, the John Muir Intrusive Suite has an unusual early period of felsic magmatism, expressed in the Morgan Creek pluton and early leucocratic phases of the Lamarck Granodiorite (Hathaway, 2002; Davis et al., 2012).

The Morgan Creek pluton has been interpreted as an isolated subdivision of the nearby Lake Edison Granodiorite, separated from the main body of the pluton by the younger Mono Creek Granite (Bateman, 1992). Recent geochronological work suggests the pluton is older than the main body of the Lake Edison Granodiorite (Porter et al., 2011). The ages have low precision and show significant scatter but, combined with the age of adjacent skarn mineralization, are adequate to show that the Morgan Creek formed before the Lake Edison Granodiorite (Porter et al., 2011; Davis et al., 2012). This paper presents field, petrographic, and geochemical data to investigate the source and evolution

of the Morgan Creek pluton. Based on these new data, the place of the Morgan Creek pluton within the John Muir Intrusive Suite is reconsidered.

Geologic setting

The John Muir Intrusive Suite

The John Muir Intrusive Suite, as defined by Davis et al. (2012), is composed of seven units (Fig. 4.1, Table 4.1). They are, from oldest to youngest, the Inconsolable Quartz Monzodiorite, the McDoogle Quartz Monzodiorite, the Lamarck Granodiorite, the Lake Edison Granodiorite, the Round Valley Peak Granodiorite, and the Mono Creek Granite. This differs from the definition of Bateman (1992), in that it includes the Inconsolable Quartz Monzodiorite and the McDoogle Quartz Monzodiorite in the south, and excludes the Evolution Alaskite, now known to be of Jurassic age, and the Mount Givens Granodiorite which is separated from the other rocks of the John Muir Intrusive Suite by unrelated Jurassic and older intrusive and volcanic rocks. Herein the definition of the John Muir Intrusive Suite follows that of Davis et al. (2012), except that the Morgan Creek pluton, which was emplaced synchronously with the early stages of the Lamarck Granodiorite, is included as a separate unit.

All plutons of the John Muir Intrusive Suite are elongate to the NNW (Fig. 4.1). Compositionally, the rocks range from diorite to leucogranite. The younger intrusions are generally more felsic than the early rocks in the suite, typical of intrusive suites of the Sierra Nevada (Bateman, 1992). Rocks in the eastern portion of the suite were emplaced at pressures less than 0.2 GPa, based on metamorphic assemblages in the wall rocks of the Morgan Creek pluton (Brown et al., 1985). Pressure estimates from wall rocks in the

southern part of the John Muir Intrusive Suite yield comparable depth estimates (Sisson et al., 1996).

Plutons in the suite were emplaced between 95 and 87 Ma, roughly coincident with the well-studied Tuolumne Intrusive Suite, some 60 km to the north (Table 4.1; Coleman et al., 2004; Miller et al., 2007). The youngest magmatism in the John Muir Intrusive Suite is coincident with the early Whitney Intrusive Suite to the south (Hirt, 2007).

The earliest rocks of the Inconsolable Quartz Monzonite in the southern part of the John Muir Intrusive Suite are the most mafic of the suite. The bulk of the pluton consists of rocks ranging in composition from quartz diorite to granodiorite; however, small bodies of more mafic and more felsic rock are locally present (Hathaway, 2002). Crystallization of the Inconsolable Quartz Monzonite took place at 94.45 ± 0.32 Ma, and marked the start of intrusive activity in the John Muir Intrusive Suite (Davis et al., 2012).

The McDoogle pluton in the southern end of the suite ranges from quartz monzodiorite to granite (Mahan et al., 2003; Stearns, 2009). Ages of the McDoogle pluton range from 95.0 ± 0.13 Ma to ~94 Ma (Table 4.1; Mahan et al., 2003; Stearns, 2009; Davis et al., 2012).

The next youngest pluton in the suite, the Lamarck Granodiorite, is a large elongate pluton approximately 10 km by 60 km (Davis et al., 2012; Porter et al., 2011). Granodiorite is the dominant rock type, but granite is locally present. The rocks trend towards more mafic compositions northward (Bateman, 1965; Frost and Mahood, 1987). Weighted average ages of zircons from several samples of the Lamarck Granodiorite show a protracted history of emplacement between 94.26 ± 0.17 Ma and 90.9 ± 0.2 Ma

(Table 4.1; Coleman et al., 1995; Davis et al., 2012). The Morgan Creek pluton is approximately time-correlative with the older parts of the Lamarck Granodiorite.

The Round Valley Peak Granodiorite is younger than, but compositionally similar to the Lamarck (Bateman, 1992); both are compositionally similar to the Half Dome Granodiorite of the Tuolumne Intrusive Suite (Bateman, 1992). The pluton is dominantly composed of granodiorite (Bateman, 1992). The Round Valley Peak Granodiorite forms the northern contact of the Morgan Creek pluton and crystallized at 89.03 ± 0.18 Ma (Davis et al., 2012).

The Lake Edison Granodiorite crystallized shortly after the Round Valley Peak Granodiorite, at 88.76 ± 0.06 Ma (Table 4.1; Davis et al., 2012). It is more felsic than earlier stages of the John Muir Intrusive Suite and is zoned from more mafic rocks near the borders of the pluton to more felsic rocks in the core. Hornblende is present throughout most of the Lake Edison Granodiorite.

Bateman (1992) refers to the southeastern lobe of the Lake Edison Granodiorite as the Basin Mountain mass. Although the area is not well-studied, specific gravity and modal data suggest the rocks in the area are distinct from the main body of the Lake Edison Granodiorite, and some older works mapped the Basin Mountain mass and the Lake Edison pluton separately (Bateman, 1965; Cray, 1981). Herein, the older interpretation is followed, and the mass will be referred to as the Basin Mountain pluton (Fig. 4.1). The age of the Basin Mountain pluton, relative to the other plutons in the John Muir Intrusive Suite is unknown.

The Mono Creek Granite is the youngest member of the John Muir Intrusive Suite and forms the southern contact of the Morgan Creek pluton (Figs. 4.1, 4.2). The Mono

Creek Granite is mainly a megacrystic granite, but local granodiorite is also present (Bateman, 1992). A series of shallow-dipping aplite to pegmatite dikes extends north from the southern part of the Mono Creek pluton, near Pine Lake; these dikes are abundant in the southern portion of the Morgan Creek pluton (Fig. 4.2). Davis et al. (2012) reported a concordant weighted mean zircon date from a sample of 87.24 ± 0.15 Ma; a few concordant single zircon analyses are as young as 83.3 Ma, suggesting a possible 4 million year lifespan for the Mono Creek Granite.

Non-John Muir Intrusive Suite wall rocks

The Morgan Creek pluton is bounded to the east by the Pine Creek pendant (Fig. 4.2), a package of near-vertically dipping metasedimentary and metavolcanic rocks (Newberry, 1982; Stevens and Greene, 1999). Siliciclastic metasediments are the dominant rocks of the pendant. Quartzite and limestone beds are nearly vertical at the contact. Correlation with the Mount Morrison Pendant, approximately 20 km to the north, suggests the rocks are Pennsylvanian to Permian in age (Bateman, 1965; Stevens and Greene, 1999).

Carbonate rocks of the Pine Creek pendant that are in contact with the Morgan Creek pluton host the polymetallic Pine Creek skarn. The Pine Creek skarn system was the largest tungsten mine in the United States, with over 16 Mt of W-Mo(-Cu) ore extracted between 1927 and 1992 (Kurtak, 2004). Phase relationships in the Pine Creek skarn establish the maximum emplacement depth of the pluton at around 5 km (Brown et al., 1985). Rhenium-osmium dates of molybdenites confirm that skarn mineralization is coincident with the emplacement of the Morgan Creek pluton at approximately 94 Ma (Porter et al., 2011).

The granite of Chickenfoot Lake forms the western contact along most of the Morgan Creek pluton (Fig. 4.2). The granite of Chickenfoot Lake was formed during the Jurassic, based on an Rb/Sr date of 172 ± 8 Ma (Bateman, 1992). It is cut by a swarm of narrow mafic dikes, probably belonging to the Independence dike swarm.

Four mafic intrusions are in contact with the Morgan Creek pluton, at or near each of the four corners of the pluton (Fig. 4.2). The quartz diorite of Pine Lake is on the southwest corner of the Morgan Creek pluton. U-Pb zircon dating has shown discordant ages ranging from 97.5 to 181 Ma (Frost and Mattinson, 1988; Davis et al., 2012). Another mafic intrusion, the Rock Creek gabbro is in contact with the Morgan Creek pluton on the northwest corner, and is probably correlative with the mafic rocks on the northeast corner of the Morgan Creek pluton. Preliminary U-Pb dating suggests it was emplaced shortly before the Morgan Creek pluton at 95.0 Ma (Gaschnig et al., 2006). A narrow dioritic pluton is also located on the east-central part of the Morgan Creek pluton; zircons from that pluton have been dated at 168.7 Ma (Stern et al., 1981).

Previous work

The Morgan Creek pluton is the smallest separately mapped pluton in the John Muir Intrusive Suite, measuring ~1.5 km wide and ~8 km long (Fig. 4.2). The pluton has received attention despite its size because of its role as the causative intrusion for the world-class Pine Creek tungsten skarn (Gray et al., 1968; Newberry, 1982). While the mine was in production, several studies mentioned the Morgan Creek pluton, though the focus was usually on the geometry, genesis, and conditions of skarn mineralization (Gray et al., 1968; Newberry, 1982; Brown and Essene, 1985, Brown et al., 1985).

In the late 1970s Cray (1981) carried out detailed mapping of the Morgan Creek pluton as part of a Ph.D. project. Cray's mapping identified two main compositional facies: the main facies, comprising over 95 percent of the exposed pluton and the siliceous facies located on the southeast flank of Mount Morgan (Fig. 4.2). The siliceous facies is small, but notable for its role as the conduit for mineralizing fluids that formed the Pine Creek tungsten skarn orebody. Cray subdivided the main facies into three parts: the coarse-grained main facies and the northern and southern fine-grained members of the main facies. Broad major element zoning was reported, although sample locations were not recorded well enough for use in this study. Cray's classification of main and siliceous facies is used herein, but both fine-grained bodies are considered together as a single subfacies.

A zone of apophyses in the vicinity of the Brownstone mine in the southern end of the pluton was identified by Bateman (1965). The granite intruding the wall rocks in the zone of apophyses is part of the main facies, although the apophyses appear to be somewhat more mafic than most of main facies (Cray, 1981). Other minor rock types, including a small zone of augen gneiss near the pluton's eastern contact, were described but, because they are very rare or were not found in-place in the field, they are not considered below.

Methods

Field work and sampling

Samples were collected throughout the pluton, but focused on two east-west transects across the pluton. The southern transect sampled the pluton on the north side of Pine Creek from Pine Lake eastward (Pine Creek traverse), and the northern traverse

started at the contact near the southern shore of Bear Lake and sampled to the old mine road at the eastern margin of the pluton (Bear Lake traverse; Fig. 4.3A). The two transects were chosen because of excellent exposure across the pluton and because they each were mapped to contain the two textural subfacies of the Morgan Creek pluton (Cray, 1981). Samples for petrography and geochemistry were collected at ~100 m intervals along each transect. All samples were collected during the summer of 2007.

Magnetic susceptibility

Magnetic susceptibility measurements were taken using a ZH Instruments SM-30 handheld meter. At most magnetic susceptibility stations (n = 98), nine measurements were taken on flat surfaces within an area of ~2 m^2. Some stations in the southern part of the pluton received less than nine measurements. Where possible, surfaces in multiple orientations were measured to average out magnetic anisotropy, if present. The nine measurements at each station were averaged to obtain a mean magnetic susceptibility of the rock. Magnetic susceptibility in the Morgan Creek pluton ranges from 0.3 to 12.9 x 10^{-3} SI units. The average standard deviation of measurements at each station is 1.1 x 10^{-3} SI units.

Magnetic susceptibility measurements were collected along the Pine Creek and Bear Lake traverses at ~50 m spacing and at a number of other stations throughout the Morgan Creek pluton (Fig. 4.3B). Measurements were taken at all sample localities along both the Pine Creek and Bear Lake traverses. Measurements were also taken from 22 stations along another transect on the southern side of Pine Creek (the Brownstone traverse) with station spacing ranging from 20 m to 275 m. Coverage was not sufficient to contour or map magnetic susceptibility over the entire pluton.

Geochemistry

All major element analyses (n = 42) were performed by X-ray fluorescence (XRF) at Brigham Young University on a Siemens SRS-303 XRF spectrometer. Samples were pulverized in a tungsten carbide shatter box. After drying overnight in a 105 °C oven, glass disks for major element analysis were prepared by fusing rock powder with a 50/50 mixture of Spectroflux 105 lithium tetraborate and metaborate flux. Pressed pellets for XRF trace element analysis (n = 24) were prepared by pressing rock powder into pellets backed by Whatman fibrous cellulose powder. Reference materials were prepared in the same way.

Twenty-eight samples including all samples from the Pine Creek traverse and selected samples from elsewhere in the pluton were analyzed by inductively coupled plasma mass spectrometry on lithium borate fusions of the samples by ALS Chemex using their ME-MS81 analytical package. Thirty-eight elements were analyzed, including the rare earth elements.

Six samples were analyzed by both XRF and ICP-MS. The average difference between concentrations determined by both methods was less than 5 percent for most elements. The differences for some of the elements, V, Cu, Zn, Ga, and Sm, were more than 10 percent. For samples analyzed by both methods the ICP-MS analyses are used below.

Petrography and automated modal mineralogy

Because of the relatively small average crystal size of Morgan Creek rocks, modal data were collected from thin sections, rather than slabs, as is common for many granitic rocks. Modal data for 40 thin sections from the Morgan Creek pluton were collected on

the QEMSCAN automated scanning electron microscope at the Department of Geology and Geophysics at the University of Utah. An approximately 1 μm beam was used for all analyses with 25 kV accelerating voltage and 5 nA beam current. On each thin section a 5 by 7 grid of fields, each 3 mm square, was analyzed providing a total analyzed area of approximately 1.5 by 2.1 cm. Points were analyzed at 40 μm horizontal spacing and 50 μm vertical spacing, resulting in approximately 17,500 analyzed points on each sample. The electron beam rests on each point until the detectors received a total of 1000 counts on the four energy dispersive collectors. The raw data were processed through a proprietary software package, iDiscover 4.3, which categorizes the data using a set database of mineral compositions. A customized version of the Barrick 710 species identification protocol was used to classify the samples.

Standard petrographic techniques were used to determine mineral relationships and to customize the identification protocol by grouping minerals that are related in thin section. In the presentation of data and discussion below, chlorite is grouped with biotite because, based on mineral relationships, >90 percent of the chlorite was formed by the replacement of biotite. On similar grounds, muscovite and other low-Fe phylosilicates were grouped with alkali feldspar, as were mixed K-Na feldspars which represent albite exsolution. These groupings should not add more than a few percent error in the modal data presented.

Results

General features

The main facies of the Morgan Creek pluton comprises the majority of the pluton and can be subdivided on the basis of both texture and composition. All rocks of the main

facies are equigranular to weakly porphyritic. The coarse-grained subfacies is the dominant textural variety of main facies granite. It is light gray and has an average crystal size of ~2 mm. The fine-grained subfacies is present in two bodies, one in the northern part of the pluton, near the peak of Mount Morgan, and one in the southern part of the pluton (Fig. 4.2). In the field, the fine-grained subfacies appears mineralogically similar to the coarse-grained rocks, but is weakly porphyritic with an average crystal size of ~1 mm.

Cray (1981) focused on the textural differences within the main facies and treated the northern and southern bodies of fine-grained rocks separately, based on minor chemical and petrographic differences between the two bodies. The contact between coarse- and fine-grained rocks is gradational over tens of meters in the southern fine-grained facies. In the north, the transition is narrower, grading from coarse- to fine-grained facies over just a few meters (Cray, 1981).

There is a sharp contact between the main facies and the mineralogically similar, but more felsic, siliceous facies. Cray (1981) reported similar crystal size for the siliceous facies as the coarse-grained subfacies; however, near the western contact, the average crystal size is ~3 mm, with 4 mm crystals common. Small pods of siliceous granite, several meters in diameter, compositionally and texturally similar to the siliceous facies are present near Lower Morgan Lake and near the Pine Creek pendant (Newberry, 1982). A swarm of pegmatite dikes spatially associated with skarn mineralization has been reported near the siliceous facies (Cray, 1981). These are probably correlative with the variably mineralized silicic dikes reported by Newberry (1982). Dikes of siliceous facies

are present near the abandoned surface workings of the Pine Creek mine (Fig. 4.2), but are better exposed in underground workings (Cray, 1981; Newberry, 1982).

Mafic minerals and sparse mafic enclaves define a weak magmatic foliation throughout the main facies. Enclaves are elongate parallel to foliation defined by the alignment of mafic minerals in the granite and are parallel where multiple mafic enclaves are present in the same outcrop. Bands of schlieren are locally present, especially near the contact with the quartz diorite of Pine Lake in the southwest corner of the pluton and northeast of the siliceous facies (Cray, 1981). Magmatic foliation generally strikes NNW and dips to the ENE between 70 degrees and vertical. Cray (1981) and Newberry (1982) also reported evidence of postmagmatic strain, consisting of weak foliation cutting the magmatic foliation and anastomosing zones of quartz and feldspar with granoblastic texture.

The textural differences in the main facies are very clear in the field but, because of modal and chemical overlap between coarse- and fine-grained facies rocks, compositional differences are used for the primary classification here. The most common are coarse-grained rocks with relatively high mafic mineral abundance, termed high-mafic (HM; Fig. 4.4A) granites. Rocks with the lowest mafic abundance and more felsic compositions are found only in the fine-grained subfacies, and are referred to as low-mafic (LM; Fig. 4.4B) rocks. A group of rocks with intermediate mafic mineral content occurs in both the coarse- and fine-grained subfacies. Because the modes and compositions of the coarse- and fine-grained rocks with intermediate mafic mineral contents overlap, they are grouped together and called intermediate-mafic (IM; Fig. 4.4C, D) rocks. Siliceous facies rocks are lighter colored than main facies granites (Fig. 4.4E).

Each of the types of the main facies appear to be coherent on the scale of tens to hundreds of meters; no sharp contacts between them were observed. Instead, the contact between the two compositional types is subtle and gradational over meters to tens of meters.

Petrography

Main facies

Plagioclase, quartz, and K-feldspar are present in subequal amounts and comprise 93.7 percent of the main facies rocks, on average. All analyzed rocks of the main facies plot within the granite field on a QAP classification plot (Fig. 4.5). Quartz is anhedral and interstitial to the feldspars. Biotite is the dominant mafic mineral, but hornblende is present in all main facies samples. Total mafic mineral content of main facies rocks ranges from 3.5 to 8.9 percent, averaging 6.0 percent (Table 4.2).

Analyzed HM rocks from the Morgan Creek pluton contain an average of 27.3, percent quartz, 30.9 percent K-feldspar, and 34.1 percent plagioclase. Feldspars are most often euhedral to subhedral, with interstitial anhedral quartz (Fig. 4.6A). High mafic rocks of the coarse-grained subfacies contain approximately 1.5 percent less quartz than IM rocks.

The mineralogy of the fine-grained facies is similar to that of the coarse-grained facies, though it is generally more felsic (Fig. 4.6B). The average felsic mineral content of fine-grained facies rocks analyzed is 31.8 percent quartz, 32.2 percent K-feldspar, and 32.0 percent plagioclase. Like the more mafic rocks, feldspars are euhedral to subhedral. Interstitial anhedral quartz and feldspars give some samples of fine-grained subfacies granites a weakly porphyritic texture, as noted by Cray (1981). Quartz content in IM

rocks is 3.3 percentage points lower than LM, and plagioclase is 1.3 percent higher. The sample from the northern fine-grained facies contains subequal amounts of quartz and K-feldspar, and plagioclase contents similar to that of fine-grained IM rocks of the southern fine-grained body (Table 4.2).

Average mafic content in HM rocks is 7.56 percent, compared to 5.09 and 3.52 percent for the IM and LM rocks, respectively. Mafic minerals in the HM and fine-grained IM occur as small clots of biotite and hornblende 2-8 mm in diameter (Fig. 4.6C). In the LM and coarse-grained IM, mafic minerals are more likely to occur as isolated crystals. Hornblende is most common in the HM, as are hornblende-rich mafic enclaves. Mafic enclaves are more common in the margins of the pluton, which are dominated by the HM main facies. Although the distribution of the main facies compositional types was not mapped in detail, there is a general trend towards more felsic compositions in the center of the pluton (Fig. 4.3). Rocks in the Brownstone MS traverse appear to have a higher mafic mineral content, although QEMSCAN data are not available for these rocks.

The sample from the northern fine-grained body is somewhat more mafic than those of the fine-grained subfacies collected along the Pine Creek traverse, with a total mafic content of 6.50 percent, consisting of 5.71 percent biotite and 0.79 percent hornblende. Cray (1981) sampled the northern fine-grained body more extensively and, although he did not report petrography, he noted that the northern fine-grained rocks were generally more mafic than those of the southern fine-grained body.

Average hornblende content of HM rocks is 1.15 percent, nearly five times the average of coarse-grained IM, 0.26 percent. The highest hornblende content of any IM sample analyzed was 0.48 percent, compared to 2.54 percent in HM rocks. Samples of

the LM type average 0.21 percent hornblende. The biotite:hornblende ratio in HM rocks averages 6.0 percent. The IM rocks have a more consistently high biotite:hornblende ratio of 17.3. The most felsic samples, from the LM rocks, average 16.9.

The trace mineral assemblage is fairly consistent across all main facies rocks (Table 4.2). Euhedral to subhedral titanite and acicular to stubby apatite are ubiquitous and form approximately 0.3 and 0.1 percent of the rock, respectively. Trace epidote in the cores of plagioclase is common in all rocks of the Morgan Creek pluton (Fig. 4.6D), but is more common in HM rocks than in the IM granites reflecting, in part, the higher plagioclase contents of the HM rocks.

Titanite in HM is similar in habit and abundance to coarse-grained rocks. Average titanite content of HM rocks is 0.28 percent. In contrast to the rest of the rocks of the main facies, titanite is sparse in LM rocks, with an average content of just 0.02 percent. The LM sample with the most abundant titanite contains only 0.05 percent (Table 4.2).

Magnetite is common throughout most of the pluton. In rocks which contain magnetite, HM rocks contain more magnetite on average, 0.48 percent, than IM and LM rocks, which average 0.33 and 0.21 percent, respectively (Table 4.2). Magnetite generally occurs as isolated euhedral crystals and locally forms clusters. Exsolution lamellae of ilmenite are present in most magnetite crystals (Fig. 4.6E).

Magnetite is essentially absent in the coarse-grained, HM rocks in samples from the Pine Creek traverse within ~200 m of the southeastern contact of the Morgan Creek pluton with the Pine Creek septum. The magnetite contents of the first and second samples in the Pine Creek traverse, near the contact and ~100 m into the pluton, were 0.01 and 0.08 percent, respectively. This is well below the average magnetite content for

any compositional type of the main facies. The zone of low magnetite content coincides with a zone of near zero magnetic susceptibility (discussed below). These two samples contain more secondary clay minerals, grouped in the "other" category, and epidote than most other HM rocks, but the total abundance of these alteration products is still below a few tenths of a percent (Table 4.2). Sample MC-49 contains trace pyrite. Except for the sample collected nearest the eastern contact in the Pine Creek traverse, the rocks appear unaltered in hand sample. In transmitted light, the samples appear to be essentially free of opaque minerals, and fractures show light brown Fe-oxide staining (Fig. 4.6G).

Ilmenite is common in LM rocks. Whereas the QEMSCAN classification "Ti-oxides" went undetected, or was only present in trace amounts (0.01%) in the rest of the main facies, "Ti-oxides" are present in all LM samples, comprising an average of 0.07 percent of the rocks. The dominant "Ti-oxide" phase in LM rocks was identified as ilmenite under reflected light. It forms as subhedral to anhedral crystals near mafic minerals and within quartz and other felsic minerals. Small blebs of exsolved Fe-oxide (hematite?) are present in all observed ilmenite crystals (Fig. 4.6F).

Siliceous facies

Only one thin section of the siliceous facies, collected near the eastern contact, southwest of the Adamson mine, was analyzed as part of this study (Fig. 4.3A). Cray (1981) noted that the siliceous facies is compositionally variable, changing over several meters. Therefore, the single thin section analyzed by QEMSCAN should serve only as a guide to the mode of the siliceous facies. Although Cray did not provide modal data, his work provides a detailed description of the variability in the siliceous facies.

Like the rocks of the main facies, the siliceous facies plots in the granite field. Quartz is more abundant in the siliceous facies; plagioclase and mafic minerals less abundant. Quartz is the dominant mineral in the thin section examined, comprising 40.7 percent of the rock, followed by 30.9 percent K-feldspar and 25.9 percent plagioclase. Mafic minerals comprise only 2.13 percent of the rock, with hornblende present, but in a very minor (0.8%) amount. Biotite is more commonly chloritized than the rocks in the main facies (Cray, 1981). The biotite:hornblende ratio of the sample of the siliceous facies is 25.6, higher than any sample of the main facies (Table 4.2).

The trace mineral assemblage is very similar to that of LM. Only trace titanite is present, and Ti-oxides are present and more abundant than titanite. Magnetite makes up 0.24 percent of the sample. The sample of the siliceous facies contains traces of zircon and epidote (Table 4.2).

Mafic enclaves

Mafic monzonite to quartz monzonite enclaves are present throughout the Morgan Creek pluton, but are much more common in HM rocks. Thin sections from three enclaves were analyzed for modal mineral abundance (Table 4.2). Quartz is much less abundant than in the main or siliceous facies, making up between 3.53 and 15.9 percent of the rocks. Plagioclase is abundant, ranging from 36.5 to 44.8 percent. Potassium feldspar content in the enclaves ranges from 11.1 to 23.2 percent. All three enclaves analyzed contain more than 26 percent mafic minerals. In contrast to the felsic rocks of the main facies, hornblende is a major component in the mafic enclaves and is the dominant mafic mineral in two of the samples. The trace mineral assemblage of mafic

enclaves is similar to that of the main facies, but titanite in the enclaves is more abundant and magnetite less abundant than in the rocks of the main facies.

Magnetic susceptibility

Magnetic susceptibility values for all stations range from 0.00 to 12.9. Magnetic susceptibility correlates well with magnetite content of samples. As such, unaltered coarse-grained HM rocks have the highest values. The highest measurement was taken from a station within unaltered HM rocks, which have an average value of 10.0. Overall, IM rocks have an average magnetic susceptibility of 8.80. Values for the coarse-grained IM have a lower, but less variable average, 7.90 +/- 0.48, in contrast to the average for the fine-grained IM, 9.53 ± 1.2 (both errors 1 σ). The interior LM rocks show the lowest magnetic susceptibility values, with an average of 6.98. These values show that all rocks, even those of the most evolved LM, are magnetite-series granites (susceptibility $\geq 3 \times 10^{-3}$ SI units; Ishihara, 1981; Takagi, 2004).

Rocks within a few hundred meters of the eastern contact in both the Pine Creek and Brownstone MS traverses have essentially zero magnetic susceptibility, as do rocks near the Pine Creek surface workings in the northern part of the pluton. All stations with near-zero magnetic susceptibility values are in HM rocks, and all are at or near contacts with the Pine Creek pendant. Rocks near the eastern contact of the Morgan Creek pluton and the southeastern Jurassic mafic intrusion have normal magnetic susceptibility values for HM rocks (Fig. 4.3B). Rocks in the Pine Creek traverse appear typical of HM rocks throughout the pluton. Sparse secondary biotite is present in the easternmost sample in the Pine Creek traverse and epidote is more abundant, but still only present in trace amounts in the rocks with low magnetic susceptibility. Limited exposure prohibits

determination of the full extent of the zone of low magnetic susceptibility in the northern part of the pluton. However, one station near the Adamson mine had lower than expected magnetic susceptibility values for HM rocks (6.18; Fig. 4.3B), and suggests that the zone of lower than average magnetic susceptibility extends a few hundred meters into the pluton in the north, as it does in the south.

Only seven of the magnetic susceptibility stations are located in the LM subtype rocks. The average magnetic susceptibility for these stations is 6.98, reflecting its low magnetite content (Appendix B). None of the stations located in the LM or IM had near-zero values like those for the HM in the eastern Pine Creek traverse. Magnetic susceptibility does increase in the fine-grained rocks near the western contact with the Jurassic Chickenfoot Lake Granite.

Whole rock geochemistry

Major and trace element data are presented in Table 4.3. The silica content of main facies rocks ranges from 70.0 to 73.7 percent SiO_2. The HM rocks contain an average of 70.2 percent SiO_2. The IM granites contain an average of 71.4 percent SiO_2. The most evolved rocks of the main facies, the LM, average 73.3 percent silica. The one analyzed sample of siliceous facies contains 76.5 percent SiO_2, which falls within the range of SiO_2, of 74.7-76.7 percent reported by Cray (1981) for four samples of the siliceous facies.

All analyzed samples of the Morgan Creek pluton plot in the granite/rhyolite field of a total alkali vs. silica plot (Fig. 4.8A). Like most rocks of the large intrusive suites, the rocks of the Morgan Creek are high-K and calc-alkaline, though a few samples are

alkali-calcic (Fig. 4.8B). Most major elements correlate well with silica and define a linear trend (Fig. 4.9).

Some samples from the Morgan Creek pluton plot off the main trend for the unit. The same samples are off trend in the various plots, suggesting that these samples have all undergone alteration or weathering that has changed their composition. Most rocks of the main facies are peralkaline, but a few samples from the main facies are weakly peraluminous (Fig. 4.10). Compatible elements, such as Mg, Fe, and Al, decrease with increasing SiO_2.

Trace elements

The main facies of the Morgan Creek pluton is characterized by very high Rb, Ba, and Zr compared to rocks with similar SiO_2 contents from plutons in the nearby Cretaceous intrusive suites, including available analyses from the Lamarck Granodiorite member of the John Muir Intrusive Suite (Fig. 4.11). The Sr contents of rocks in the main facies fall on the lower part of the trend defined by the other rocks of the intrusive suites. The ratio of Rb to Sr in the Morgan Creek pluton is elevated, compared to other rocks in the nearby intrusive suites, suggesting a different source or evolution for the pluton (Fig. 4.12).

Trace element compositions of the various rock types of the main facies form distinctive trends, as they do for the major element concentrations. The average Ba, Sr, and Zr contents decrease from HM to LM rocks. Rubidium is high in all Morgan Creek granites and shows only a modest increase with increasing silica from HM to LM rock types. One sample of fine-grained IM, MC-65, has anomalously low trace element

concentrations, suggesting alteration or a bad analysis. This sample was excluded when calculating average trace element concentrations of IM rocks.

The siliceous facies has similar trace element compositions to the Johnson Porphyry in the Tuolumne Intrusive Suite and the leucogranites of the Whitney Intrusive Suite to the south (Fig. 4.11; Hirt, 2007). The siliceous facies has much lower Zr contents than the rest of the main facies, with the one sample analyzed containing just 99 ppm Zr, compared to an average of 175 ppm for the main facies.

The rocks of the Morgan Creek pluton plot within the syn-collisional fields in Rb-Y-Nb and Rb-Yb-Ta space, as defined by Pearce et al. (1984). In contrast, almost all other rocks in the Sierra Nevada batholith fall within the volcanic arc field (Fig. 4.13). The difference between compositions of the Morgan Creek and other Sierran suites suggests a different source for the Morgan Creek pluton than even the rocks of the John Muir Intrusive Suite, to which it belongs. The data suggest magmas that formed the Morgan Creek pluton formed as a result of melting of the upper crust.

Spatial variations in whole rock geochemistry

Spatial variations of major and trace element compositions are prominent in both the Pine Creek and Bear Lake traverses. Silica and incompatible elements (e.g., K, Pb, U) increase towards the center of the pluton and compatible elements (e.g., Mg, Ca, Sr) show a decrease (Figs. 4.14, 4.15). The increase occurs, regardless of the subtype, i.e., SiO_2 increases in HM rocks as they approach the IM and fine-grained subfacies contacts in the Pine Creek and Bear Lake traverses. Major and trace element variations across the pluton in the Bear Lake traverse, are similar to those in the Pine Creek traverse. Similar spatial variation is also observed in modal data (Fig. 4.16).

Rare earth elements

Normalized REE patterns for all main facies rocks, using the mantle compositions of McDonough and Sun (1995), have similar shape, but differ in their REE concentrations (Fig. 4.17). All main facies rocks are enriched in light REE (LREE), have a moderate negative Eu anomaly, and a flat heavy REE (HREE) pattern. Although there is some overlap between the different rock types in the Morgan Creek pluton, REE concentrations tend to decrease with increasing silica.

The mean normalized La/Yb in the main facies decreases from an average of approximately 18 for the HM and IM types to an average of 16.6 for the siliceous LM granites. The fine-grained IM rocks tend to have higher normalized La/Yb ratios than do the coarse-grained IM, with La contents similar to those of the HM type, but lower HREE concentrations. The HREE pattern of the LM rocks is more concave than the other rocks from the pluton, a common feature in evolved rocks (Glazner et al., 2008). The normalized REE pattern of the lone sample of siliceous facies is distinct compared to the main facies rocks. The LREE content of the siliceous facies is slightly lower than that of the main facies, with a similar slope, but the Eu anomaly is deeper. Heavy REE show a concave up pattern, as opposed to the nearly flat pattern of the main facies rocks. The heaviest REE, Tm, Yb, and Lu, are more abundant than in any other main facies rocks. The REE pattern for the siliceous facies is similar to that of many Sierran aplites, but the siliceous facies sample is less depleted in middle REE than most aplites (Glazner et al., 2008).

Discussion

Trace element modeling

Simple trace element models were constructed to understand the cause of the distinct trace element composition of the Morgan Creek pluton, with its elevated Rb, Zr, and Ba, compared to rocks in nearby Cretaceous intrusive suites. With the assumption that the Morgan Creek pluton crystalized inward, the HM compositions should reflect a composition near that of the initial magma. Modeled partial melting of a variety of sources did not yield compositions near those of the high-Ba, low-Sr HM rocks, except when partition coefficients were used that are unrealistic for the mineralogy of the proposed sources. Nor could a starting composition on the trend defined by the main facies be derived by mixing or contamination of a magma along the compositional trend defined by the Sierran intrusive suites (Fig. 4.18); no contaminants or hypothetical melts contain high enough Ba, Rb, and Zr to define a mixing trend that contained the HM composition.

The consistent compositional trends in the Morgan Creek pluton can be modeled by fractional crystallization of a magma with the starting composition of the HM rocks using reasonable partition coefficients for granitic rocks (Table 4.4). The Rb distribution is more diffuse than for the others, but shows the same trend. The scatter in the Zr-Rb plot may be a combination of Rb mobilization and possibly the result of zircon inheritance causing deviation on the Zr axis. This model is consistent with the Morgan Creek pluton being emplaced as one batch of magma and crystallizing from the outside in. There are no breaks in the compositional trends that suggest the magma was formed by the repeated injection of discrete magma pulses; if multiple pulses of magma

contributed to the main facies of the Morgan Creek pluton, they must have homogenized enough to obscure any compositional differences between pulses.

Low degree (~5-10 %) partial melting of typical Sierran granitoids did yield an appropriate composition (Fig. 4.18). A modified average composition of the granitoids from the John Muir, Whitney, and Tuolumne Intrusive Suites was used as one possible source composition. The average Ba, Rb, and Zr contents of the intrusive suite granitoids were used as the starting composition, but a higher Sr content was needed to derive HM composition through partial melting (Table 4.4). Using distribution coefficients consistent with a biotite and K-feldspar bearing rock, a low degree partial melt (~5-10%) yields compositions similar to those of the HM rocks. Early Jurassic zircon ages in the Morgan Creek suggest some contact with the early Sierran granitoids and are consistent with this model (Porter et al., 2011). A melt derived from partial melting of a granitoid may also explain the negative Eu anomalies, present in all Morgan Creek rocks (Fig. 4.17). Granitoids from the Tuolumne and Whitney Intrusive Suites do not generally show strong Eu anomalies; only high silica aplites typically have negative Eu anomalies (Hirt, 2007; Glazner et al., 2008; Gray et al., 2008).

The sample of the siliceous facies plots off the main fractionation trend defined by the main facies. As noted above, the siliceous facies is in most regards compositionally similar to the most siliceous products of the Tuolumne and Whitney Intrusive Suites, except in terms of Zr content.

Fractional crystallization can explain much of the compositional evolution of the Morgan Creek pluton, but the starting composition is well removed from the main compositional trend for time equivalent intrusive suites. Removal of a plagioclase-

pyroxene cumulate from an average Lamarck starting composition, with some assimilation of upper crustal rocks can push the residual liquid composition towards the composition of HM rocks. However, it is unlikely that assimilation or fractional crystallization of any magma along the main trend of the intrusive suites would evolve towards the starting composition of the Morgan Creek pluton. The overall trend in the suites is derived by a combination of *in situ* fractionation and variations from a fractionating and evolving source (Coleman et al., 2012).

The difference between the Morgan Creek composition and that of the other rocks of the intrusive suites is most likely related to a significantly different source than most of the granitoids in the Sierra Nevada batholith. Isotopic evidence from the Tuolumne and Whitney intrusive suites show that they were derived from a mix of primitive and crustal sources (Kistler et al., 1986; Hirt, 2007; Coleman et al., 2012; Nelson et al., 2013). Although isotopic data are not available for the Morgan Creek pluton, the trace element data suggest a significant crustal contribution (Fig. 4.13).

A crustal source for the Morgan Creek pluton is also consistent with the tungsten mineralization associated with the pluton; tungsten skarns are most often associated with crustal melts (Einaudi et al., 1981; Meinert, 2005). Being on the eastern edge of the Sierra Nevada, the Morgan Creek pluton is also very near Triassic and Jurassic plutons that are some of the earliest rocks of the batholith (Barth et al., 2011). The rocks of the Scheelite Intrusive Suite, just east of the Morgan Creek pluton, are good candidates for a magma source. This hypothesis is supported by the presence of inherited Late Triassic zircons in the Morgan Creek pluton (Porter et al., 2011). The trace element data show a different source for the Morgan Creek pluton than the other Cretaceous Sierran plutons.

The Morgan Creek magma likely formed as a result of crustal thickening, or the incursion of early magmas related to the John Muir Intrusive Suite heating and partially melting the upper crustal granitoids. Better geochemical data for the nearby Triassic and Jurassic rocks and isotopic data for the Morgan Creek and older Sierran rocks would increase the confidence in this model.

Oxygen fugacity in the Morgan Creek pluton

Most of the main facies of the Morgan Creek pluton contains titanite, indicating a high fO_2 (Wones, 1989). Titanite is nearly absent and ilmenite is present in all samples of the chemically evolved LM rocks. Cray (1981) reported microprobe analyses of biotite that average over 2 percent TiO_2 but, given the distribution of samples in that study, it is unlikely any were obtained from the LM rocks. The near-absence of titanite and presence of ilmenite in LM rocks may reflect a lower fO_2 in the innermost parts of the pluton where the LM rocks are found.

A few microprobe analyses of biotites in the Morgan Creek pluton are consistent with lower fO_2 in the interior of the pluton (Cray, 1981). Biotite from the margins of the pluton has lower Fe/(Fe + Mg) than those in the center of the pluton. The highest Fe/(Fe + Mg) reported (0.64) is from a sample in the titanite-free siliceous facies. The highest ratio in the rest of the pluton comes from a sample which was reported to contain ilmenite and lacked reported titanite (Cray, 1981). Wones and Eugster (1965) determined that decreased fO_2 is one factor that can lead to high Fe/(Fe + Mg) ratios in igneous rocks.

Ilmenite may have formed at the expense of titanite under more reduced conditions than in the rest of the rocks in the main facies. One reaction that may have

been responsible for the consumption of titanite and creation of ilmenite was proposed by Wones (1989):

$$12 \text{ titanite} + 14 \text{ magnetite} + 36 \text{ silica} + 6 H_2O =$$

$$12 \text{ ilmenite} + 6 \text{ ferroactinolite} + 7 O_2. \qquad 4.1$$

This could, in part, account for the low magnetic susceptibility in the LM rocks. Hornblende is present, though not abundant in LM rocks. It is possible that much of the average 0.21 percent hornblende was created through this reaction. A similar reaction can be written involving biotite and feldspars:

$$\text{titanite} + 3 \text{ K-feldspar} + 2 \text{ magnetite} + 2 H^+ =$$

$$\text{biotite} + \text{anorthite} + \text{ilmenite} + 5 \text{ silica} + O_2 + 2 K^+. \qquad 4.2$$

This reaction involves a reduced, acidic fluid.

Exsolution of a volatile phase has been implicated in increases of fO_2 throughout the evolution of some plutons associated with porphyry systems (Panguna: Eastoe, 1983; Yerington: Dilles, 1987). Experimental work shows a similar relationship with the exsolution of a Cl-bearing fluid phase, common in many ore deposits (Bell and Simon, 2011). Fluid was released from the Morgan Creek pluton, probably coincident with the emplacement of the siliceous facies. However, the fluids that formed the Pine Creek skarn were reduced, approximately 1 log unit below the quartz-fayalite-magnetite buffer (Brown and Essene, 1985).

The presence of CO_2 in hydrothermal fluids has been linked to a lowering of fO_2 in ascending magmas (Burgisser and Scaillet, 2007). It is possible that CO_2 from limestone in the Pine Creek pendant may have interacted with the magma, buffering it to

a lower fO_2. Given that the rocks which lack titanite and are interpreted to have low fO_2 are in the interior of the pluton, this is unlikely.

The cause of the reduced fO_2 in the central Morgan Creek pluton is unknown, but it likely indicates open system behavior during the magmatic evolution (Dilles, 1987). An oxidized fluid may have been released before the reduced fluid responsible for ore deposition.

The lack of titanite in the interior of the pluton may, instead, be the result of highly evolved compositions of the LM and siliceous facies. Mustard (2004) suggested that the change from titanite-bearing rocks to ilmenite-bearing rocks in the Sandy Creek syenogranite of the Timbarra Tablelands pluton in New South Wales, Australia was the effect of a Ca-limited magma owing to extensive fractionation. The rocks in the pluton core are very potassic, and have low CaO contents (<1%). The lack of titanite in the siliceous facies may be related to a Ca-limited magma, but it is unlikely that the same is true for the LM rocks.

Low magnetic susceptibility and cryptic alteration in the Morgan Creek pluton

The low magnetic susceptibility and the lack of magnetite in the southeast corner of the Morgan Creek pluton is not interpreted to be the result of a changing fO_2, but is the result of hydrothermal alteration of the rocks. All rocks in the Morgan Creek pluton show some evidence of alteration in the form of epidote cores in plagioclase and titanite crystals; chlorite replacing biotite and hornblende; and a dusting of sericite on most feldspar crystals. The rocks with low magnetic susceptibility in the Pine Creek traverse contain more chlorite and epidote coupled with lower magnetite than other HM rocks

(Table 4.2). Secondary biotite is present in the sample closest to the eastern contact of the Pine Creek traverse (MC-48) and weak Fe-oxide staining occurs along intramineral fractures.

Hydrothermal alteration of the Morgan Creek pluton margin near the mineralized skarn has been described by Newberry (1982) and Cray (1981). Endoskarn and silicification are common within a few meters of the mineralized sediment-pluton contact (Cray, 1981; Keith et al., 1989). The rocks of the Pine Creek traverse are not adjacent to mineralized skarn, but the traverse shows alteration extends farther from the contact than reported by earlier workers. In the Pine Creek traverse, and likely in the rocks on the south side of Pine Creek, the alteration is zoned with weak biotite alteration within several meters of the contact. The absence of magnetite in QEMSCAN data and the low magnetic susceptibility values in the south and north ends of the pluton show that magnetite replacement extended ~300 m from the pluton-sediment contact. Semi-quantitative QEMSCAN data show a higher albite component to plagioclase compositions and suggest that weak Na-exchange in the plagioclase extends at least another 100 m beyond the zone of magnetite removal.

Emplacement and crystallization model for the Morgan Creek pluton

The size and variations in the texture and composition of the Morgan Creek pluton resemble similar variations in the Half Dome Granodiorite in the termed lobes and cycles (Figure 4.18; Memeti et al. 2010; Coleman et al., 2012). Lobes are small portions of the larger plutons in the suite that are interpreted to have evolved independently from the rest of the pluton and are interpreted to be composed of a single intrusive pulse, or

multiple pulses emplaced very rapidly, forming a single magma that evolved as a unified whole. As in the Morgan Creek, enclaves are more abundant in the outer units of the Half Dome lobes. Most of the compositional variations are gradational; however, some of the compositional subtypes are separated by sharp contacts. Cycles are compositional gradients from granodiorite to leucocratic granite on similar scale to the Morgan Creek, ~1-1.5 km wide, which are present within the main body of the Half Dome Granodiorite (Fig. 4.19; Coleman et al., 2012).

In the Half Dome Granodiorite cycles, magnetic susceptibility decreases from the granodiorite to the granite. These variations took place at the km-scale; most mapped cycles are only modestly smaller than the Morgan Creek pluton. The variations were interpreted as the result of *in situ* differentiation and crystal-liquid separation, whereas larger variations at the intrusive suite scale have been attributed to an evolving source and multiple intrusions emplaced at different times (Coleman et al., 2012).

Trace element trends consistent with compositional evolution through fractional crystallization, together with the similarities with the lobes and cycles of the Half Dome Granodiorite suggest that the Morgan Creek was emplaced as a single batch of magma or multiple rapid pulses allowing the magma that formed the pluton to evolve as a unit. Crystallization of the magma took place from the outside in, and compositional changes were possibly the result of sidewall boundary differentiation (Lee and Christiansen, 1983; Sawka et al., 1990). Newberry (1982) noted that the crystal size increases at depth, consistent with the sidewall boundary differentiation model. As crystallization proceeded, the more fractionated liquid was concentrated in the interior of the pluton, giving rise to the relatively more mafic borders. This outside-in crystallization concentrates the

evolving magma towards the center of the pluton and is consistent with the mineralogical and compositional variations in the Morgan Creek pluton.

The contact between HM and IM is gradational, grading from HM to a relatively thin zone of coarse-grained IM rocks. At the transition between the compositionally equivalent coarse- and fined-grained IM rocks something in the crystallizing pluton changed, forcing the reduction in crystal size. This may have been a rapid release of pressure, in effect pressure quenching the fine-grained rocks, perhaps related to the emplacement of the siliceous facies and its associated dike swarm and mineralizing fluids (Cray, 1981). Rapid crystallization via pressure quenching may also have contributed to the finer groundmass that gives the fine-grained facies its weakly porphyritic texture (Cray, 1981). The siliceous facies cuts both the coarse-grained facies and northern fine-grained facies. The northern fine-grained subfacies may have been partially liquid at the time of emplacement of the siliceous facies. The absolute timing of emplacement between the reduction in crystal size that formed the fine-grained subfacies and the siliceous facies is not certain, but field relationships between the siliceous facies and the LM rocks make this a permissible explanation for the reduction in crystal size.

The LM rocks may have crystallized soon after the fine-grained IM, accounting for the similar crystal size between the two distinct compositional rock types. The LM rocks represent the final product in the differentiation of the Morgan Creek magma. They are weakly peraluminous, probably owing to the crystallization of hornblende in the earlier rock types (Chappell et al., 2012).

The sparse data from the siliceous facies suggests a magma with a different compositional evolution than the rest of the Morgan Creek pluton. Crystallization of

titanite and other trace minerals (e.g., allanite, monazite) in the parent magma probably led to the distinct REE pattern of the siliceous facies (Glazner et al., 2008). Trace element data suggest that the siliceous facies is more closely related to typical rocks of the intrusive suites than the main facies rocks. The differences may reflect an evolving source in the lower crust. However, more data are needed to determine whether the sample from the siliceous facies is representative of the facies as a whole.

The place of the Morgan Creek pluton within the John Muir Intrusive Suite

The age and distinct geochemistry of the Morgan Creek pluton show that it is not correlative with the main body of the Lake Edison Granodiorite, as previously interpreted (Bateman, 1992). The data presented here suggest that the Basin Mountain and Morgan Creek plutons were part of a coherent whole before the emplacement of the Mono Creek Granite isolated them. Detailed petrography, geochronology, and whole rock and isotope geochemistry are required to firmly establish the relationship of the two bodies.

As a granite *sensu stricto* in the earliest parts of a large intrusive suite, the Morgan Creek occupies an unusual place in the time-composition space of large magmatic systems in the Sierra Nevada batholith. In general, the intrusive suites evolve towards more silicic compositions with time (Bateman, 1992). Silicic rocks of the intrusive suites are commonly emplaced late, which has been attributed to be evidence of compositional evolution in the magma source region (e.g., Coleman et al., 2012).

The Indian Peak caldera complex field on the border of Utah and Nevada has a similar areal extent to the Sierran intrusive suites (Best et al., 1989, 2013) and shows some parallels with the compositional evolution of the John Muir Intrusive Suite. Most of

the rocks of the caldera complex are dacitic, but were preceeded by a period of bimodal magmatism, characterized by andesites and a small volume of rhyolite tuffs and flows (Best et al., 1989, 2013). The early tuffs of the Indian Peak caldera complex are also compositionally distinct from most of the younger rocks in the volcanic suite. In similar fashion, the Morgan Creek has a distinct composition compared to younger rocks in the John Muir Intrusive Suite with similar silica contents. This difference in the John Muir Intrusive Suite likely represents an early stage of the evolution of the source region, before the magma source had reached an equilibrium that leads to a "typical" source composition for Sierran arc granitoids. In the case of the Morgan Creek, partial melting of relatively felsic crustal rocks played a dominant role in the unique composition. As time passed, partial melts of rocks that are interpreted as the source for the Morgan Creek were either extracted or strongly diluted by more mafic magmas. Some rocks of the Lamarck Granodiorite, which overlaps in age with the emplacement of the Morgan Creek (Porter et al., 2011; Davis et al., 2012), contain elevated Ba, suggesting some component of the high-Ba Morgan Creek source in that magma.

Conclusions and future work

The geochemistry and geochronology of the Morgan Creek pluton show that although it is part of the John Muir Intrusive Suite, there are important differences between the Morgan Creek pluton and the other rocks of the intrusive suite. The relationship of the Morgan Creek pluton to the Basin Mountain pluton should be established to determine the volume of magmatism associated with this early, crustally sourced felsic stage of John Muir Intrusive Suite magmatism. The relationship of the Morgan Creek pluton to the Basin Mountain pluton could also lead to insights about the

source of smaller W skarns south of Pine Creek (Hanging Valley and Tungstar mines; Bateman, 1965, 1992).

A more comprehensive geochemical and radiogenic isotope study of the John Muir Intrusive Suite as a whole would provide further insight into the evolution of the suite through time. Trace element geochemistry has only been published for rocks of the Lamarck Granodiorite (Frost and Mahood, 1987). The mix of high Ba contents and Ba contents more typical of the Whitney and Tuolumne Intrusive Suites, suggest that the John Muir Intrusive Suite may have undergone a compositional evolution distinct from that of its nearby cousins. A broad survey may yield insights into what caused the shift in source from the early rocks of the Morgan Creek to more typical rocks, showing an expected evolution towards more felsic compositions through time. Despite the difficulties involved in collecting samples from remote parts of the John Muir Intrusive Suite, the work may provide insight into the evolution of the Sierran arc, and large magmatic systems in general.

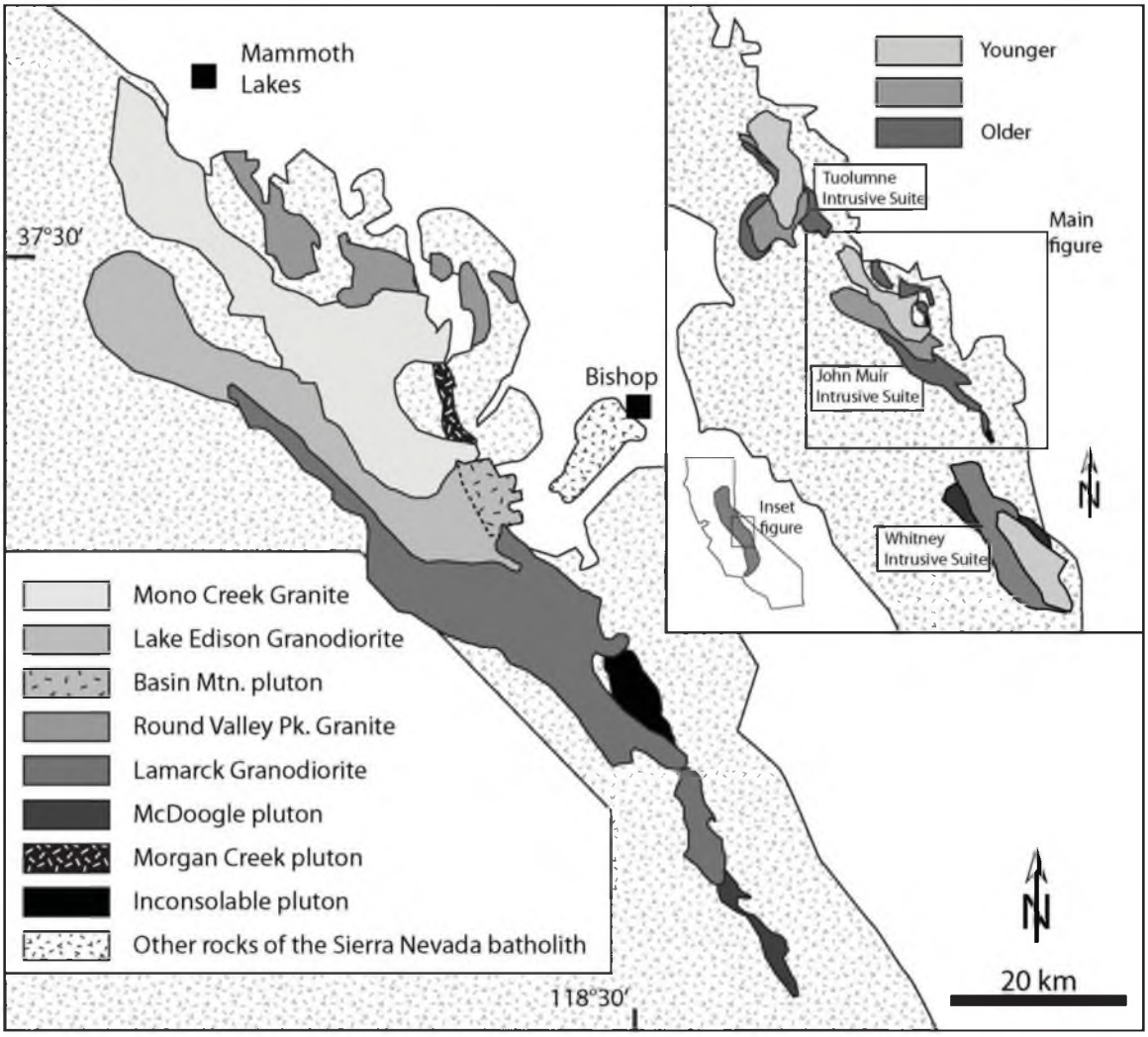

Figure 4.1. Simplified geologic map of the Sierra Nevada batholith in the vicinity of the Morgan Creek pluton (modified from Davis et al., 2012).

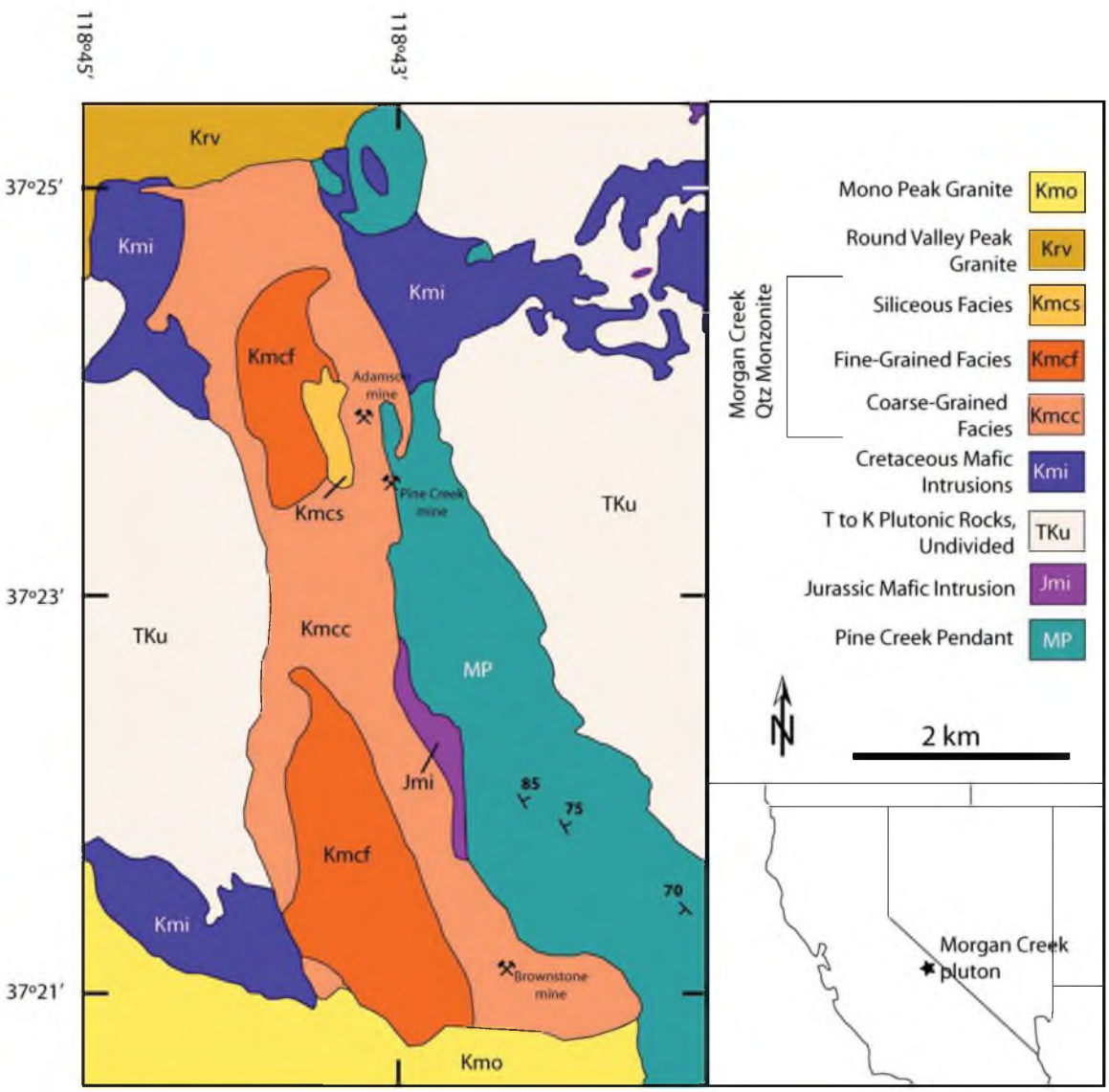

Figure 4.2. Simplified geologic map of the Morgan Creek pluton (modified from Cray, 1981).

Figure 4.3. A. Simplified geologic map of the Morgan Creek pluton with locations of samples analyzed for modal mineralogy and/or geochemistry by rock type. B. Simplified geologic map of the Morgan Creek pluton showing magnetic susceptibility stations. Magnetic susceptibility values less than 5×10^{-3} SI units, in purple, are anomalously low and are discussed later in the text (map outline modified from Cray, 1981).

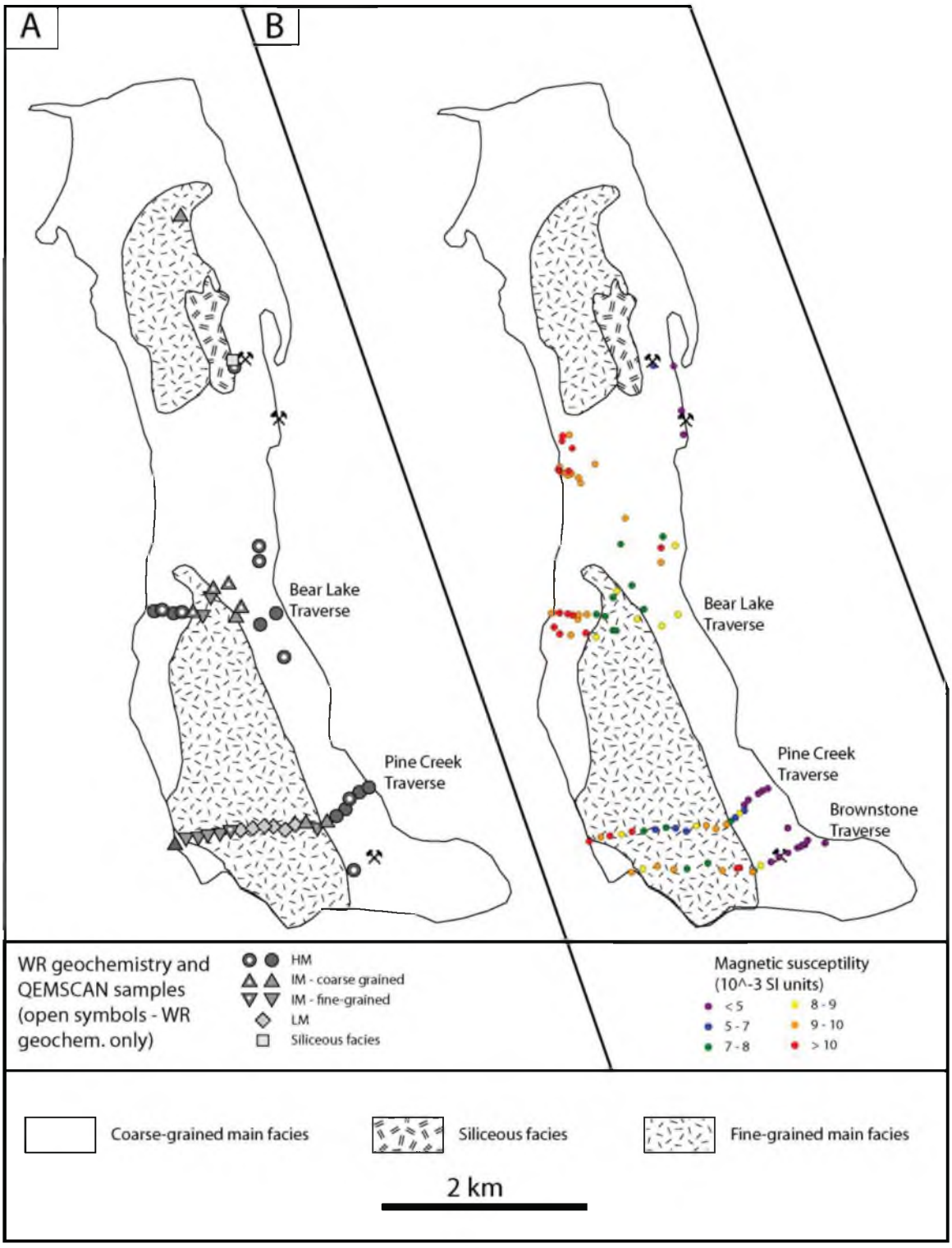
A
B
Bear Lake Traverse
Pine Creek Traverse
Bear Lake Traverse
Pine Creek Traverse
Brownstone Traverse
WR geochemistry and QEMSCAN samples (open symbols - WR geochem. only)
HM
IM - coarse grained
IM - fine-grained
LM
Siliceous facies
Magnetic susceptility (10^-3 SI units)
< 5
5 - 7
7 - 8
8 - 9
9 - 10
> 10
Coarse-grained main facies
Siliceous facies
Fine-grained main facies
2 km

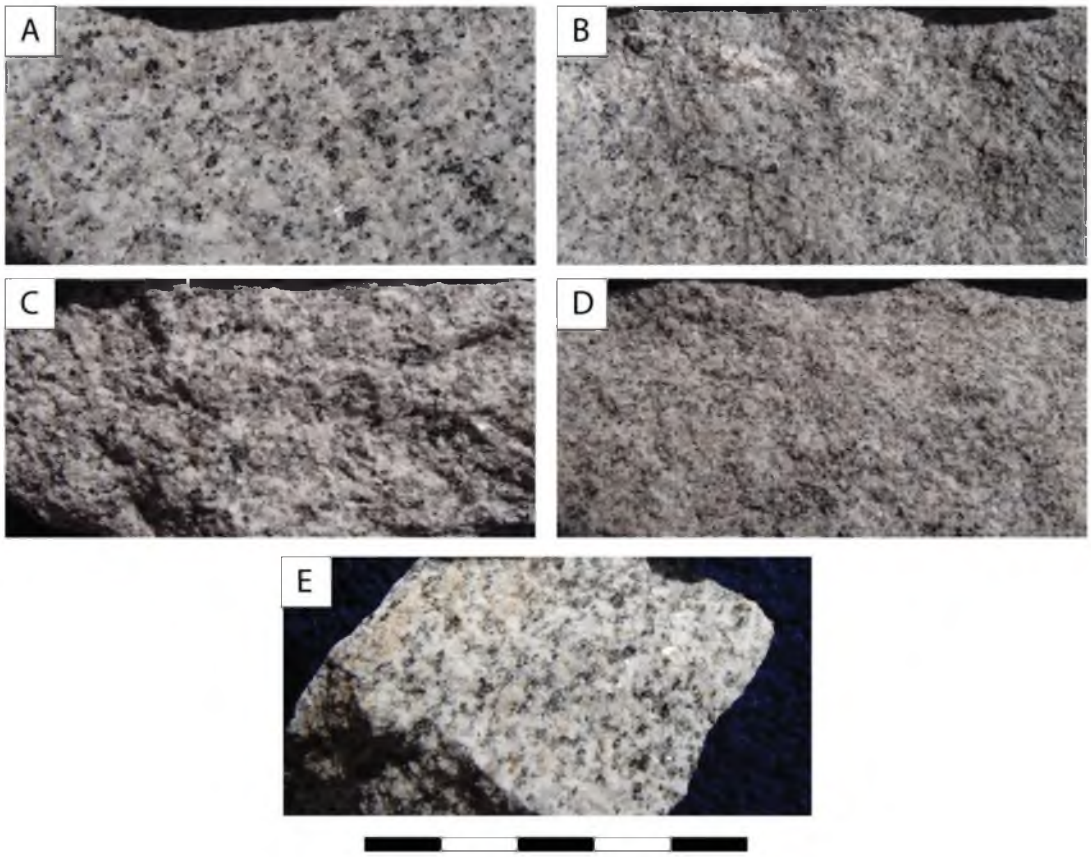

Figure 4.4. Photographs of the rocks from the Morgan Creek pluton. All photographs are at the same scale; the scale bar is 5 cm long, with 1 cm divisions. A. Morgan Creek high mafic granite (HM). B. Morgan Creek low mafic granite (LM). C. Coarse-grained Morgan Creek intermediate mafic granite (IM). D. Fine-grained intermediate mafic granite (IM). E. Siliceous facies granite.

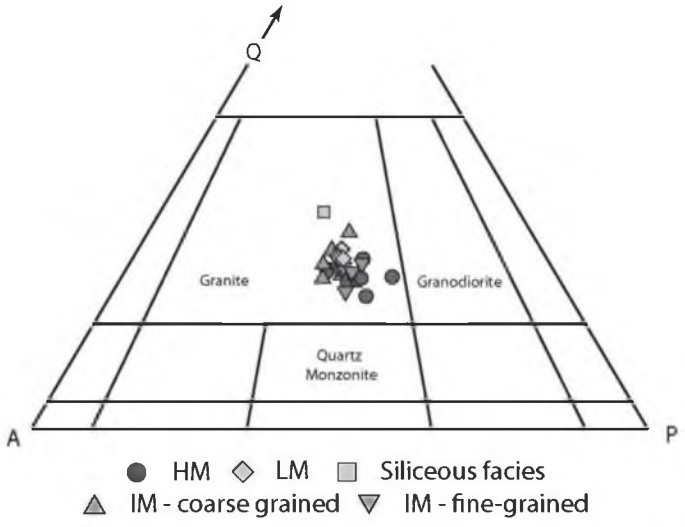

Figure 4.5. Quartz-alkali feldspar-plagioclase plot of rocks from the Morgan Creek pluton. All rocks plot in the granite field (modified from Le Maitre, 2002)

Figure 4.6. Photomicrographs of rocks from the Morgan Creek pluton. The scale bar associated with each image is 25 μm. A. Transmitted, cross-polarized light (XPL) photomicrograph of a thin section from sample MC-51, showing typical HM mineralogy and relationships. B. Transmitted XPL photomicrograph of a thin section of sample MC-61, showing typical mineralogy and relationships in the LM granite. Note the finer crystal size, but similar habit and alteration to the HM. C. Transmitted plane-polarized light photomicrograph (PPL) of a typical clot of mafic minerals common in the HM and fine-grained IM rocks. This clot is dominated by biotite, but in the HM and fine grained IM, hornblende is a common constituent of the clots. D. Transmitted XPL photomicrograph of a thin section from MC-51, showing the partial replacement of the core of a plagioclase crystal by epidote. This relationship is found in all Morgan Creek rock types. E. Reflected PPL photomicrograph from sample MC-42, showing typical magnetite crystals. Note the planar lamellae of exsolved ilmenite(?). F. Reflected PPL photomicrograph from sample MC-61 showing typical habit and exsolution style of ilmenite crystals in the LM. The exsolved phase (hematite?) is more spotty and rounded than the exsolved phase in magnetite crystals in all rock types. Ilmenite crystals are generally less euhedral than magnetite. G. Transmitted PPL photomicrograph of sample MC-48, from the southeastern contact of the pluton with the Pine Creek pendant. Chlorite and secondary biotite represent hydrothermal alteration. The weak, brown iron oxide staining along some fractures is interpreted to be related to the removal of magnetite in the zone of low magnetic susceptibility.

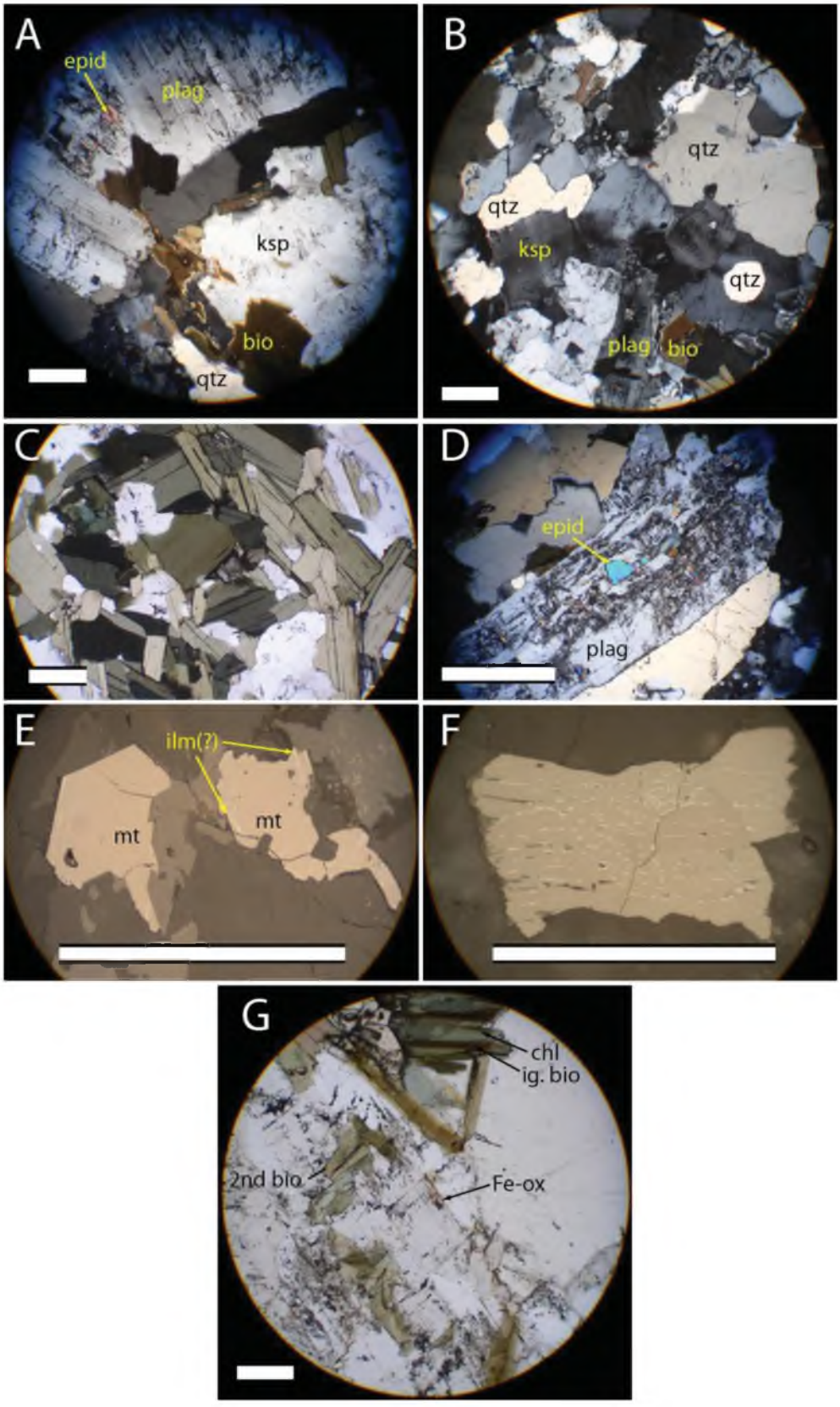
A
epid
plag
ksp
bio
qtz
B
qtz
qtz
ksp
qtz
plag
bio
C
D
epid
plag
E
ilm(?)
mt
mt
F
G
chl
ig. bio
2nd bio
Fe-ox

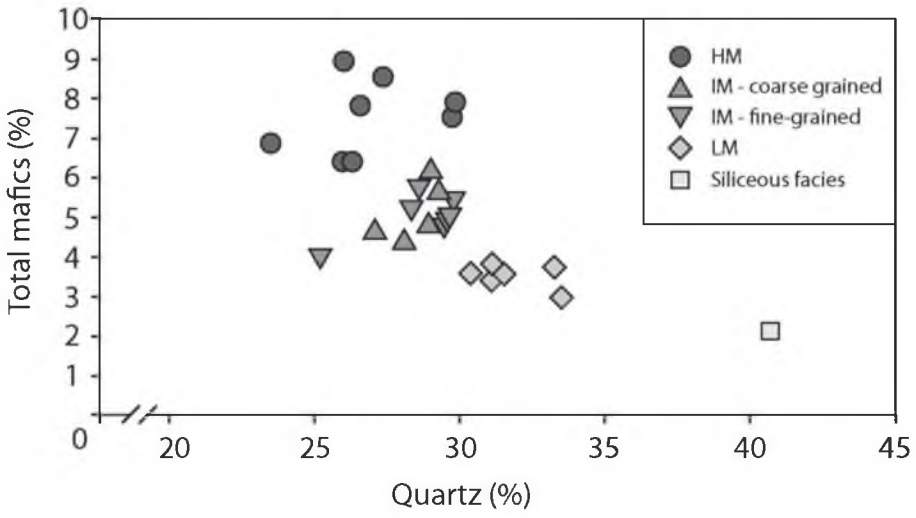

Figure 4.7. Plot of QEMSCAN quartz and total mafic mineral abundances for rocks of the Morgan Creek pluton. Clear groupings of the different rock types are apparent. Mafic enclaves are not plotted on this figure or in the following figures.

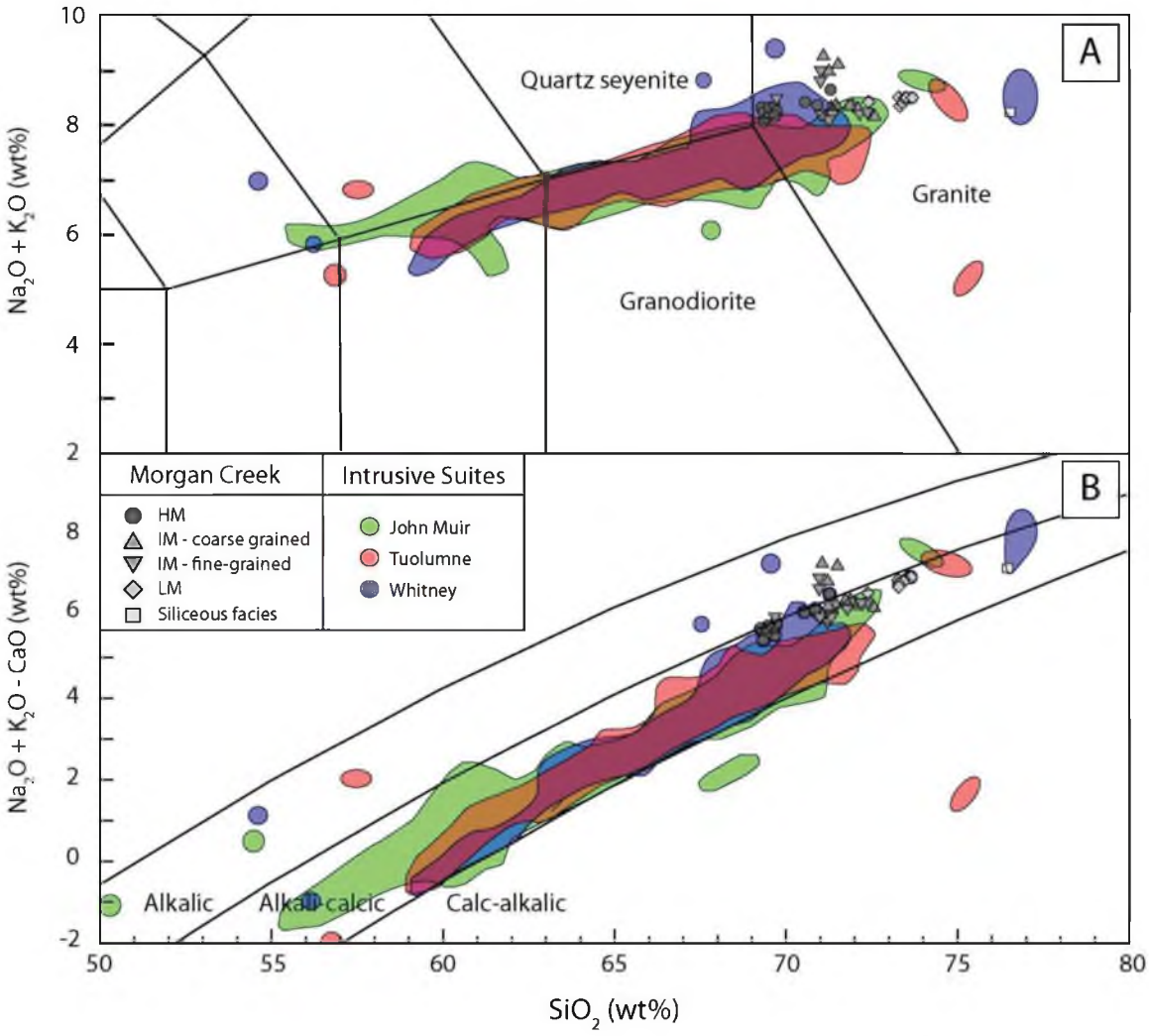

Figure 4.8. A. Total alkali-silica plot of Morgan Creek samples and fields representing analyses from the John Muir, Tuolumne, and Whitney Intrusive Suites. All rocks of the Morgan Creek plot in the granite field and contain slightly higher total alkali content than rocks with similar silica contents in the intrusive suites. B. Plot of $K_2O + Na_2O - CaO$ vs. SiO_2 (Frost et al., 2001) for rocks of the Morgan Creek pluton with fields representing the distribution of compositions in the John Muir, Tuolumne, and Whitney Intrusive Suites. Data used to construct this and major element figures in the rest of the paper are from Gray et al. (2008: Tuolumne Intrusive Suite); Bateman et al. (1984: Tuolumne and John Muir Intrusive Suites), Frost and Mahood (1987: John Muir Intrusive Suite); and Hirt (2007: Whitney Intrusive Suite).

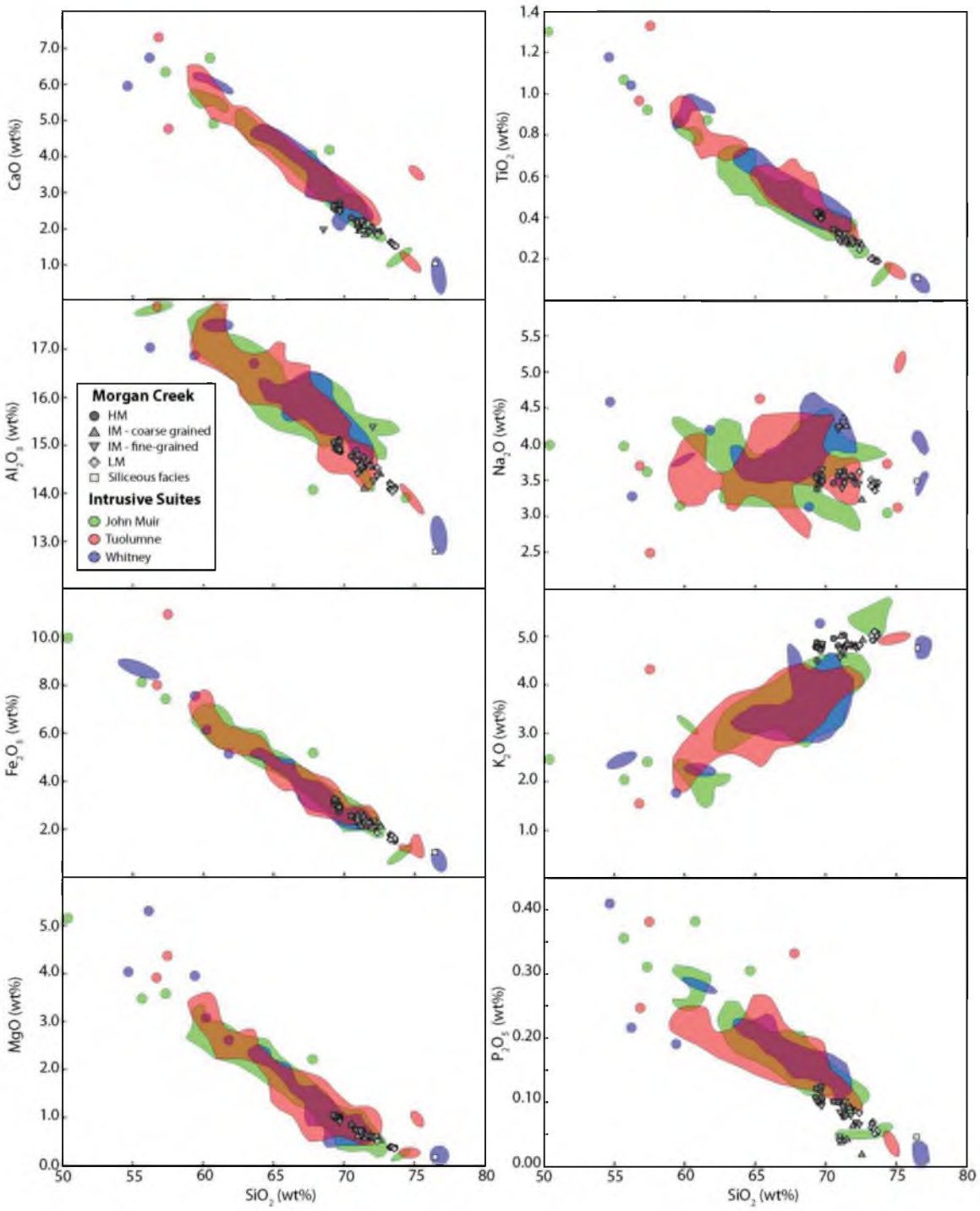

Figure 4.9. Major element variation diagrams for rocks of the Morgan Creek pluton and fields representing the JMIS, TIS, and WIS. Major element variations in the Morgan Creek mirror variations in the higher silica portions of the intrusive suites. A. CaO vs. SiO_2. B. TiO_2 vs. SiO_2. C. Al_2O_3 vs. SiO_2. D. Na_2O vs. SiO_2. E. Fe_2O_3 vs. SiO_2. F. K_2O vs. SiO_2. G. MgO vs. SiO_2. H. P_2O_5 vs. SiO_2.

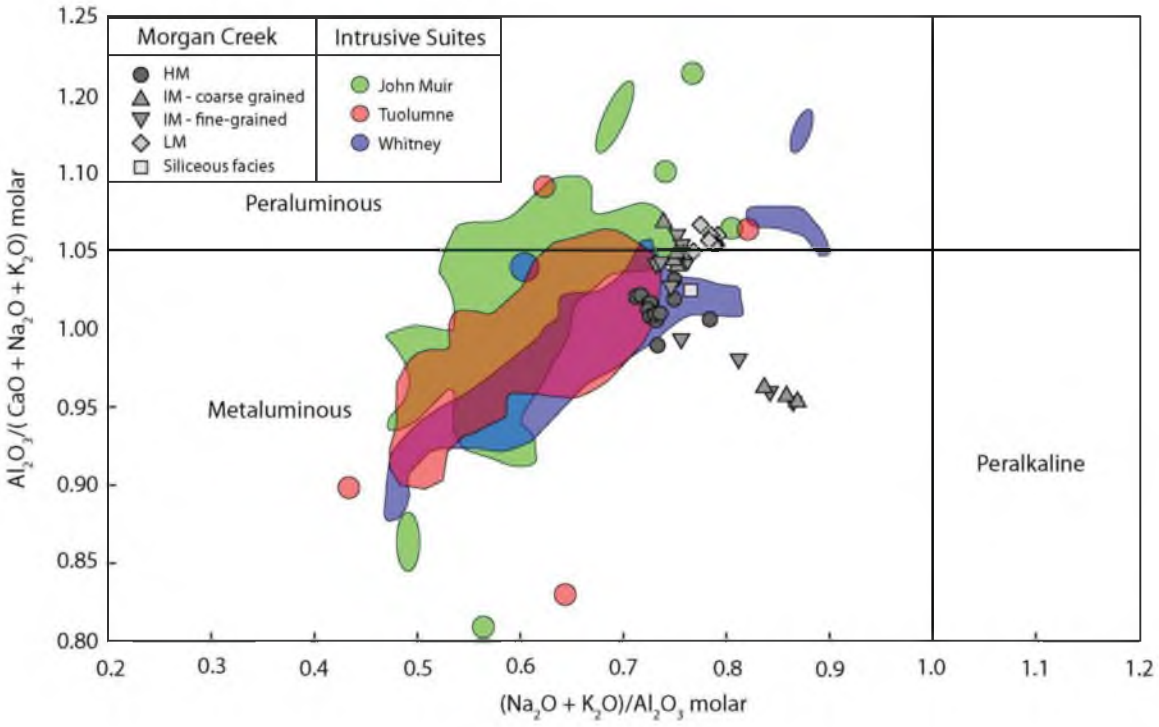

Figure 4.10. A/CNK vs. A/NK plot of Morgan Creek rocks and fields representing the same intrusive suites as in Figure 4.8. Note that LM rocks plot as peraluminous, as do many samples of the older Morgan Creek data. The "tail" of data trending to the lower right of the plot are likely the result of alteration.

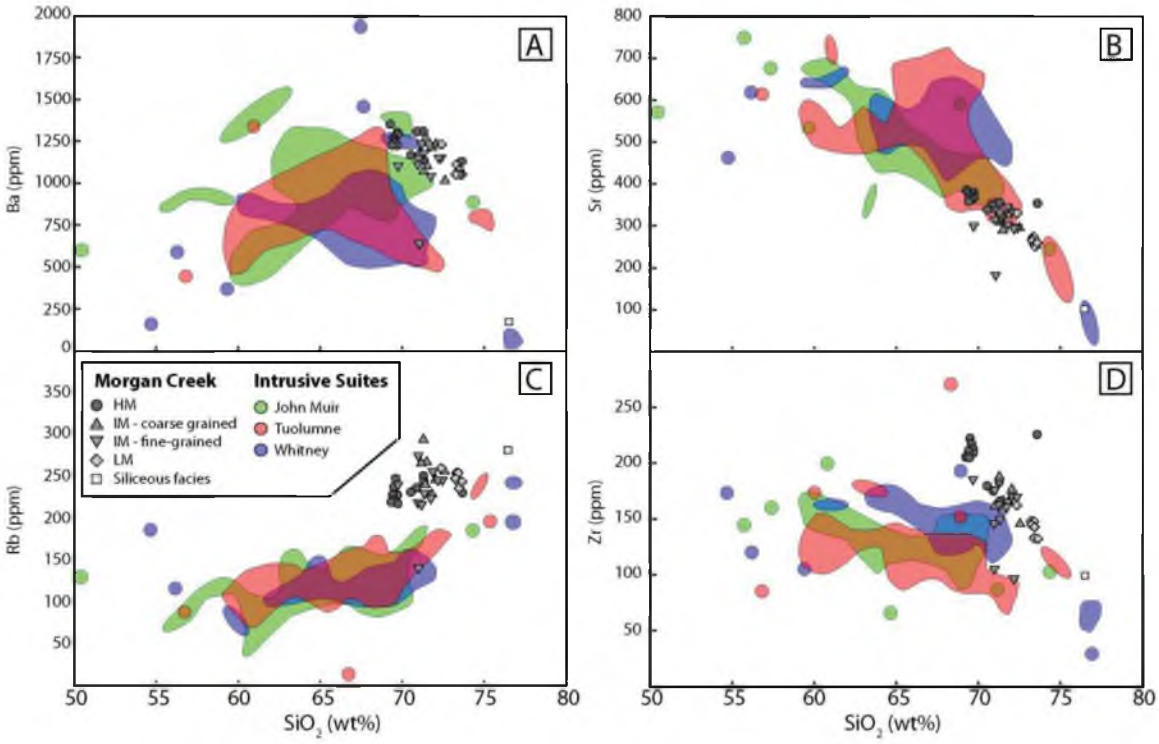

Figure 4.11. Trace element variation diagrams showing the relationship of the Morgan Creek rocks to rocks of the TIS, WIS, and Lamarck Granodiorite. Only Sr shows similar contents at equivalent SiO_2 as rocks of the intrusive suits. A. Ba vs. SiO_2. B. Sr vs. SiO_2. C. Rb vs. SiO_2. D. Zr vs. SiO_2.

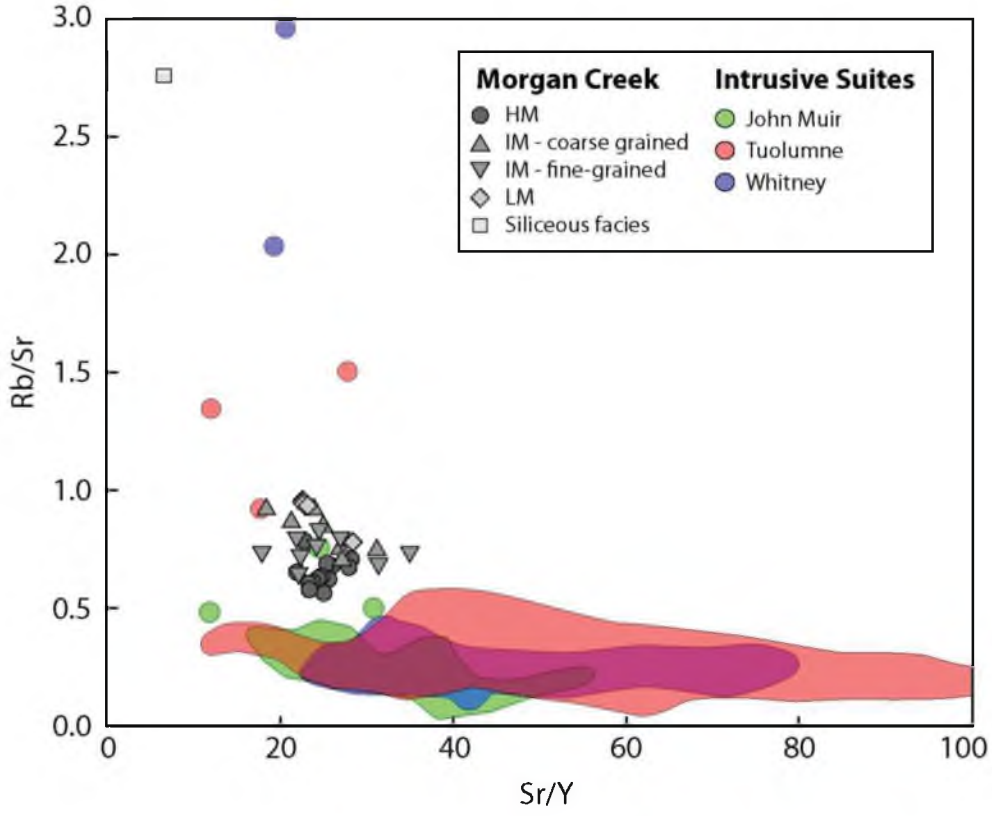

Figure 4.12. Rb/Sr vs. Sr/Y plot showing the rocks of the Morgan Creek pluton and samples from the Tuolumne and Whitney Intrusive Suites and the Lamarck Granodiorite (John Muir Intrusive Suite). Note the high Rb/Sr of the Morgan Creek main facies samples at similar Sr/Y of rocks of the intrusive suites. The sample of siliceous facies has an Rb/Sr comparable to the most evolved rocks of the intrusive suites.

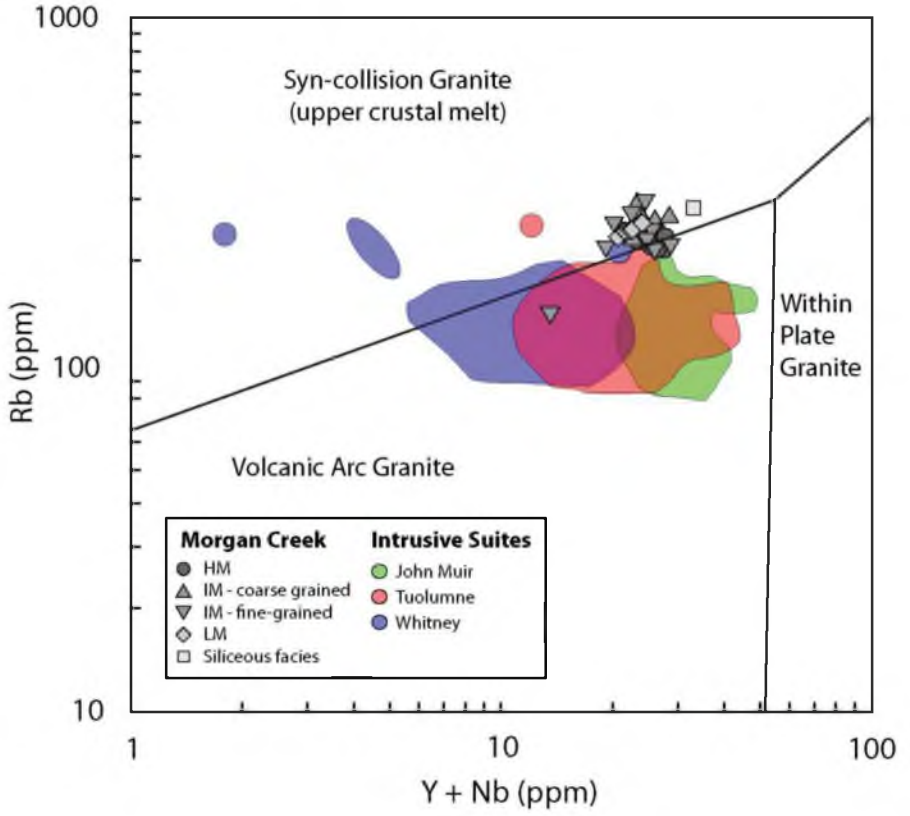

Figure 4.13. Plot of Rb vs. Y + Nb, with tectonic classification after Pearce et al., 1984. Morgan Creek rocks and fields showing the compositions of rocks from the TIS, WIS, and Lamarck Granodiorite. No data are available for other rocks of the JMIS. Most of the rocks from the Morgan Creek plot in the syn-collisional field, in contrast to the strong arc signature of the intrusive suites. Data for this figure and trace element figures below are from Gray et al. (2008: Tuolumne Intrusive Suite), Hirt (2007: Whitney Intrusive Suite), and Frost and Mahood (1987: John Muir Intrusive Suite – Lamarck Granodiorite).

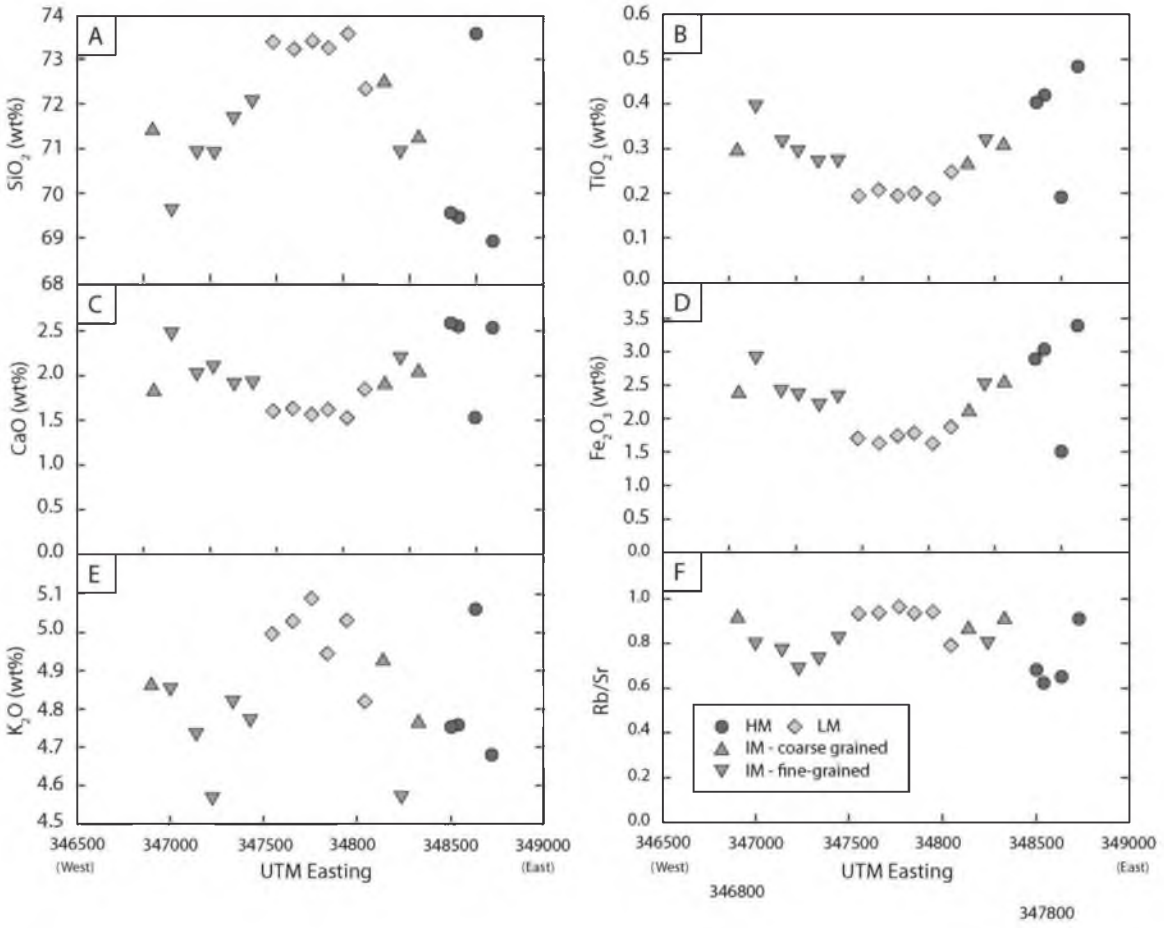

Figure 4.14. East-west variations in whole rock geochemistry across the Pine Creek traverse. All elements show a similar trend towards more evolved rocks in the central LM rocks.

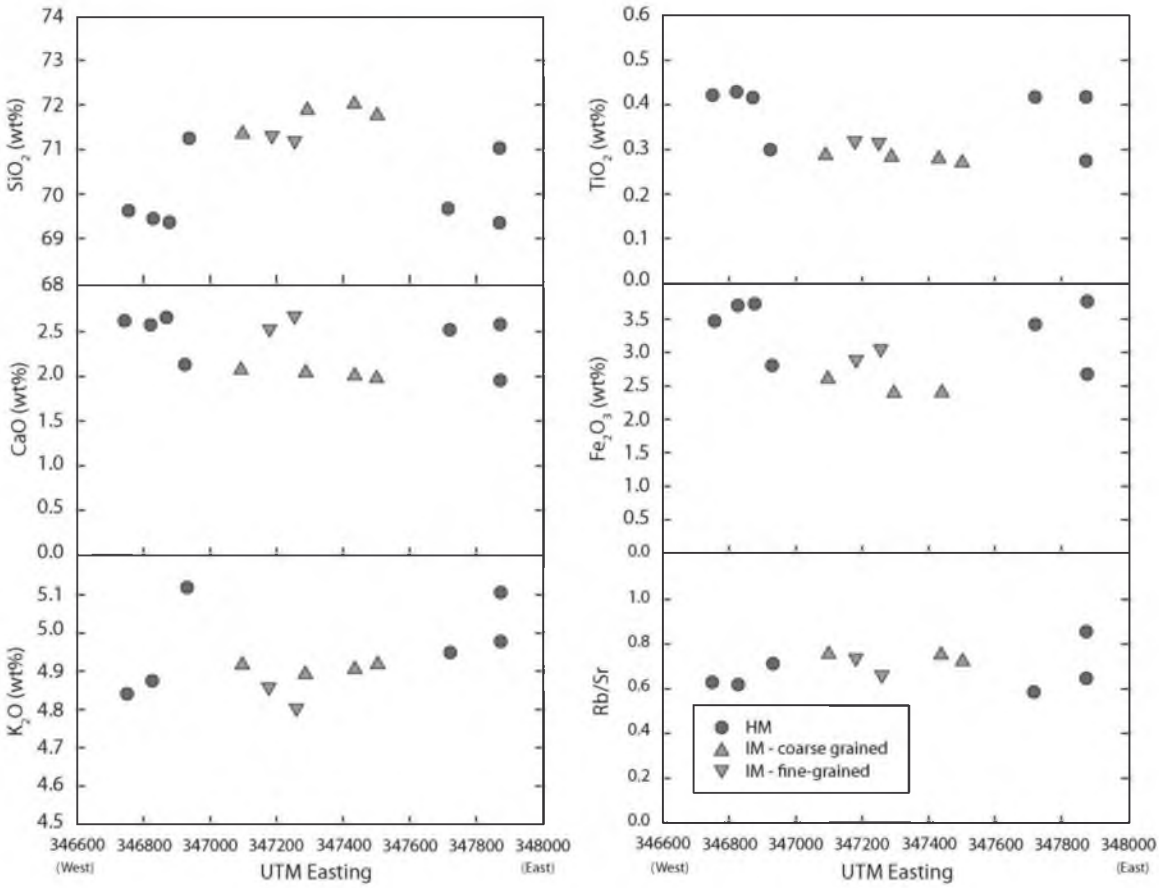

Figure 4.15. East-west variations in whole rock geochemistry across the Bear Lake traverse. As with the Pine Creek traverse, rocks become more evolved away from the contacts, although the trends are not as smooth as in the Pine Creek traverse.

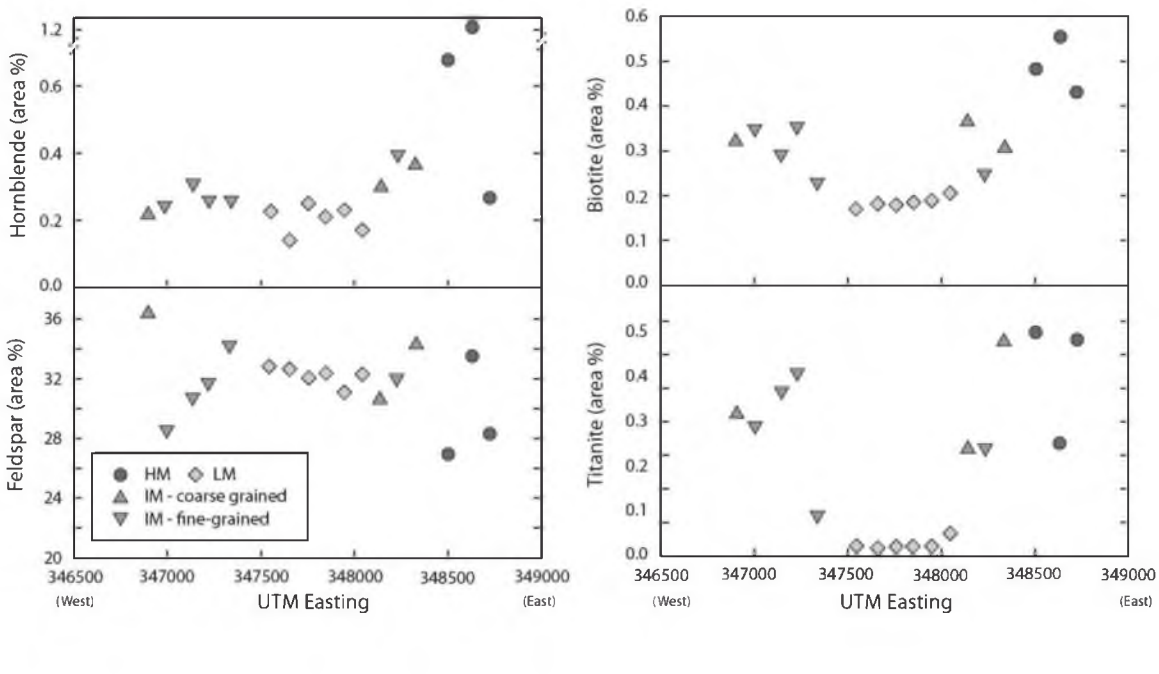

Figure 4.16. East-west variations in mineralogy across the Pine Creek traverse.

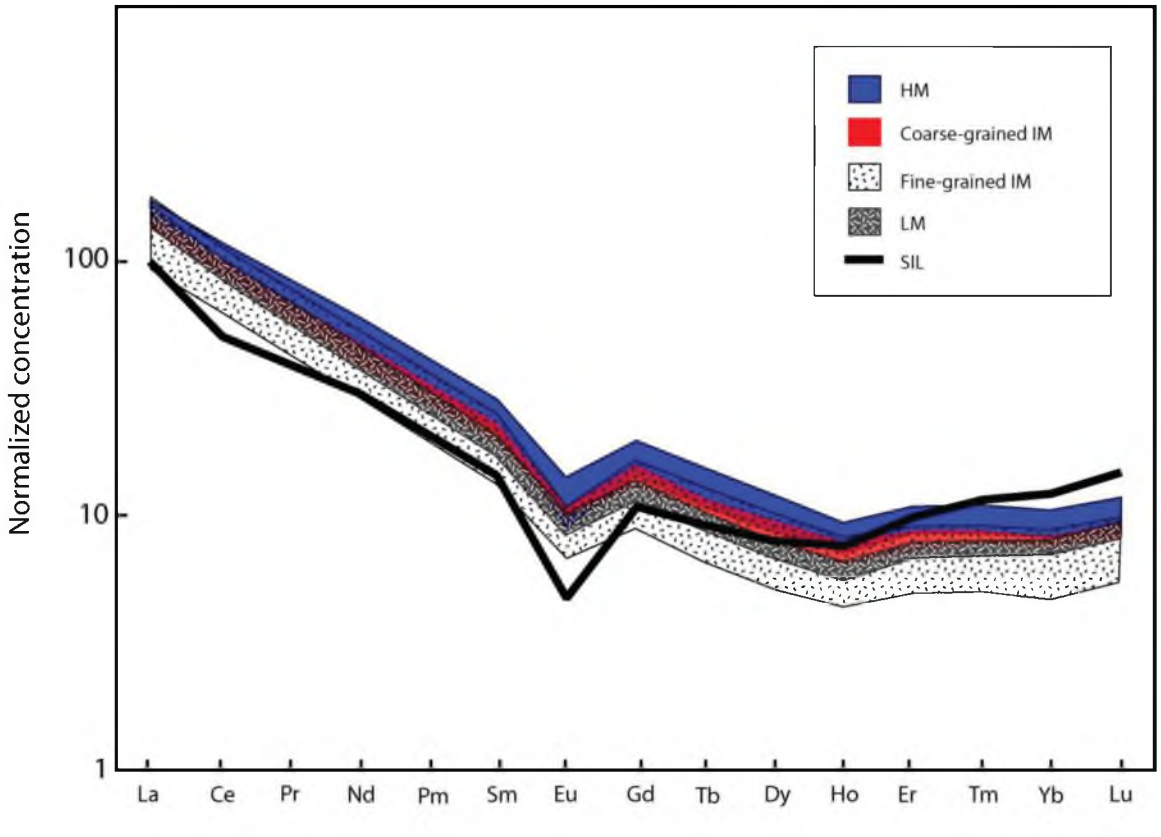

Figure 4.17. Normalized REE plots for rocks of the Morgan Creek pluton.

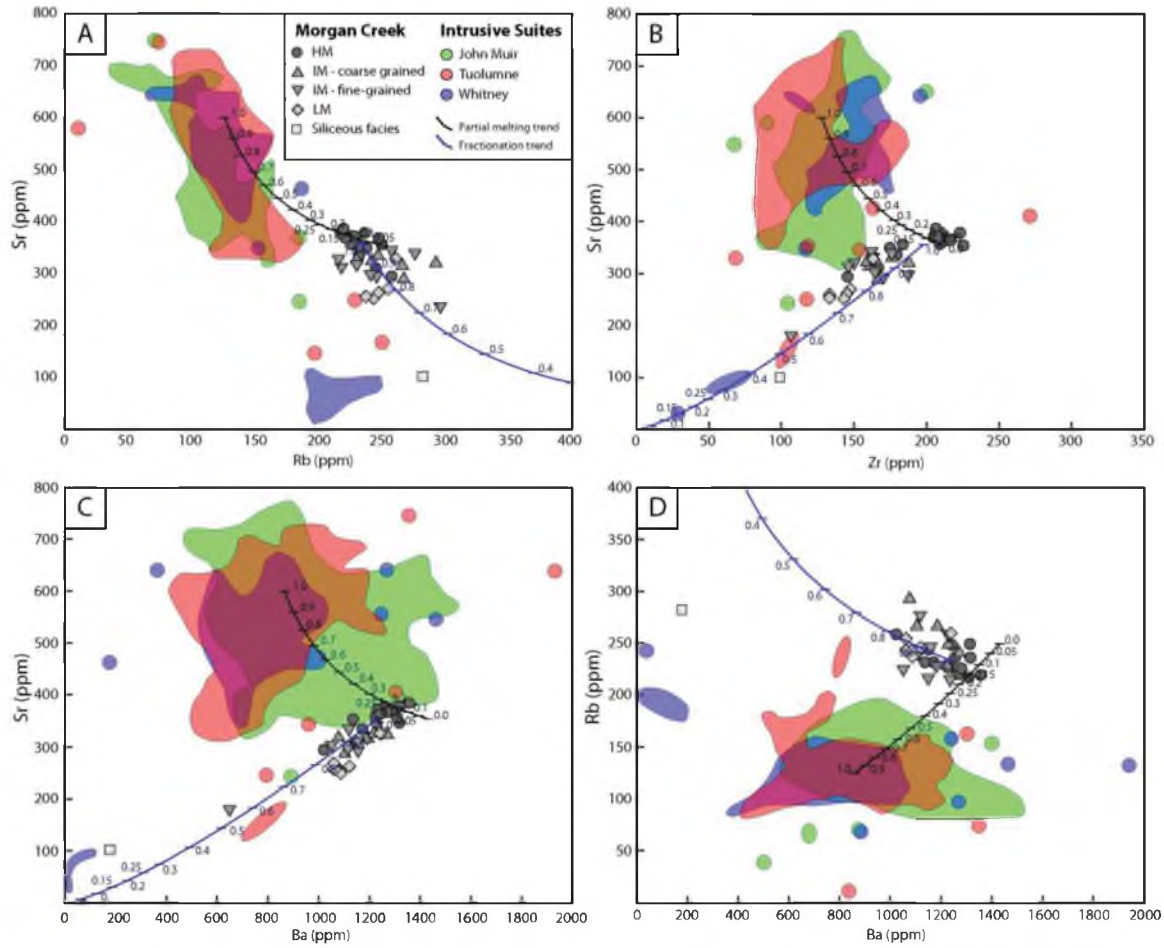

Figure 4.18. Bivariate plots of trace elements from the Morgan Creek pluton and the TIS, WIS, and Lamarck Granodiorite. Trace element models for batch partial melting of modified average composition of rocks from all samples from the intrusive suites, in an effort to represent "average" Sierran arc rocks. A starting value of 600 ppm Sr is used, rather than the bulk average of 510 ppm. The fractional crystallization model starts at average high mafic Morgan Creek composition on all panels. Melt fraction is displayed by the numbers adjacent to both the batch partial melting and fractional crystallization trends. The general compositional trend for the intrusive suites is shown by the red arrow. A. Sr-Rb variation and model. B. Sr-Zr variation and model. The Zr contents may be off the fractionation trend because of zircon inheritance. C. Sr-Ba variation and model. D. Rb-Ba variation and model.

Figure 4.19. Comparison at identical scales of the Morgan Creek pluton (A), the lobes of the porphyrytic (B) and equigranular (C) Half Dome Granodiorite of the Tuolumne Intrusive Suite (modified from Memeti et al., 2010), and the cycles of the main body of the Half Dome Granodiorite (D; modified from Coleman et al., 2012). The scales and compositional variations (more silicic interiors) in these bodies are similar, suggesting similar processes involved in the creation of the compositional patterns. See text for discussion.

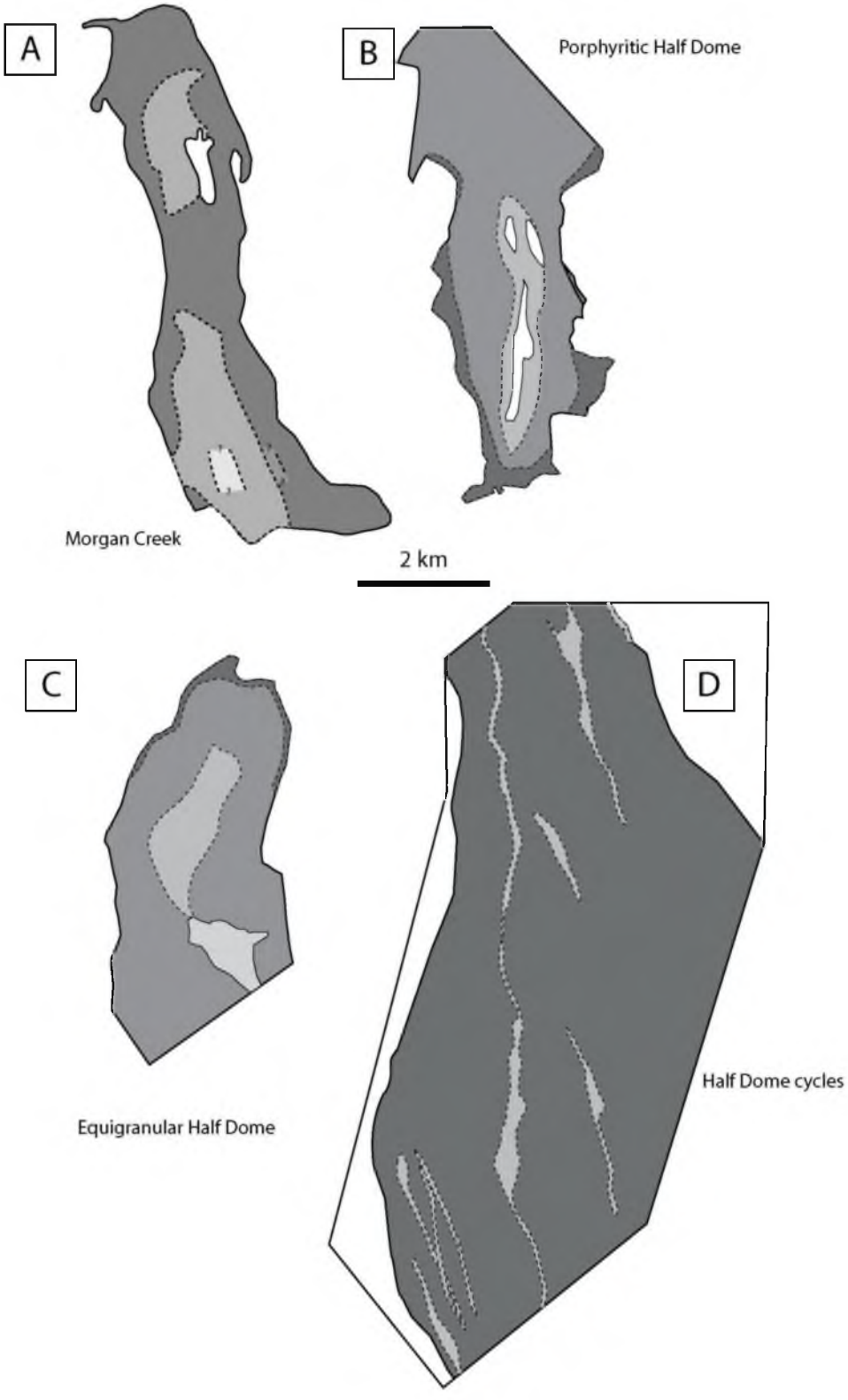
A
B
Porphyritic Half Dome
Morgan Creek
2 km
C
D
Equigranular Half Dome
Half Dome cycles

Table 4.1. Intrusions in the John Muir Intrusive Suite

Unit Name	Prominent Rock type(s)	Color Index - range (avg.)	Age (Ma)	References
Inconsolable pluton	Granodiorite, granite, quartz diorite	1 - 44 (~20)	95.45	Hathaway, 2002; Davis et al., 2012
McDoogle pluton	Quartz monzodiorite, quartz monzonite	16 - 27 (~25)	~95	Mahan et al., 2003; Stearns, 2009; Davis et al., 2012
Morgan Creek pluton	Granite	2 - 9 (~5)	~94	Cray, 1981; Porter et al., 2011; this study
Lamarck Granodiorite	Granodiorite, granite	4 - 24 (16)	94.26 - 90.9	Gracely, 2007; Davis et al., 2012
Round Valley Peak Granodiorite	Granodiorite	5 - 15 (~9)	89.03	Bateman, 1992; Davis et al., 2012
Lake Edison Granodiorite	Granodiorite, granite	1 - 18 (~10)	88.76	Bateman, 1992; Davis et al., 2012
Mono Creek Granite	Granite	2 - 16 (~5)	87.24 (to ~83.5)	Bateman, 1992; Davis et al., 2012

Table 4.2. QEMSCAN Modal data

					High Mafic (HM)
Sample	MC-11	MC-12	MC-14	MC-27	MC-42
Traverse	BL		BL	BL	BL
Easting	346751	346876	347873	347720	347010
Northing	4137382	4137361	4137366	4137262	4137368
elev	10218	10213	10117	9942	10171
Quartz	26.1	26.6	26.0	23.5	26.3
Feldspar	32.0	24.2	28.6	30.3	29.9
Plagioclase	34.5	40.0	35.0	38.4	35.7
Amphibole	1.42	0.75	2.54	1.04	1.29
Biotite	3.47	5.45	4.64	4.05	3.38
Chlorite	1.54	1.63	1.76	1.79	1.74
Magnetite	0.48	0.5	0.38	0.19	0.86
Apatite	0.08	0.16	0.13	0.13	0.14
Epidote	0.16	0.09	0.4	0.05	0.07
Titanite	0.21	0.53	0.41	0.41	0.52
Fe-Ti Oxides	nd	nd	0.01	nd	0.01
Zircon	0.05	0.02	0.06	0.02	0.04
Others	0.07	0.04	0.06	0.05	0.11
bio:hbl	3.5	9.4	2.5	5.6	4.0

MC-48 PC	MC-49 PC	MC-51 PC
348726	348635	348504
4135764	4135718	4135562
8995	9118	9290
29.7	27.4	29.8
28.4	33.6	27.0
33.6	29.7	34.0
0.27	1.21	0.68
4.32	5.54	4.83
2.94	1.79	2.38
nd	0.01	0.08
0.1	0.11	0.11
0.01	0.26	0.44
0.48	0.25	0.5
nd	nd	nd
0.05	0.01	0.03
0.14	0.18	0.12
26.9	6.1	10.6

Table 4.2 (cont.).

	Coarse-Grained Intermediate-Mafic (IM)				
Sample	MC-13	MC-15	MC-71	MC-53	MC-55
Traverse	BL	BL	PC	PC	PC
Easting	347436	347504	346905	348331	348143
Northing	4137635	4137319	4135180	4135435	4135424
elev	10215	9825	9944	9517	9684
Quartz	28.1	28.9	27.1	29.3	29.0
Feldspar	32.8	31.3	36.4	34.4	30.7
Plagioclase	34.0	34.1	30.9	29.4	33.3
Amphibole	0.15	0.28	0.22	0.37	0.3
Biotite	2.75	2.87	3.25	3.11	3.71
Chlorite	1.54	1.71	1.21	2.22	2.19
Magnetite	0.26	0.37	0.43	0.42	0.35
Apatite	0.1	0.04	0.05	0.09	0.09
Epidote	0.08	0.07	0.01	0.06	0.03
Titanite	0.14	0.3	0.32	0.48	0.24
Fe-Ti Oxides	nd	nd	nd	nd	0.01
Zircon	0.04	0.04	0.03	0.03	0.05
Others	0.07	0.06	0.05	0.05	0.04
bio:hbl	28.6	16.4	20.3	14.4	19.7

Table 4.2 (cont.).

	Fine Grained Intermediate Mafic (IM)						
Sample	MC-54	MC-63A	MC-63B	MC-65	MC-66	MC-25	MC-24
Traverse	PC	PC	PC	PC	PC	BL	BL
Easting	348234	347338	347228	347142	347002	347182	347258
Northing	4135395	4135343	4135330	4135318	4135279	4137350	4137523
elev	9584	10127	10165	10024	9997	9978	10273
Quartz	29.5	25.2	28.6	28.4	29.8	29.7	29.4
Feldspar	31.9	34.2	31.7	30.8	28.6	31.5	32.8
Plagioclase	32.9	36.1	32.9	34.7	35.5	32.9	32.3
Amphibole	0.39	0.26	0.26	0.31	0.25	0.48	0.3
Biotite	2.51	2.31	3.56	2.92	3.55	2.35	2.35
Chlorite	2.03	1.4	1.89	1.95	1.66	2.29	2.14
Magnetite	0.3	0.32	0.43	0.33	0.27	0.23	0.27
Apatite	0.05	0.07	0.06	0.07	0.04	0.05	0.05
Epidote	0.1	0.02	0.07	0.1	0.06	0.11	0.07
Titanite	0.24	0.09	0.41	0.37	0.29	0.28	0.21
Fe-Ti Oxides	nd	nd	nd	nd	0.01	nd	nd
Zircon	0.01	0.02	0.04	0.02	0.03	0.02	0.03
Others	0.09	0.06	0.06	0.06	0.05	0.06	0.06
bio:hbl	11.6	14.3	21.0	15.7	20.8	9.7	15.0

Table 4.2 (cont.).

	Fine Grained Low Mafics (LM)					
Sample	MC-56	MC-57	MC-58	MC-59	MC-60	MC-61
Traverse	PC	PC	PC	PC	PC	PC
Easting	348046	347951	347850	347759	347659	347550
Northing	4135421	4135372	4135400	4135405	4135388	4135373
elev	9763	9852	9907	10020	10094	10076
Quartz	31.5	33.3	31.1	30.4	31.1	33.5
Feldspar	32.3	31.2	32.4	32.1	32.6	32.8
Plagioclase	32.0	31.4	32.3	33.4	32.4	30.3
Amphibole	0.17	0.23	0.21	0.25	0.14	0.23
Biotite	2.06	1.86	1.84	1.81	1.83	1.71
Chlorite	1.34	1.66	1.78	1.53	1.45	1.04
Magnetite	0.18	0.2	0.17	0.26	0.23	0.24
Apatite	0.05	0.04	0.02	0.03	0.01	0.04
Epidote	0.05	0.05	0.01	0.07	0.05	0.02
Titanite	0.05	0.02	0.02	0.02	0.01	0.02
Fe-Ti Oxides	0.05	0.06	0.08	0.06	0.09	0.05
Zircon	0.02	0.03	0.03	0.05	0.03	0.03
Others	0.1	0.03	0.04	0.07	0.07	0.04
bio:hbl	20.0	15.3	17.2	13.4	23.4	12.0

Table 4.2 (cont.).

	Northern Fine Gr.	Siliceous Facies	Enclaves			
Sample	MC-18	MC-39	MC-10	MC-27E	MC-41E	MC-41H
Traverse						
Easting	347000	347557	346751	347720	347010	347010
Northing	4141392	4139647	4137382	4137262	4137368	4137368
elev	13207	11565	10218	9942	10171	10171
Quartz	29.6	40.7	3.5	15.9	7.6	25.4
Feldspar	29.8	30.9	23.2	11.1	16.3	26.4
Plagioclase	33.1	25.9	39.6	44.8	36.5	38.8
Amphibole	0.79	0.08	27.18	12.29	21.2	1.88
Biotite	3.54	1.25	2.91	10.13	9.86	4.4
Chlorite	2.17	0.8	1.71	3.87	5.9	1.85
Magnetite	0.25	0.24	0.06	0.1	0.11	0.34
Apatite	0.09	0.02	0.3	0.33	0.46	0.16
Epidote	0.29	0.01	0.46	0.55	0.9	0.24
Titanite	0.32	0.01	0.97	0.85	1.04	0.45
Fe-Ti Oxides	nd	0.03	nd	nd	nd	0.01
Zircon	0.04	0.01	0.08	0.04	0.06	0.02
Others	0.04	0.07	0.06	0.02	0.16	0.06
bio:hbl	7.2	25.6	0.2	1.1	0.7	3.3

nd = not detected

Table 4.3. Geochemical analyses of the Morgan Creek pluton.

	High Mafic (HM)										
Sample	MC-11	MC-12	MC-14	MC-27	MC-42	MC-49	MC-51	MC-16	MC-35	MC-38	MC-43
Traverse	BL		BL	BL	BL	PC	PC				BL
Easting	346751	346876	347873	347720	347010	348635	348504	347941	348581	347561	346931
Northing	4137382	4137361	4137366	4137262	4137368	4135718	4135562	4136964	4134997	4139611	4137365
elev	10218	10213	10117	9942	10171	9118	9290	9700	9539	11598	10240
Normalized major elements											
SiO2	69.7	69.4	69.4	69.7	70.5	73.6	69.6	69.7	70.9	71.3	71.3
TiO2	0.42	0.42	0.42	0.42	0.34	0.19	0.40	0.42	0.33	0.31	0.30
Al2O3	14.94	15.07	14.94	14.89	14.77	14.12	15.11	15.07	14.89	14.54	14.53
Fe2O3	3.02	3.22	3.27	2.98	2.57	1.52	2.90	2.75	2.47	2.52	2.41
MnO	0.07	0.10	0.10	0.09	0.10	0.07	0.06	0.07	0.05	0.08	0.04
MgO	1.01	1.03	1.00	0.99	0.86	0.37	0.98	0.99	0.76	0.73	0.62
CaO	2.59	2.64	2.56	2.51	2.30	1.53	2.59	2.58	2.18	2.15	2.09
Na2O	3.46	3.57	3.37	3.47	3.46	3.44	3.47	3.56	3.56	3.47	3.63
K2O	4.73	4.50	4.88	4.85	4.97	5.06	4.75	4.77	4.81	4.79	5.02
P2O5	0.10	0.10	0.12	0.10	0.10	0.05	0.12	0.12	0.10	0.09	0.08
Totals	100.00	100.00	100.00	100.00	100.00	100.00	100.00	100.00	100.00	100.00	100.00
LOI	0.51	0.56	0.46	0.45	0.53	0.38	0.52	0.47	0.68	0.45	0.45
Analytical	100.41	100.08	99.62	99.25	99.24	99.34	98.65	97.73	100.07	99.75	99.44
Trace elements used in modeling											
Ba	*1285*		1230	*1307*	*1172*	1135	1245		*1314*	*1143*	*1313*
Rb	*227*		226	*218*	*231*	231	248		*236*	*245*	*250*
Sr	*369*		358	*379*	*337*	354	365		*349*	*312*	*356*
Zr	*209*		210	*209*	*180*	226	217		*175*	*167*	*184*

Table 4.3 (cont.)..

Sample	MC-11	MC-12	MC-14	MC-27	MC-42	MC-49
V	*47*		47	*48*	*42*	53
Ni	*5*		5	*4*	*4*	6
Zn	*30*		68	*34*	*27*	53
Cu	*13*		93	*11*	*8*	18
Sn			2			1
Ga	*15*		18.3	*15*	*14*	19.1
Y	*16*		14.6	*16*	*13*	16.2
Nb	*11*		10.3	*11*	*10*	11.5
Cs			7.78			5.39
La	*27*		37.3	*31*	*28*	41.3
Ce	*59*		64.7	*65*	*59*	72.5
Pr			7.06			7.99
Nd	*31*		24.7	*30*	*25*	27.6
Sm	*7*		4	*7*	*7*	4.36
Eu			0.74			0.76
Gd			3.65			4.05
Tb			0.5			0.57
Dy			2.57			3.04
Ho			0.48			0.53
Er			1.51			1.76
Tm			0.24			0.26
Yb			1.41			1.75
Lu			0.22			0.27
Hf			6			7.2
Ta			1.2			1.5
Tl			0.8			0.8
Pb	*19*		19	*18*	*18*	20
Th	*22*		20.2	*21*	*21*	24.5
U	*6*		4.57	*5*	*7*	6.74

MC-51	MC-16	MC-35	MC-38	MC-43
50		*31*	*35*	*57*
6		*2*	*3*	*5*
52		*24*	*23*	*35*
12		*5*	*8*	*10*
1				
18.5		*14*	*13*	*15*
14.2		*13*	*14*	*13*
10.3		*10*	*11*	*11*
5.59				
35.3		*29*	*23*	*32*
60.3		*64*	*48*	*61*
6.61				
23.3		*32*	*21*	*23*
3.84		*7*	*7*	*7*
0.81				
3.58				
0.52				
2.67				
0.49				
1.54				
0.23				
1.49				
0.24				
7				
1.4				
0.9				
19		*19*	*21*	*20*
17.1		*25*	*26*	*23*
6.07		*6*	*8*	*7*

	High Mafic (HM)			
Sample	MC-44	MC-50	MC-67	MC-68
Traverse	BL	PC		
Easting	346828	348541	347713	347712
Northing	4137373	4135661	4137982	4137847
elev	10194	9216	10511	10511
Normalized major elements				
SiO2	69.5	69.5	69.3	69.7
TiO2	0.43	0.42	0.42	0.40
Al2O3	14.91	14.96	15.07	14.87
Fe2O3	3.21	3.04	3.08	2.95
MnO	0.06	0.09	0.07	0.04
MgO	1.05	1.02	1.03	0.98
CaO	2.55	2.56	2.62	2.71
Na2O	3.44	3.55	3.53	3.49
K2O	4.77	4.76	4.77	4.77
P2O5	0.10	0.10	0.11	0.11
Totals	100.00	100.00	100.00	100.00
LOI	0.45	0.50	0.52	0.54
Analytical	99.97	99.77	99.04	99.85
Trace elements used in modeling				
Ba	*1267*	1255	*1355*	1230
Rb	*221*	236	*219*	228
Sr	*368*	378	*385*	372
Zr	*205*	223	*205*	212

Table 4.3 (cont.).

Coarse-Grained Intermediate Mafic (IM)						
MC-13	MC-15	MC-71	MC-53	MC-55	MC-28	MC-40
BL	BL	PC	PC	PC		BL
347436	347504	346905	348331	348143	347549	347099
4137635	4137319	4135180	4135435	4135424	4137415	4137369
10215	9825	9944	9517	9684	10111	10049
72.1	71.8	71.5	71.3	72.6	71.2	71.4
0.28	0.27	0.30	0.31	0.27	0.28	0.29
14.54	14.56	14.10	14.61	14.39	14.55	14.74
2.09	2.26	2.40	2.55	2.12	2.15	2.29
0.06	0.07	0.09	0.06	0.04	0.08	0.07
0.61	0.61	0.59	0.69	0.52	0.64	0.64
1.99	1.96	1.85	2.06	1.91	2.07	2.07
3.49	3.54	4.25	3.56	3.23	4.37	3.56
4.80	4.82	4.87	4.77	4.93	4.61	4.81
0.09	0.09	0.04	0.10	0.02	0.04	0.08
100.00	100.00	100.00	100.00	100.00	100.00	100.00
0.50	0.57	0.38	0.58	0.35	0.45	0.45
99.25	100.47	100.41	99.75	98.53	98.54	99.49
1235	*1218*	*1104*	1075	1025		*1270*
247	*230*	*267*	293	258		*242*
333	*325*	*290*	321	295		*324*
176	*164*	*167*	188	146		*159*

Table 4.3 (cont.).

Sample	MC-44	MC-50	MC-67	MC-68	MC-13	MC-15
V	*49*	55	*45*	52	27	*26*
Ni	*5*	7	*5*	6	<5	*2*
Zn	*34*	53	*28*	53	54	*19*
Cu	*10*	11	*13*	23	7	*6*
Sn		2		1	1	
Ga	*15*	20.2	*14*	19.3	17.4	*14*
Y	*16*	15.5	*15*	14.6	12.4	*12*
Nb	*11*	11.2	*11*	10.4	11.1	*11*
Cs		3.89		7.26	7.54	
La	*30*	38.9	*29*	33.7	31.8	*28*
Ce	*64*	67.6	*63*	59.9	54.4	*58*
Pr		7.41		6.7	5.49	
Nd	*31*	26.1	*31*	24.1	18.6	*25*
Sm	*7*	4.17	*7*	3.96	2.98	*7*
Eu		0.77		0.76	0.61	
Gd		3.93		3.58	2.73	
Tb		0.55		0.5	0.39	
Dy		2.86		2.7	2.04	
Ho		0.52		0.48	0.37	
Er		1.79		1.6	1.24	
Tm		0.25		0.24	0.2	
Yb		1.66		1.54	1.3	
Lu		0.27		0.25	0.21	
Hf		7.3		6.8	5.2	
Ta		1.4		1.3	1.7	
Tl		0.8		0.7	0.9	
Pb	*19*	20	*17*	19	23	*22*
Th	*23*	23.7	*20*	24.5	25.6	*25*
U	*7*	5.85	*6*	4.63	5.51	*6*

MC-71	MC-53	MC-55	MC-28	MC-40
26	38	28		*39*
3	<5	<5		*3*
18	47	39		*18*
11	12	9		*7*
	1	1		
13	18.4	17.1		*14*
16	13.4	13.9		*10*
13	10.3	11.8		*11*
	6.67	5.7		
28	35.9	37.6		*23*
59	61.8	55.8		*45*
	6.55	6.26		
28	22.3	21.1		*19*
8	3.53	3.2		*7*
	0.6	0.52		
	3.21	2.97		
	0.43	0.41		
	2.41	2.22		
	0.44	0.41		
	1.42	1.42		
	0.22	0.22		
	1.4	1.46		
	0.24	0.25		
	6.3	5.1		
	1.5	2.1		
	1	0.9		
19	29	24		*23*
25	31.7	27.2		*26*
9	8.06	9.95		*8*

Table 4.3 (cont.).

Fine Grained Intermediate Mafic (IM)

Sample	MC-54	MC-63A	MC-63B	MC-65	MC-66	MC-25	MC-24	MC-62
Traverse	PC	PC	PC	PC	PC	BL	BL	PC
Easting	348234	347338	347228	347142	347002	347182	347258	347437
Northing	4135395	4135343	4135330	4135318	4135279	4137350	4137523	4135368
elev	9584	10127	10165	10024	9997	9978	10273	10092
Normalized major elements								
SiO2	71.0	71.8	71.0	71.0	69.7	71.3	71.2	72.2
TiO2	0.32	0.27	0.30	0.32	0.40	0.32	0.32	0.28
Al2O3	14.81	14.68	14.67	14.40	14.90	14.52	14.59	14.27
Fe2O3	2.53	2.24	2.37	2.45	2.93	2.51	2.65	2.36
MnO	0.10	0.06	0.08	0.09	0.05	0.10	0.08	0.10
MgO	0.74	0.61	0.65	0.65	0.93	0.70	0.73	0.59
CaO	2.20	1.92	2.11	2.03	2.49	2.21	2.24	1.93
Na2O	3.63	3.54	4.23	4.26	3.65	3.46	3.40	3.47
K2O	4.57	4.82	4.57	4.74	4.86	4.75	4.70	4.78
P2O5	0.08	0.08	0.04	0.04	0.09	0.10	0.09	0.07
Totals	100.00	100.00	100.00	100.00	100.00	100.00	100.00	100.00
LOI	0.56	0.41	0.56	0.59	0.36	0.57	0.43	0.48
Analytical	98.95	99.52	100.54	100.34	98.81	100.04	99.19	100.17
Trace elements used in modeling								
Ba	1120	1225	1150	649	1110	*1185*	1235	1155
Rb	276	257	218	141.5	240	*230*	216	246
Sr	340	345	314	182	299	*318*	328	295
Zr	176	162	146	106	187	*150*	163	170

All major elements reported in wt%.
Trace elements reported in ppm

Table 4.3 (cont.).

Sample	MC-54	MC-63A	MC-63B	MC-65	MC-66
V	40	33	30	19	32
Ni	5	<5	<5	<5	<5
Zn	49	43	41	23	40
Cu	11	8	7	<5	6
Sn	1	1	1	1	1
Ga	18.7	19.6	17.1	10.3	18
Y	12.5	9.9	10.1	7.5	13.7
Nb	10.1	10.3	8.8	6.1	10.7
Cs	6.92	7.91	8.37	4.53	9.33
La	34.8	40.5	37.2	22.1	39.9
Ce	59.3	64.7	61.2	38.9	67.8
Pr	6.28	6.77	6.39	4.09	7.27
Nd	21.4	21.9	21	13.7	24.7
Sm	3.43	3.2	3.01	2.02	3.79
Eu	0.6	0.59	0.59	0.4	0.62
Gd	3.03	2.72	2.58	1.86	3.37
Tb	0.42	0.36	0.34	0.25	0.48
Dy	2.19	1.79	1.81	1.32	2.6
Ho	0.39	0.33	0.32	0.25	0.46
Er	1.33	1.08	1.1	0.83	1.5
Tm	0.19	0.15	0.17	0.13	0.23
Yb	1.29	1.11	1.1	0.81	1.5
Lu	0.21	0.18	0.19	0.14	0.25
Hf	5.9	5.4	4.8	3.5	6.2
Ta	1.7	1.8	1.6	1	1.7
Tl	1	1.1	0.8	<0.5	0.9
Pb	24	23	21	13	23
Th	32.5	26.6	26.2	17.55	30.7
U	10.1	9.37	7.91	5.02	8.08

MC-25	MC-24	MC-62
29	39	29
3	<5	<5
23	44	42
8	10	9
	1	1
12	16.7	18.2
14	14.7	12.1
11	11.3	12.8
	4.49	7.99
28	35.2	42.4
59	60.4	70.7
	6.32	7.25
29	21.7	23.9
7	3.55	3.38
	0.69	0.6
	3.32	3
	0.47	0.39
	2.58	2.07
	0.46	0.4
	1.54	1.36
	0.24	0.2
	1.59	1.43
	0.25	0.24
	5.1	5.7
	1.8	1.9
	0.8	1
23	23	24
24	24.7	28.1
9	7.56	10.2

Table 4.3 (cont.).

Fine Grained Low Mafic						
Sample	MC-56	MC-57	MC-58	MC-59	MC-60	MC-61
Traverse	PC	PC	PC	PC	PC	PC
Easting	348046	347951	347850	347759	347659	347550
Northing	4135421	4135372	4135400	4135405	4135388	4135373
elev	9763	9852	9907	10020	10094	10076
Normalized major elements						
SiO2	72.4	73.6	73.3	73.5	73.3	73.4
TiO2	0.25	0.19	0.20	0.20	0.21	0.20
Al2O3	14.54	14.07	14.18	14.04	14.21	14.07
Fe2O3	1.86	1.62	1.78	1.74	1.62	1.71
MnO	0.08	0.03	0.08	0.09	0.08	0.08
MgO	0.52	0.36	0.40	0.39	0.38	0.39
CaO	1.85	1.53	1.62	1.57	1.63	1.60
Na2O	3.62	3.47	3.43	3.37	3.50	3.46
K2O	4.82	5.03	4.95	5.09	5.03	5.00
P2O5	0.08	0.05	0.07	0.06	0.06	0.05
Totals	100.00	100.00	100.00	100.00	100.00	100.00
LOI	0.32	0.39	0.49	0.36	0.32	0.36
Analytical	99.43	98.61	99.66	100.21	98.73	99.79
Trace elements used in modeling						
Ba	1240	1060	1060	1085	1115	1085
Rb	261	244	255	243	247	237
Sr	330	259	272	252	263	255
Zr	163	133	148	143	145	133

	Siliceous Facies	Altered HM	
MC-18	MC-39	MC-52 PC	MC-48 PC
347000	347557	348415	346905
4141392	4139647	4135495	4135180
13207	11565	9402	9944
71.8	76.5	64.6	69.0
0.30	0.10	0.39	0.48
14.42	12.79	18.59	15.26
2.32	1.07	2.45	3.39
0.07	0.06	0.04	0.06
0.62	0.18	0.97	1.13
2.08	1.04	2.63	2.54
3.57	3.48	4.02	3.36
4.75	4.76	6.19	4.68
0.09	0.05	0.11	0.12
100.00	100.00	100.00	100.00
0.33	0.36	0.49	0.77
99.67	99.65	98.47	99.67
1050	177.5	1545	1255
225	282	699	353
304	102	455	387
165	99	239	229

Table 4.3 (cont.).

Sample	MC-56	MC-57	MC-58	MC-59	MC-60	MC-61
V	27	15	19	15	16	15
Ni	<5	<5	<5	<5	<5	<5
Zn	41	25	26	36	25	29
Cu	9	15	11	9	7	7
Sn	1	1	1	1	1	1
Ga	19	15.7	16.3	15.4	16.3	15.4
Y	11.7	11.5	11.7	11.2	11.5	10.4
Nb	12.1	10.7	12.3	10.4	10.9	10.3
Cs	7.66	6.28	7.42	7.06	7.09	5.06
La	39.2	34.5	32.3	32.8	34	32.3
Ce	63	57.3	53	54.5	55.3	52.2
Pr	6.45	5.76	5.35	5.51	5.73	5.27
Nd	21.2	18.8	17.8	18.1	18.8	17.2
Sm	3.12	2.78	2.71	2.82	2.84	2.61
Eu	0.58	0.52	0.53	0.52	0.53	0.49
Gd	2.8	2.66	2.57	2.46	2.64	2.39
Tb	0.38	0.36	0.36	0.36	0.36	0.33
Dy	1.98	2	1.95	1.93	1.95	1.76
Ho	0.35	0.36	0.37	0.36	0.35	0.32
Er	1.24	1.26	1.29	1.22	1.23	1.14
Tm	0.18	0.2	0.2	0.2	0.19	0.18
Yb	1.29	1.34	1.35	1.28	1.29	1.22
Lu	0.21	0.23	0.24	0.22	0.22	0.21
Hf	5.5	4.8	5.3	4.8	5	4.6
Ta	2.3	2	3.1	2	2	2
Tl	0.9	1	1.1	0.9	1	0.9
Pb	27	32	32	28	30	26
Th	28.1	31.1	32.2	30.6	30.3	30.2
U	11.1	11.5	12.05	11	11.3	10.2

All major elements reported in wt%

Trace elements reported in ppm; XRF trace element data in italics

MC-18	MC-39	MC-52	MC-48
31	7	36	59
<5	<5	<5	7
42	30	108	75
7	82	156	6
1	1	6	<1
17	16.3	27.5	19
17	15.7	16.9	6.9
11.6	17.2	17.9	8.8
6.18	5.06	24.7	13.45
34	23.4	41	37.5
61.2	31.6	71.1	59.7
6.69	4.26	7.42	6.03
23.6	14.5	24.9	19.4
4.02	2.27	3.97	2.47
0.68	0.28	0.81	0.71
3.57	2.26	3.8	2.4
0.53	0.35	0.53	0.27
2.88	2.07	2.85	1.23
0.52	0.44	0.52	0.22
1.74	1.66	1.75	0.79
0.26	0.3	0.28	0.11
1.75	2.12	1.78	0.82
0.29	0.38	0.3	0.15
5.2	4.5	7.7	7.1
2	3.1	1.8	0.8
0.8	0.9	2.8	1.2
23	31	32	20
26.8	32.7	26.2	13.7
6.76	23.7	6.48	4.37

Table 4.4. Trace element modeling parameters.

	Zr	Rb	Sr	Ba	
Batch partial melting					
Bulk partition coeff.	0.6	0.5	1.7	0.6	
Starting composition (ppm)	128	126	600	864	(Avg. of intrusive suites, increased Sr)
Fractional Crystallization					
Bulk partition coeff.	2.0	0.5	2.3	2.0	
Starting composition (ppm)	198	234	356	1234	(Avg. high mafic Morgan Creek)

References

Barth, A.P., Walker, J.D., Wooden, J.L., Riggs, N.R., and Schweickert, R.A., 2012, Birth of the Sierra Nevada magmatic arc: Early Mesozoic plutonism and volcanism in the east-central Sierra Nevada of California: Geosphere, v. 7, p. 877-897.

Bateman, P.C., 1965, Geology and tungsten mineralization of the Bishop district, California: USGS Professional Paper 470, 208 p.

Bateman, P.C., 1992, Plutonism in the central part of the Sierra Nevada batholith, California: USGS Professional Paper 1483, 186 p.

Bateman, P.C., Dodge, F.C.W., and Bruggman, P.E., 1984, Major oxide analyses, CIPW norms, modes, and bulk specific gravities of plutonic rocks from the Mariposa 1° x 2° sheet, central Sierra Nevada, California: USGS Open File Report 84-162, 50 p.

Bell, A.S. and Simon, A., 2011, Experimental evidence for the alteration of the $Fe^{3+}/\sum Fe$ of silicate melt caused by the degassing of chlorine-bearing aqueous volatiles: Geology, v. 39, p. 499-502.

Best, M.G., Christiansen, E.H., and Blank, R.H., 1989, Oligocene caldera complex and calc-alkaline tuffs and lavas of the Indian Peak volcanic field, Nevada and Utah: GSA Bulletin, v. 101, p. 1076-1090.

Best, M.G., Christiansen, E.H., Deino, A.L., Gromme, S., Hart, G.L., and Tingey, D.G., 2013, The 36–18 Ma Indian Peak–Caliente ignimbrite field and calderas, southeastern Great Basin, USA: Multicyclic super-eruptions: Geosphere, v. 9, p. 684-950.

Brown, P.E. and Essene, E.J., 1985, Activity variations attending tungsten skarn formation, Pine Creek, California: Contributions to Mineralogy and Petrology, v. 89, p. 358-369.

Brown, P.E., Bowman, J.R., and Kelly, W.C., 1985, Petrologic and stable isotope constraints on the source and evolution of skarn-forming fluids at Pine Creek, California: Economic Geology, v. 80, p. 72-95.

Burgisser, A. and Scaillet, B., 2007, Redox evolution of a degassing magma rising to the surface: Nature, v. 445, p. 194-197.

Cecil, M.R., Rotberg, G.L., Ducea, M.N., Saleeby, J.B., and Gehrels, G.E., 2012, Magmatic growth and batholithic root development in the northern Sierra Nevada, California: Geosphere, v. 8, p. 592-606.

Chappell, B.W., Bryant, C.J., and Wyborn, D., 2012, Peraluminous I-type granites: Lithos, v. 153, p. 142-153.

Chen, J.H., and Tilton, G.R., 1991, Applications of lead and strontium isotopic relationships to the petrogenesis of granitoid rocks, central Sierra Nevada batholith, California: Geological Society of America Bulletin, v. 103, p. 439–447.

Coleman, D.S. and Glazner A.F., 1998, The Sierra Crest magmatic event: Rapid formation of juvenile crust during the Late Cretaceous in California: *in* Ernst, W.G., and Nelson, C.A., eds., Integrated Earth and Environmental Evolution of the Southwestern United States; the Clarence A. Hall, Jr. volume. Bellwether Publishing, USA, pp. 253-272.

Coleman, D.S., Glazner, A.F., Miller, J.S., Bradford, K.J., Frost, T.P., Joye, J.L., and Bachl, C.A., 1995, Exposure of a Late Cretaceous layered mafic-felsic magma system in the central Sierra Nevada batholith, California: Contributions to Mineralogy and Petrology, v. 120, p. 129-136.

Coleman, D.S., Gray, W. and Glazner, A.F., 2004, Rethinking the emplacement and evolution of zoned plutons: Geochronologic evidence for incremental assembly of the Tuolumne Intrusive Suite, California: Geology, v. 32, p., 433–436.

Coleman, D.S., Bartley, J.M., Glazner, A.F., and Pardue, M.J., 2012, Is chemical zonation in plutonic rocks driven by changes in source magma composition or shallow crustal differentiation: Geospherre, v. 8 p. 1568-1587.

Cray, 1981, The geochemistry and petrology of the Morgan Creek pluton, Inyo County, California: Unpublished PhD thesis, University of California, Davis, 454 p.

Davis, J.W., Coleman, D.S., Gracely, J.T., Gaschnig, R., and Stearnes, M., 2012, Magma accumulation rates and thermal histories of plutons of the Sierra Nevada batholith, CA: Contributions to Mineralogy and Petrology, v. 163, p. 449-465.

Dilles, J.H., 1987, Petrology of the Yerington batholith, Nevada: Evidence for evolution of porphyry copper ore fluids: Economic Geology, v. 82, p. 1750-1789.

Eastoe, C., 1983, Sulfur isotope data and the nature of the hydrothermal systems at the Panguna and Frieda porphyry copper deposits, Papua new Guinea: Economic Geology, v. 78, p. 201-213.

Einaudi, M.T., Meinert, L.D., and Newberry, R.J., 1981, Skarn deposits: Economic Geology 75th Anniversary Volume, p. 317–391.

Frost, T.P. and Mahood, G.A., 1987, Field, chemical, and physical constraints on mafic-felsic magma interaction in the Lamarck Granodiorite, Sierra Nevada, California: GSA Bulletin, v. 99, p. 272-291.

Frost, T.P. and Mattinson, J.M., 1988, Late Cretaceous U-Pb age of a mafic intrusion from the eastern Sierra Nevada, California: Isohcron/West, no. 51, p. 15-18.

Frost, R.B., Barnes, C.G., Collins, W.J., Arculus, R.J., Ellis, D.J., and Frost, C.D., 2001, A geochemical classification for Granitic Rocks: Journal of Petrology, v. 42, p. 2033-2048.

Gaschnig, R.M., Coleman, D.S., and Glazner, A.F., 2006, Twin of the Tuolumne: New geochronology from the Mono Pass intrusive suite: GSA Abstracts With Programs, v. 38, p. 559.

Glazner, A.F., Coleman, D.S., and Bartley, J.M., 2008, The tenuous connection between high-silica rhyolites and granodiorite plutons: Geology, v. 36, p. 183-186.

Gray, R. F., Hoffman, V. J., Bagan, R. J., and McKinley, H. L., 1968, Bishop tungsten district, California: *in* Ridge, J. D., ed., Ore deposits of the United States, 1933-1967 (Graton-Sales vol.): New York, Am. Institute of Mining Metallurgy and Petroleum Engineers, p. 1531-1554.

Gray, W., Glazner, A.F., Coleman, D.S., and Bartley, J.M., 2008, Long-term geochemical variability of the Late Cretaceous Tuolumne Intrusive Suite, central Sierra Nevada, California: Geological Society, London, Special Publications, v. 308, p. 183-201.

Hathaway, G.M., 2002, Geology of the Inconsolable Range, east-central Sierra Nevada, Kings Canyon National Park and John Muir Wilderness, California: Magmatic emplacement and the dynamic evolution of composite intrusions: Unpublished PhD thesis, University of California, Los Angeles, 474 p.

Hirt, W.H., 2007, Petrology of the Mount Whitney Intrusive Suite, eastern Sierra Nevada, California: Implications for the emplacement and differentiation of composite felsic intrusions: GSA Bulletin, v. 119, p. 1185-1200.

Ishihara, S., 1981, The granitoid series and mineralization: Economic Geology, 75th Anniversary Volume, p. 458-484.

Keith, J.D., van Middelaar, W.T., Clark, A.H., and Hodgson, C.J., 1989, Granitoid textures, compositions, and volatile fugacities associated with the formation of tungsten-dominated skarn deposits: Reviews in Economic Geology, v. 4, p. 235–250.

Kistler, R.W., and Peterman, Z.E., 1973, Variations in Sr, Rb, K, Na, and initial $^{87}Sr/^{86}Sr$ in Mesozoic granitic rocks and intruded wall rocks in central California: Geological Society of America Bulletin, v. 84, p. 3489–3512,

Kistler, R.W., Chappell, B.W., Peck, D.L., and Bateman, P.C., 1986, Isotopic variation in the Tuolumne Intrusive Suite, central Sierra Nevada, California: Contributions to Mineralogy and Petrology, v. 94, p. 205-220.

Kurtak, J.M., 2004, Mine in the Sky: The history of California's Pine Creek Tungsten Mine and the people who were part of it: Publication Consultants, Anchorage, Alaska, 220 p.

Lackey, J.S., Cecil, M.R., Windham, C.J., Frazer, R.E., Bindeman, I.N., and Gehrels, G.E., 2012, The Fine Gold Intrusive Suite: The roles of basement terranes and magma source development in the Early Cretaceous Sierra Nevada batholith: Geosphere, v. 8, p. 292-313.

Le Maitre, R.W., ed., 2002, Igneous rocks: A classification and glossary of terms – recommendations of the International Union of Geological Sciences Subcommission on the Systematics of Igneous Rocks: Cambridge, United Kingdom, Cambridge University Press, 236 p.

Lee, D.E. and Christiansen, E.H., 1983, The granite problem as exposed in the southern Snake Range, Nevada: Contributions to Mineralogy and Petrology, v. 83, p. 99-116.

Mahan, D.H., Bartley, J.M., Coleman, D.S., Glazner, A.F., and Carl, B.S., 2003, Sheeted intrusion of the synkinematic McDoogle pluton, Sierra Nevada, California: GSA Bulletin, v. 115, p. 1570-1582.

McDonough, W.F. and Sun, S.-s., 1995, The composition of the Earth: Chemical Geology, v. 120, p. 223-253.

Meinert, L.D., Dipple, G.M., and Nicolescu, S., 2005, World Skarn Deposits: Economic Geology 100th Anniversary Volume, p. 299-336.

Memeti, V., Paterson, S., Matzel, J., Mundil, R., and Okaya, D., 2010, Magmatic lobes as "snapshots" of magma chamber growth and evolution in large, composite batholiths: An example from the Tuolumne intrusion, Sierra Nevada, California: GSA Bulletin, v. 122, p. 1912-1931.

Miller, J.S., Matzel, J.E.P., Miller, C.F., Burgess, S.D., and Miller, R.B., 2007, Zircon growth and recycling during the assembly of large, composite arc plutons: Journal of Volcanology and Geothermal Research v. 167, p. 282–299.

Mustard, R., 2004, Textural , mineralogical and geochemical variation in the zoned Timbarra Tablelands pluton, New South Wales: Australian Journal of Earth Sciences, v. 51, p. 385-405.

Nelson, W.R., Dorais, M.J., Christiansen, E.H., and Hart, G.L., 2013, Petrogenesis of Sierra Nevada plutons inferred from the Sr, Nd, and O isotopic signatures of mafic igneous complexes in Yosemite Valley, California: Contributions to Mineralogy and Petrology, v. 165, p. 397-417.

Newberry, R.J., 1982, Tungsten-bearing skarns of the Sierra Nevada. I. The Pine Creek mine, California: Economic Geology, v. 77, p. 823-844.

Pearce, J.A., Harris, N.B.W., and Tindle, A.G., 1984, Trace element discrimination diagrams for the tectonic interpretation of granitic rocks: Journal of Petrology, v. 25, p. 956-983.

Porter, J.P., Bartley, J., Petersen, E., and Barra, F., 2011, Timing of the Pine Creek tungsten skarn and the causative Morgan Creek pluton, California: Implications for ore genesis and regional geology: *in* R. Steininger and B. Pennell, eds. Great Basin Evolution and Metallogeny: Geological Society of Nevada Symposium Proceedings, p. 397-417.

Sawka, W.N., Chappell, B.W., and Kistler, R.W., 1990, Granitoid compositional zoning by side-wall boundary layer differentiation: Evidence from the Palisade Crest Intrusive Suite, central Sierra Nevada, California: Journal of Petrology, v. 31, p. 519-553.

Sisson, T.W., Grove, T.L., and Coleman, D.S., 1996, Hornblende gabbro sill complex at Onion Valley, California, and a mixing origin for the Sierra Nevada batholith: Contributions to Mineralogy and Petrology, v. 126, p. 81-108.

Solomon, G. and Taylor, H., 1989, Isotopic evidence for the origin of Mesozoic and Cenozoic granitic plutons in the northern Great Basin: Geology, v. 17, p. 591-594.

Stearns, M.A., 2009, Anatomy and assembly of the McDoogle pluton near Sawmill Lake, central Sierra Nevada, California: Unpublished MS thesis, University of Utah, 109 p.

Stern, T.W., Bateman, P. C., Morgan, B.A., Newell, M.F. and Peck, D.L., 1981, Isotopic U-Pb ages of zircon from the granitoids of the central Sierra Nevada, California: USGS Professional Paper No. 1185, 17 p.

Stevens, C.H. and Greene, D.C., 1999, Stratigraphy, depositional history, and tectonic evolution of Paleozoic continental-margin rocks in roof pendants of the eastern Sierra Nevada, California: GSA Bulletin, v. 111, p. 919-933.

Takagi, T., 2004, Origin of the magnetite- and ilmenite-series granitic rocks in the Japan arc: American Journal of Science, v. 304, p. 169-202.

Wones, D.R., 1989, Significance of the assemblage titanite + magnetite + quartz in granitic rocks: American Mineralogist, v. 74, p. 744-749.

Wones, D. and Eugster, H., 1965, Stability of biotite: experiment, theory, and application: American Mineralogist, v. 50, p. 1228-1272.

CHAPTER 5

FUTURE WORK

The work on the Morgan Creek pluton presented in the preceding pages may not have accomplished the initial goal of answering some of the larger problems of how incremental emplacement is related to ore genesis. The pluton was chosen for this study because of its temporal and spatial relationship with other protracted, incrementally emplaced plutons and its associated W-Mo mineralization. The high silica content of the Morgan Creek pluton, common to plutons associated with tungsten deposits (Meinert et al., 2005; Seedorff et al.,, 2005), led to a complicated U-Pb zircon dataset. The spread in Re-Os ages of molybdenite from the Pine Creek skarn is more likely the result of analytical anomalies than extremely protracted mineralization (~16 Myr). These problems with the geochonological dataset may have been alleviated by selecting a less-silicic pluton as the area of study.

For all the complications in the geochronology presented in Chapter 3, the geochemical data presented in Chapter 4 shows interesting differences between the Morgan Creek pluton and the rest of the John Muir Intrusive Suite, and raises questions about the early evolution of this and other large intrusive suites. However, the geochemistry alone does not offer conclusive evidence of crustal origins.

Isotope geochemistry, both stable and radiogenic, would help determine the source of the Morgan Creek magma, and similar work could help the understanding of the source for entire John Muir Intrusive Suite. This kind of work would help evaluate the contributions of various magma sources that may have contributed to the suite. Chapter 3 proposes an upper crustal source for the Morgan Creek, and speculates that some crustal component may also be present in the rocks of the Lamarck Granodiorite. Isotopic work could confirm or refute those conclusions. They are also an important piece required for the full comparison of the processes involved in the generation of large intrusive suites in the Mesozoic Sierra Nevada arc (e.g., Tuolumne Intrusive Suite; Kistler et al., 1986; intrusive suite of Yosemite Valley; Nelson et al., 2013).

There is also work to be done to confirm the extent of Morgan Creek related rocks. A detailed characterization of the Basin Mountain pluton rocks should be undertaken to determine the relationship, if any, of the Morgan Creek, Basin Mountain, and Lake Edison plutons. Petrography, geochemistry, and geochronology of the Basin Mountain pluton will, together, advance the understanding of the place of that pluton within the larger John Muir Intrusive Suite.

The results presented in this dissertation do not shed much light on the interplay between incremental pluton emplacement and magmatic-hydrothermal deposits. However, there are also opportunities to increase the understanding of the emplacement processes of plutons related to magmatic-hydrothermal systems. Those shallow plutons provide a link to the well-studied plutonic and volcanic systems. These three environments must be treated together to obtain a complete, robust model of the transport and emplacement of magmatic systems.

References

Kistler, R.W., Chappell, B.W., Peck, D.L., and Bateman, P.C., 1986, Isotopic variation in the Tuolumne Intrusive Suite, central Sierra Nevada, California: Contributions to Mineralogy and Petrology, v. 94, p. 205-220.

Meinert, L.D., Dipple, G.M., Nicolescu, S., 2005, World skarn deposits: *in* Hedenquist, J.H., Thompson, J.F.H., Goldfarb, R.J., and Richards, J.P., eds., Economic Geology 100th Anniversary Volume, p. 299-336.

Nelson, W.R., Dorais, M.J., Christiansen, E.H., and Hart, G.L., 2013, Petrogenesis of Sierra Nevada plutons inferred from the Sr, Nd, and O isotopic signatures of mafic igneous complexes in Yosemite Valley, California: Contributions to Mineralogy and Petrology, v. 165, p. 397-417.

Seedorff, E. and Einaudi, M.T,. 2004, Henderson porphyry molybdenum system, Colorado: I. Sequence and abundance of hydrothermal mineral assemblages, flow paths of evolving fluids, and evolutionary style: Economic Geology, v. 99, p. 3-37.

Seedorff, E., Dilles, J.H., Proffett, J.M., Einaudi, M.T., Zurcher, L., Stavast, W.J.A., Johnson, D.A., and Barton, M.D., 2005, Porphyry deposits: Characteristics and origin of hypogene features: *in* Hedenquist, J.H., Thompson, J.F.H., Goldfarb, R.J., and Richards, J.P., eds., Economic Geology 100th Anniversary Volume, p. 251-298.

APPENDIX A

U-PB ANALYTICAL DATA

Table A.1

	Concentration					
	U (ppm)	U/Th	206Pb 204Pb	206Pb* 238U	± (%)	207Pb* 235U*
Sample 07-MC-009						
01	1483	1.42	15138	0.01469	1	0.10352
03	297	1.14	3138	0.01454	1	0.09674
04	356	1.08	3504	0.01448	1	0.10047
08	212	1.35	3208	0.01408	2	0.08913
09	237	1.29	2320	0.01478	1	0.09054
10	169	1.53	2282	0.01488	1	0.10910
12	330	1.13	3146	0.01446	1	0.08983
13	174	2.11	2444	0.01462	2	0.09733
14	174	1.38	1364	0.01461	1	0.08789
15	179	1.23	1680	0.01449	1	0.10069
16	129	1.46	1680	0.01456	2	0.10378
19	131	1.31	1216	0.01437	3	0.08838
21	266	1.26	1944	0.01460	1	0.10615
22	282	1.36	2694	0.01398	1	0.10119
23	234	1.65	2906	0.01464	1	0.10044
24	478	1.23	4426	0.01441	3	0.09044
25	135	1.61	1440	0.01476	2	0.10311
27	164	2.01	2550	0.01385	2	0.09213
29	195	1.72	1800	0.01445	1	0.08686
30	348	1.60	4460	0.01474	1	0.09841
32	362	1.80	4856	0.03090	2	0.22706
33	730	2.38	7558	0.01460	1	0.09944
34	204	1.51	2896	0.01451	2	0.10685
35	187	2.02	2054	0.01494	1	0.10878

. LA ICP-MS U-Pb zircon results

Isotope ratios						Apparent ages (Ma)			
± (%)	error corr.	206Pb* 207Pb*	± (%)	206Pb* 238U*	± (Ma)	207Pb* 235U	± (Ma)	206Pb* 207Pb*	± (Ma)
4	0.24	19.57	4	94.0	0.9	100.0	3.9	245.2	92.4
6	0.18	20.72	5	93.1	0.9	93.8	5.0	111.7	129.1
9	0.11	19.87	9	92.7	0.9	97.2	8.1	210.1	202.0
5	0.33	21.78	5	90.1	1.6	86.7	4.5	-6.9	122.8
9	0.12	22.50	9	94.6	1.0	88.0	7.7	-86.2	223.5
13	0.08	18.81	13	95.2	0.9	105.1	13.0	336.2	295.0
10	0.10	22.20	10	92.5	0.9	87.3	8.7	-52.7	253.3
19	0.09	20.71	19	93.6	1.6	94.3	16.8	113.1	440.3
11	0.09	22.93	11	93.5	0.9	85.5	9.2	-132.4	277.7
9	0.11	19.84	9	92.7	0.9	97.4	8.7	214.0	217.3
18	0.11	19.34	18	93.2	1.8	100.3	17.5	272.3	420.5
35	0.09	22.41	35	91.9	2.9	86.0	28.8	-76.4	874.7
15	0.10	18.97	15	93.4	1.3	102.4	14.6	317.0	341.9
12	0.08	19.05	12	89.5	0.9	97.9	11.2	306.5	273.2
16	0.06	20.09	16	93.7	1.0	97.2	15.0	184.3	378.5
7	0.39	21.96	7	92.2	2.6	87.9	6.1	-27.0	162.7
17	0.10	19.74	17	94.5	1.6	99.6	16.2	225.1	395.4
13	0.16	20.73	13	88.7	1.8	89.5	11.0	110.8	299.4
11	0.11	22.93	11	92.5	1.1	84.6	8.6	-132.7	261.5
4	0.24	20.65	4	94.3	0.9	95.3	3.7	119.8	93.4
4	0.53	18.77	4	196.2	4.3	207.8	7.9	341.1	81.4
4	0.26	20.25	4	93.5	0.9	96.3	3.5	166.1	86.6
12	0.19	18.72	12	92.9	2.2	103.1	12.2	346.3	278.1
17	0.06	18.93	17	95.6	0.9	104.9	17.2	321.0	393.2

	Concentration					
	U (ppm)	U/Th	206Pb 204Pb	206Pb* 238U	± (%)	207Pb* 235U*
36	354	2.01	3292	0.01468	1	0.09816
37	237	1.94	2918	0.01437	2	0.09322
38	314	2.54	4454	0.01452	3	0.09078
39	621	5.34	24778	0.01537	1	0.09857
02a	393	1.48	5211	0.01488	1	0.09999
07a	1958	4.19	28095	0.01553	2	0.10443
08a	675	2.93	12948	0.01767	1	0.12754
11a	1218	2.19	16386	0.01514	1	0.09972
12a	562	1.41	4110	0.01591	1	0.11205
13a	631	2.26	4725	0.01560	2	0.11218
14a	1303	1.59	861	0.01677	2	0.11544
15a	790	4.37	13485	0.01747	1	0.11785
16a	655	2.04	5901	0.01616	1	0.10936
17a	1485	3.15	22305	0.01614	1	0.10972
18a	173	1.59	2505	0.01530	1	0.09516
19a	1298	2.39	16455	0.01539	1	0.10354
23a	459	2.60	4788	0.01546	1	0.10504
24a	255	2.18	5802	0.01682	1	0.10780
Sample 07-MC-017						
01	369	1.69	2297	0.01462	1	0.09597
02	300	1.43	1994	0.01433	3	0.09598
03	453	4.04	8529	0.03210	1	0.22585
05	292	2.54	2519	0.01562	1	0.11146
07	210	1.51	1600	0.01427	2	0.09963
08	191	1.80	1811	0.01491	1	0.10464
09	215	1.86	2287	0.01481	1	0.09439

Table A.1 (cont.).

Isotope ratios						Apparent ages (Ma)			
± (%)	error corr.	206Pb* 207Pb*	± (%)	206Pb* 238U*	± (Ma)	207Pb* 235U	± (Ma)	206Pb* 207Pb*	± (Ma)
14	0.10	20.62	14	93.9	1.3	95.1	12.7	124.1	328.3
7	0.28	21.25	7	92.0	1.9	90.5	6.3	51.7	166.5
13	0.21	22.06	13	92.9	2.6	88.2	11.1	-37.3	311.7
5	0.28	21.49	5	98.3	1.3	95.5	4.3	25.1	108.2
11	0.05	20.52	11	95.2	0.5	96.8	10.0	135.0	255.6
3	0.76	20.51	2	99.4	2.1	100.9	2.7	136.5	42.7
10	0.10	19.10	10	112.9	1.2	121.9	11.6	300.6	230.2
3	0.51	20.93	2	96.9	1.3	96.5	2.4	87.8	53.7
4	0.12	19.57	4	101.7	0.5	107.8	4.4	244.7	97.4
5	0.36	19.17	5	99.8	1.9	108.0	5.3	292.8	109.1
13	0.11	20.03	13	107.2	1.6	110.9	14.0	191.7	309.2
3	0.26	20.44	3	111.6	1.0	113.1	3.7	144.7	78.5
4	0.14	20.37	4	103.3	0.5	105.4	3.6	152.3	83.4
1	0.52	20.29	1	103.2	0.7	105.7	1.4	161.6	27.1
7	0.08	22.17	7	97.9	0.5	92.3	6.3	-49.8	172.8
2	0.39	20.50	2	98.5	0.6	100.0	1.6	137.7	36.3
5	0.10	20.30	5	98.9	0.5	101.4	4.7	160.7	114.0
5	0.09	21.51	5	107.5	0.5	104.0	5.3	22.7	127.6
10	0.10	21.01	10	93.6	0.9	93.0	8.6	79.4	227.9
10	0.32	20.58	10	91.7	3.0	93.1	9.1	128.1	229.4
3	0.32	19.60	3	203.7	2.0	206.8	5.9	242.2	68.9
10	0.11	19.32	10	99.9	1.1	107.3	10.3	275.3	229.9
23	0.09	19.75	23	91.4	1.9	96.4	21.6	223.9	546.4
19	0.05	19.65	19	95.4	0.9	101.1	18.6	236.2	449.8
11	0.09	21.63	11	94.8	0.9	91.6	9.4	9.7	258.7

Table A.1 (cont.).

	Concentration					Isotope ratios			
	U (ppm)	U/Th	206Pb 204Pb	206Pb* 238U	± (%)	207Pb* 235U*	± (%)	error corr.	206Pb* 207Pb*
10	175	2.62	2052	0.01545	1	0.09750	13	0.08	21.85
11	234	1.66	2572	0.01529	1	0.10348	23	0.06	20.38
12	522	3.22	10192	0.01490	1	0.09258	7	0.15	22.19
14	178	1.99	1413	0.01421	1	0.08519	17	0.07	23.00
16	146	1.26	1091	0.01432	2	0.09934	20	0.08	19.88
17	903	3.18	9758	0.01475	1	0.09698	4	0.27	20.98
18	278	2.02	2256	0.01415	2	0.09105	10	0.18	21.43
19	174	2.41	2479	0.01373	1	0.08490	17	0.06	22.30
22	375	2.35	7422	0.01679	1	0.11421	5	0.19	20.27
24	454	1.57	2967	0.01493	1	0.10362	10	0.10	19.86
25	938	3.38	5603	0.01447	1	0.09687	6	0.19	20.59
26	188	1.67	1217	0.01500	1	0.09502	10	0.11	21.77
27	182	2.07	3308	0.01453	1	0.10458	16	0.06	19.16
28	249	2.97	2423	0.01447	1	0.09967	12	0.08	20.02
29A	448	1.84	3160	0.01447	5	0.09899	10	0.46	20.15
30	383	2.42	2761	0.01554	1	0.10154	7	0.16	21.10
32	784	3.71	7092	0.01458	3	0.10339	5	0.47	19.45
33	240	2.25	3624	0.01432	1	0.09722	13	0.09	20.32
34	199	2.01	3618	0.01385	1	0.09434	18	0.06	20.24
35	212	2.04	1775	0.01436	1	0.09216	19	0.05	21.48
36	226	1.56	1846	0.01430	2	0.08964	14	0.12	22.00
37	763	3.26	5952	0.01587	1	0.10456	4	0.26	20.93
39	357	2.93	3378	0.01601	1	0.11124	9	0.11	19.84
40	279	2.12	2795	0.01577	2	0.11457	13	0.17	18.98
02a	128	1.57	2968	0.01491	1	0.09308	13	0.04	22.09

Apparent ages (Ma)						
± (%)	206Pb* 238U*	± (Ma)	207Pb* 235U	± (Ma)	206Pb* 207Pb*	± (Ma)
13	98.8	1.0	94.5	11.6	-14.2	310.7
23	97.8	1.3	100.0	22.1	151.2	548.0
7	95.3	0.9	89.9	5.7	-51.7	159.8
17	91.0	1.1	83.0	13.7	-140.2	427.1
20	91.7	1.4	96.2	18.3	209.0	464.2
4	94.4	0.9	94.0	3.4	82.9	85.8
10	90.6	1.6	88.5	8.7	31.6	242.5
17	87.9	0.9	82.7	13.4	-64.0	412.7
5	107.3	1.1	109.8	5.4	164.0	119.7
10	95.5	0.9	100.1	9.8	211.0	238.9
5	92.6	1.0	93.9	5.0	127.0	129.1
9	96.0	1.0	92.2	8.4	-5.2	229.2
16	93.0	0.9	101.0	15.1	294.2	359.9
12	92.6	1.0	96.5	11.5	192.2	289.3
9	92.6	4.4	95.8	9.5	177.3	215.9
7	99.4	1.2	98.2	6.9	69.0	174.4
5	93.3	2.4	99.9	5.2	259.7	110.9
13	91.7	1.1	94.2	11.9	158.4	308.3
18	88.7	1.0	91.5	15.9	166.7	425.7
19	91.9	0.9	89.5	16.0	26.6	449.4
14	91.5	1.6	87.2	11.9	-31.2	344.0
4	101.5	1.0	101.0	3.7	88.1	88.6
9	102.4	1.0	107.1	9.1	213.8	207.1
13	100.9	2.1	110.1	13.3	315.6	287.6
13	95.4	0.5	90.4	11.4	-40.9	321.3

Table A.1 (cont.).

	Concentration					Isotope ratios			
	U (ppm)	U/Th	206Pb 204Pb	206Pb* 238U	± (%)	207Pb* 235U*	± (%)	error corr.	206Pb* 207Pb*
05a	258	6.58	8688	0.01500	1	0.10282	6	0.10	20.12
06a	225	2.96	5740	0.01525	2	0.09265	17	0.09	22.70
07a	251	1.88	6900	0.01496	1	0.09421	6	0.26	21.90
08a	258	1.19	5876	0.01507	1	0.09922	15	0.09	20.94
09a	568	6.06	14388	0.01593	1	0.10392	4	0.28	21.13
10a	109	1.39	2964	0.01517	1	0.09151	10	0.05	22.86
12a	256	1.84	5068	0.01569	1	0.11511	8	0.14	18.80
13a	172	1.27	4980	0.01519	1	0.09446	7	0.07	22.17
14a	242	1.21	4948	0.01473	1	0.09852	10	0.12	20.61
15a	162	1.23	4044	0.01493	1	0.09125	10	0.06	22.56
16a	203	1.20	4984	0.01567	1	0.10016	21	0.02	21.57
17a	460	1.20	9696	0.01534	1	0.09969	6	0.11	21.21
19a	156	1.43	3968	0.01504	2	0.09076	9	0.23	22.85
20a	211	1.07	4648	0.01468	1	0.09122	6	0.24	22.19
21a	146	1.65	3752	0.01497	4	0.09202	9	0.42	22.43
22a	253	3.09	5428	0.01516	1	0.09732	4	0.20	21.47
23a	1164	2.35	64500	0.03147	2	0.21960	2	0.77	19.76
24a	322	1.05	6304	0.01491	2	0.09804	5	0.41	20.97
Sample 07-MC-018									
01	361	1.84	3623	0.01381	1	0.08902	8	0.13	21.40
02	2967	3.05	4146	0.01479	2	0.10715	5	0.32	19.03
03	206	1.79	1658	0.01387	1	0.09793	15	0.07	19.53
05	230	2.03	1715	0.01438	2	0.09907	20	0.08	20.01
06	549	7.12	5964	0.01431	1	0.09457	2	0.41	20.86

Apparent ages (Ma)						
± (%)	206Pb* 238U*	± (Ma)	207Pb* 235U	± (Ma)	206Pb* 207Pb*	± (Ma)
6	96.0	0.6	99.4	5.9	181.6	144.1
17	97.6	1.5	90.0	14.6	-107.6	418.1
5	95.8	1.4	91.4	4.9	-20.4	130.7
14	96.4	1.2	96.1	13.3	86.9	345.3
4	101.9	1.2	100.4	3.9	65.5	92.2
10	97.1	0.5	88.9	8.5	-124.9	247.6
8	100.4	1.1	110.6	8.8	337.4	189.7
7	97.2	0.5	91.6	6.0	-49.6	166.5
10	94.3	1.1	95.4	8.8	124.1	225.8
10	95.5	0.6	88.7	8.2	-92.6	237.1
21	100.2	0.5	96.9	19.7	16.0	516.8
6	98.1	0.7	96.5	5.7	56.2	145.8
9	96.2	2.0	88.2	7.8	-124.2	222.0
6	94.0	1.4	88.6	5.3	-52.3	148.1
8	95.8	3.5	89.4	7.5	-78.8	193.9
4	97.0	0.9	94.3	4.1	27.4	105.6
2	199.8	3.7	201.6	4.4	222.9	35.2
5	95.4	2.1	95.0	5.0	83.9	118.8
7	88.4	0.9	86.6	6.2	35.8	178.7
5	94.6	1.5	103.4	5.0	309.6	110.0
15	88.8	0.9	94.9	13.3	249.6	338.3
20	92.0	1.5	95.9	18.4	193.6	469.8
2	91.6	0.9	91.8	2.1	95.7	52.4

Table A.1 (cont.).

	Concentration					Isotope ratios			
	U (ppm)	U/Th	206Pb 204Pb	206Pb* 238U	± (%)	207Pb* 235U*	± (%)	error corr.	206Pb* 207Pb*
08	1033	2.59	4238	0.01421	1	0.09594	2	0.49	20.42
09	992	3.73	5712	0.01403	3	0.09395	8	0.34	20.59
10	461	2.82	3189	0.01403	1	0.08930	4	0.23	21.66
11	1524	2.49	4437	0.01477	1	0.10692	7	0.13	19.04
14	780	2.95	6611	0.01466	4	0.10554	20	0.23	19.16
16	280	2.09	1766	0.01476	1	0.10130	8	0.13	20.10
18	166	2.68	1180	0.01451	1	0.09611	26	0.04	20.82
19	298	2.18	1799	0.01573	1	0.10625	13	0.08	20.41
20	186	1.79	3798	0.01441	6	0.08670	12	0.54	22.91
21	648	12.87	6785	0.01405	1	0.09218	14	0.07	21.02
22	193	2.39	1617	0.01404	3	0.08907	18	0.16	21.73
24	2131	4.60	4107	0.01416	1	0.09821	2	0.52	19.88
25	410	2.30	1715	0.01486	1	0.10646	5	0.24	19.25
26	790	2.46	3267	0.01606	9	0.11599	12	0.76	19.09
30	188	2.77	1669	0.01510	2	0.10469	27	0.07	19.89
31	479	2.61	2307	0.01438	1	0.09968	7	0.14	19.89
33	802	2.15	4301	0.01504	1	0.10580	5	0.29	19.60
34	479	2.81	2854	0.01454	2	0.10277	9	0.19	19.50
35	798	7.42	3359	0.01399	1	0.09734	3	0.29	19.81
36	1041	1.17	4821	0.01500	1	0.10375	9	0.13	19.93
37	588	3.98	3531	0.01366	3	0.08887	6	0.52	21.19
40	1541	1.99	3810	0.01421	3	0.10268	7	0.50	19.08
03a	1632	1.65	10604	0.01455	1	0.10261	2	0.56	19.55
05a	455	2.11	7908	0.01525	1	0.09963	6	0.12	21.10
07a	182	1.76	2868	0.01488	1	0.09569	7	0.16	21.44
08a	1225	1.96	21056	0.01500	1	0.09752	3	0.18	21.21

Apparent ages (Ma)						
± (%)	206Pb* 238U*	± (Ma)	207Pb* 235U	± (Ma)	206Pb* 207Pb*	± (Ma)
2	91.0	0.9	93.0	1.8	146.5	42.2
7	89.8	2.2	91.2	6.5	127.4	166.6
4	89.8	0.9	86.9	3.6	6.6	102.1
7	94.5	0.9	103.1	7.3	307.6	168.6
19	93.8	4.2	101.9	19.1	294.0	441.5
8	94.5	0.9	98.0	7.1	183.9	176.1
26	92.9	0.9	93.2	23.0	101.0	619.3
13	100.6	1.0	102.5	12.7	147.2	305.1
10	92.2	5.8	84.4	9.5	-130.8	244.8
14	90.0	0.9	89.5	11.6	78.1	322.5
18	89.9	2.5	86.6	15.1	-1.1	434.9
2	90.6	0.9	95.1	1.7	209.2	37.7
5	95.1	1.1	102.7	4.9	283.3	112.5
8	102.7	9.2	111.4	12.6	302.6	178.4
27	96.6	1.9	101.1	25.8	207.8	630.7
7	92.0	0.9	96.5	6.4	207.4	160.3
5	96.2	1.4	102.1	4.9	242.1	112.3
9	93.0	1.6	99.3	8.8	253.3	209.4
3	89.5	0.9	94.3	3.1	217.1	75.2
9	96.0	1.1	100.2	8.7	203.1	209.5
5	87.5	2.7	86.5	5.0	58.9	122.1
6	90.9	3.1	99.2	6.5	303.8	134.6
2	93.1	1.1	99.2	2.0	247.6	41.3
6	97.5	0.7	96.4	5.9	69.1	151.6
7	95.2	1.2	92.8	6.6	30.7	175.5
3	96.0	0.5	94.5	2.6	57.0	66.8

Table A.1 (cont.).

	Concentration					Isotope ratios			
	U (ppm)	U/Th	206Pb 204Pb	206Pb* 238U	± (%)	207Pb* 235U*	± (%)	error corr.	206Pb* 207Pb*
11a	1089	2.77	9528	0.01517	1	0.10756	4	0.32	19.45
13a	1877	1.55	28024	0.01501	2	0.10144	3	0.69	20.40
17a	1418	1.55	9468	0.01506	1	0.10939	4	0.14	18.98
19a	269	1.21	4860	0.01519	1	0.09633	7	0.19	21.74
21a	1199	1.19	7724	0.01530	1	0.11128	3	0.29	18.96
23a	1240	1.64	15960	0.01532	1	0.10094	2	0.30	20.92
24a	356	2.86	13372	0.03392	1	0.24097	3	0.35	19.41
25a	355	1.40	9108	0.01511	1	0.10037	6	0.13	20.76
Sample 07-MC-039									
01	949	2.23	4650	0.01508	1	0.10321	4	0.24	20.15
03	585	2.44	3293	0.01642	1	0.12022	6	0.24	18.84
05	311	1.62	2358	0.01484	2	0.10041	9	0.17	20.37
06	253	1.95	2196	0.01523	1	0.09418	6	0.17	22.30
07	851	1.68	5423	0.01557	2	0.10718	6	0.30	20.03
09	1099	2.42	5136	0.01539	2	0.11142	7	0.29	19.05
11	319	2.11	5867	0.01600	1	0.10891	7	0.14	20.26
13	214	2.27	1576	0.01519	3	0.10626	21	0.16	19.71
14	1730	9.42	35401	0.01523	2	0.10385	3	0.73	20.22
15	216	3.08	1921	0.01469	1	0.09832	10	0.14	20.60
17	2580	2.25	15259	0.01470	3	0.10253	3	0.93	19.77
18	534	3.19	4930	0.01499	1	0.10563	5	0.23	19.57
19	265	2.39	10379	0.03014	1	0.20518	3	0.34	20.25
20	2333	3.14	5562	0.01432	1	0.10160	3	0.31	19.43
22	467	2.73	5005	0.01464	2	0.09711	13	0.13	20.78

Apparent ages (Ma)						
± (%)	206Pb* 238U*	± (Ma)	207Pb* 235U	± (Ma)	206Pb* 207Pb*	± (Ma)
4	97.1	1.2	103.7	3.7	259.1	82.5
2	96.0	1.7	98.1	2.4	149.0	42.7
4	96.4	0.5	105.4	3.6	315.0	80.8
7	97.2	1.3	93.4	6.1	-2.8	160.9
2	97.9	0.7	107.1	2.6	318.3	55.2
2	98.0	0.5	97.6	1.6	89.3	37.8
2	215.0	1.9	219.2	5.0	264.4	54.3
6	96.7	0.7	97.1	5.2	107.5	132.4
4	96.5	1.0	99.7	4.0	178.1	96.5
6	105.0	1.4	115.3	6.2	332.5	125.2
9	94.9	1.5	97.2	8.6	151.6	215.8
6	97.5	1.0	91.4	5.3	-64.2	145.0
5	99.6	1.7	103.4	5.7	192.0	127.5
6	98.5	1.9	107.3	6.9	307.1	147.2
7	102.3	1.0	105.0	7.0	165.3	161.9
21	97.2	3.3	102.5	20.7	228.6	488.1
2	97.4	2.3	100.3	3.1	169.4	51.4
10	94.0	1.2	95.2	8.9	125.4	228.4
1	94.1	3.0	99.1	3.3	221.4	29.1
5	95.9	1.2	102.0	5.2	244.8	121.1
3	191.4	2.0	189.5	5.5	166.0	70.0
3	91.7	0.9	98.3	3.1	261.4	71.3
13	93.7	1.6	94.1	11.8	105.0	309.2

Table A.1 (cont.).

	Concentration					Isotope ratios			
	U (ppm)	U/Th	206Pb 204Pb	206Pb* 238U	± (%)	207Pb* 235U*	± (%)	error corr.	206Pb* 207Pb*
23	329	2.91	3981	0.02938	1	0.21472	7	0.14	18.87
26	545	1.70	3592	0.01530	1	0.10574	6	0.26	19.95
28	1867	3.41	7839	0.01357	6	0.09840	7	0.79	19.01
30	1132	3.19	8587	0.01495	3	0.10105	5	0.56	20.40
33	1091	4.09	9806	0.01455	2	0.09809	4	0.54	20.45
34	461	3.15	3709	0.01523	1	0.10897	8	0.13	19.27
36	400	2.09	7465	0.02983	1	0.20499	5	0.20	20.07
38	334	2.77	2434	0.01475	2	0.10870	7	0.22	18.71
43	1969	3.66	9665	0.01621	2	0.11333	3	0.61	19.72
45	3180	3.41	7584	0.01509	6	0.11078	7	0.77	18.78
01a	377	0.99	7500	0.01496	1	0.09516	4	0.23	21.68
04a	328	1.07	5764	0.01497	1	0.09870	11	0.07	20.91
07a	444	1.06	10532	0.01498	1	0.09831	3	0.17	21.01
09a	352	0.96	7716	0.01533	3	0.09676	6	0.46	21.85
10a	295	0.96	6272	0.01557	3	0.09925	9	0.31	21.63
11a	149	1.45	4160	0.01472	1	0.08816	10	0.06	23.03
12a	369	1.02	7660	0.01491	2	0.09494	5	0.49	21.65
13a	167	1.24	3496	0.01572	2	0.09737	9	0.19	22.26
14a	133	1.75	3788	0.01513	1	0.09446	12	0.11	22.08
15a	149	1.50	3640	0.01456	1	0.08862	10	0.06	22.66
16a	213	1.64	4028	0.01539	1	0.10869	9	0.07	19.52
18a	559	1.24	13196	0.01466	1	0.09486	4	0.11	21.30
19a	887	1.38	8168	0.01445	1	0.10324	6	0.08	19.30
20a	291	2.22	4736	0.01525	1	0.11191	16	0.04	18.78

Apparent ages (Ma)						
± (%)	206Pb* 238U*	± (Ma)	207Pb* 235U	± (Ma)	206Pb* 207Pb*	± (Ma)
7	186.7	1.8	197.5	12.5	329.0	156.5
6	97.9	1.4	102.1	5.5	200.2	128.0
4	86.9	4.9	95.3	6.5	311.4	99.5
4	95.7	2.8	97.7	5.0	148.7	104.4
3	93.1	1.8	95.0	3.3	143.1	72.3
8	97.4	1.0	105.0	7.6	280.7	172.8
5	189.5	1.9	189.3	8.5	187.3	111.8
7	94.4	1.5	104.8	7.0	347.5	154.9
2	103.7	1.8	109.0	3.0	227.3	52.4
5	96.5	5.3	106.7	7.3	339.9	103.8
4	95.8	0.9	92.3	3.6	3.8	94.5
11	95.8	0.7	95.6	9.6	90.5	249.6
3	95.8	0.5	95.2	2.7	79.5	68.7
5	98.1	2.5	93.8	5.0	-14.3	120.3
9	99.6	2.9	96.1	8.6	9.7	214.9
10	94.2	0.5	85.8	8.0	-143.1	240.2
4	95.4	2.1	92.1	4.1	7.1	97.8
8	100.6	1.6	94.4	7.7	-59.8	204.4
12	96.8	1.3	91.7	10.6	-40.4	291.5
10	93.2	0.6	86.2	8.4	-103.6	248.5
9	98.4	0.6	104.8	8.7	250.9	200.7
4	93.8	0.5	92.0	3.9	46.4	105.9
6	92.5	0.5	99.8	6.0	276.7	143.3
16	97.5	0.7	107.7	16.0	338.9	357.1

Table A.1 (cont.).

	Concentration					Isotope ratios			
	U (ppm)	U/Th	206Pb 204Pb	206Pb* 238U	± (%)	207Pb* 235U*	± (%)	error corr.	206Pb* 207Pb*
Sample 07-MC-053									
01	106	2.33	709	0.01459	1	0.09923	27	0.04	20.27
03	428	1.61	3176	0.01539	1	0.10681	10	0.10	19.86
05	318	1.50	2434	0.01426	2	0.10310	18	0.08	19.07
07	225	1.55	2072	0.01444	1	0.09682	8	0.15	20.57
08	418	1.62	2880	0.01549	1	0.10302	8	0.12	20.74
09	153	1.86	889	0.01479	1	0.09145	20	0.05	22.30
11	249	1.53	1467	0.01492	2	0.10664	12	0.13	19.29
14	346	2.13	2637	0.01575	1	0.10084	8	0.12	21.54
15	760	1.14	4238	0.01493	1	0.09980	5	0.18	20.63
16	520	1.66	4551	0.01525	1	0.10363	9	0.11	20.29
17	713	2.73	41659	0.01494	1	0.09792	4	0.26	21.04
19	751	24.56	14171	0.01407	1	0.09364	5	0.19	20.72
20	279	1.52	2781	0.01455	1	0.08711	8	0.12	23.04
22	177	1.77	2164	0.01459	2	0.09893	14	0.15	20.33
23	254	2.10	1885	0.01409	2	0.09310	17	0.12	20.86

Apparent ages (Ma)						
± (%)	206Pb* 238U*	± (Ma)	207Pb* 235U	± (Ma)	206Pb* 207Pb*	± (Ma)
27	93.4	1.0	96.1	25.1	163.4	649.9
10	98.4	1.0	103.0	10.1	210.7	238.5
18	91.3	1.4	99.6	17.4	304.9	419.1
8	92.4	1.1	93.8	6.8	129.5	177.4
8	99.1	1.0	99.6	7.6	110.2	188.6
20	94.7	0.9	88.9	16.8	-64.3	486.5
12	95.4	1.5	102.9	11.5	278.9	267.5
8	100.7	1.0	97.5	7.5	20.0	193.5
5	95.6	0.9	96.6	5.0	122.3	126.0
9	97.6	1.0	100.1	8.4	161.1	204.1
4	95.6	1.1	94.9	4.0	76.3	100.3
5	90.1	0.9	90.9	4.7	111.7	124.2
8	93.2	0.9	84.8	6.9	-144.2	207.7
14	93.4	1.9	95.8	12.5	156.7	318.5
17	90.2	1.8	90.4	14.5	96.3	397.5

Table A.1 (cont.).

	Concentration					Isotope ratios			
	U (ppm)	U/Th	206Pb 204Pb	206Pb* 238U	± (%)	207Pb* 235U*	± (%)	error corr.	206Pb* 207Pb*
24	278	2.34	1952	0.01559	2	0.10104	13	0.14	21.27
25	76	2.21	978	0.02445	2	0.17841	17	0.11	18.90
26	992	12.24	8141	0.01416	2	0.10027	9	0.17	19.47
27	223	1.69	2960	0.02833	3	0.20454	16	0.18	19.10
28	160	1.82	1029	0.01487	2	0.10624	18	0.09	19.30
29	182	1.46	1981	0.01505	1	0.09525	16	0.06	21.78
31	426	2.45	6389	0.01533	1	0.09637	6	0.15	21.93
32	234	2.88	1540	0.01503	1	0.10970	11	0.10	18.89
33	229	2.07	1481	0.01447	2	0.09420	4	0.37	21.18
34	188	1.91	1911	0.01540	1	0.09647	8	0.12	22.02
35	285	2.42	1437	0.01472	1	0.10384	13	0.07	19.54
36	736	2.37	5046	0.01456	1	0.09769	4	0.35	20.55
38	284	2.18	1858	0.01503	2	0.11096	12	0.16	18.68
39	880	1.21	5552	0.01473	1	0.09753	4	0.28	20.83
40	162	2.22	1506	0.01519	3	0.10133	14	0.18	20.67
01a	475	2.75	7155	0.01453	2	0.09783	4	0.38	20.49
02a	127	1.79	2022	0.01465	2	0.09221	19	0.08	21.90
03a	164	1.75	2952	0.01506	2	0.09039	12	0.13	22.97
05a	420	2.63	9351	0.01455	1	0.09516	6	0.22	21.08
07a	297	1.94	12378	0.03040	2	0.21608	4	0.38	19.40
08a	201	2.14	4482	0.01523	1	0.09814	7	0.07	21.40
09a	193	1.50	4308	0.01505	1	0.09083	9	0.07	22.85
11a	269	1.65	4830	0.01462	3	0.09188	7	0.38	21.94
12a	172	1.35	1959	0.01499	3	0.10212	16	0.17	20.24
13a	173	1.83	3360	0.01473	1	0.09019	8	0.17	22.52

Apparent ages (Ma)						
± (%)	206Pb* 238U*	± (Ma)	207Pb* 235U	± (Ma)	206Pb* 207Pb*	± (Ma)
13	99.7	1.8	97.7	12.2	49.5	310.5
17	155.7	3.0	166.7	26.1	325.5	385.4
9	90.6	1.4	97.0	8.6	256.7	210.9
16	180.1	5.3	189.0	28.0	301.1	366.4
18	95.1	1.5	102.5	17.4	277.7	410.6
16	96.3	1.0	92.4	14.2	-7.2	388.5
6	98.1	1.0	93.4	5.8	-23.9	155.5
11	96.2	1.0	105.7	11.2	325.6	253.0
4	92.6	1.4	91.4	3.7	59.9	93.4
8	98.5	1.0	93.5	7.4	-33.1	199.6
13	94.2	0.9	100.3	12.9	248.7	310.3
4	93.2	1.2	94.6	3.5	131.3	86.3
12	96.2	1.9	106.8	12.5	351.6	274.7
4	94.3	1.1	94.5	3.6	100.0	90.7
14	97.2	2.5	98.0	13.4	118.0	333.6
4	93.0	1.5	94.8	3.9	139.0	93.0
19	93.7	1.5	89.6	16.6	-20.5	470.6
12	96.3	1.4	87.9	9.8	-136.8	285.6
6	93.1	1.2	92.3	5.1	71.3	135.2
4	193.1	3.2	198.6	8.0	265.4	93.7
7	97.4	0.5	95.1	6.5	35.7	171.4
9	96.3	0.6	88.3	7.7	-124.1	225.6
6	93.6	2.3	89.3	5.7	-24.8	149.7
16	95.9	2.6	98.7	15.3	167.4	377.5
8	94.2	1.2	87.7	6.4	-87.7	185.0

Table A.1 (cont.).

	Concentration					Isotope ratios			
	U (ppm)	U/Th	206Pb 204Pb	206Pb* 238U	± (%)	207Pb* 235U*	± (%)	error corr.	206Pb* 207Pb*
14a	129	1.82	1467	0.01486	2	0.09411	19	0.09	21.77
15a	311	1.64	8166	0.01499	2	0.09371	6	0.33	22.05
16a	283	2.80	5232	0.01501	2	0.09620	5	0.46	21.51
17a	302	2.13	5364	0.01494	2	0.10253	10	0.20	20.08
18a	214	2.33	5796	0.01506	3	0.09144	11	0.24	22.71
19a	362	1.35	5895	0.01438	1	0.09114	5	0.27	21.76
20a	269	1.72	3786	0.01480	1	0.09214	15	0.09	22.15
21a	229	2.18	585	0.01453	19	0.09087	73	0.26	22.05
22a	220	1.85	5781	0.01490	1	0.10237	10	0.12	20.07
23a	316	1.15	6204	0.01479	1	0.09205	6	0.22	22.16
24a	195	1.70	2967	0.01514	1	0.09934	5	0.23	21.02
25a	281	2.99	6462	0.01480	1	0.09378	6	0.09	21.76
Sample 07-MC-058									
01	187	1.53	1654	0.01404	1	0.08564	8	0.13	22.61
02	1568	1.45	13608	0.01408	1	0.09126	2	0.49	21.27
03	229	1.57	1908	0.01408	1	0.08447	10	0.10	22.98
06	2192	3.21	16520	0.01454	1	0.09453	2	0.43	21.20
07	194	1.28	1570	0.01376	1	0.09275	14	0.07	20.45
10	170	1.83	1542	0.01428	2	0.09388	10	0.21	20.97
11	2240	1.26	14144	0.01466	2	0.09678	2	0.86	20.88
12	243	2.24	2112	0.01458	1	0.09189	7	0.15	21.88
13	1435	2.80	11688	0.01400	1	0.09408	3	0.41	20.52
14	212	1.93	2132	0.01492	1	0.10517	14	0.07	19.57
15	2300	1.40	14326	0.01494	3	0.10424	7	0.39	19.76
16	1668	1.56	14126	0.01495	1	0.09858	2	0.50	20.91

Apparent ages (Ma)						
± (%)	206Pb* 238U*	± (Ma)	207Pb* 235U	± (Ma)	206Pb* 207Pb*	± (Ma)
19	95.1	1.7	91.3	16.8	-5.7	464.7
6	95.9	2.0	90.9	5.5	-36.8	145.8
4	96.0	2.2	93.3	4.4	23.3	106.3
10	95.6	1.8	99.1	9.2	185.3	221.6
10	96.4	2.4	88.8	9.0	-108.9	252.8
5	92.1	1.2	88.6	4.0	-4.5	110.2
15	94.7	1.3	89.5	12.9	-47.3	366.8
71	93.0	17.4	88.3	62.1	-36.7	1980.6
10	95.3	1.1	99.0	9.4	187.0	229.8
6	94.7	1.2	89.4	5.2	-48.4	143.9
5	96.9	1.1	96.2	4.6	78.6	116.3
5	94.7	0.5	91.0	4.8	-4.2	132.7
8	89.9	1.0	83.4	6.8	-98.0	205.5
2	90.1	0.9	88.7	1.7	50.3	42.7
10	90.1	0.9	82.3	8.2	-137.8	255.2
2	93.0	0.9	91.7	2.0	57.8	49.4
14	88.1	0.9	90.1	11.8	143.2	322.6
10	91.4	1.9	91.1	8.8	84.2	233.7
1	93.8	1.6	93.8	1.8	93.7	24.0
7	93.3	0.9	89.3	5.8	-17.4	163.7
2	89.6	1.0	91.3	2.3	135.4	56.7
14	95.5	0.9	101.5	13.3	245.8	317.8
7	95.6	2.6	100.7	6.8	223.0	150.5
2	95.7	0.9	95.5	1.8	90.5	40.7

Table A.1 (cont.).

	Concentration					Isotope ratios			
	U (ppm)	U/Th	206Pb 204Pb	206Pb* 238U	± (%)	207Pb* 235U*	± (%)	error corr.	206Pb* 207Pb*
17	4137	1.32	25726	0.01540	1	0.10108	2	0.47	21.00
18	1578	1.82	5530	0.01485	1	0.10215	2	0.47	20.04
19	204	2.85	2184	0.01528	2	0.09861	10	0.16	21.36
20	141	1.41	1636	0.01450	1	0.08820	12	0.08	22.67
21	514	2.62	10134	0.03240	1	0.22614	2	0.41	19.76
24	1334	2.18	9226	0.01503	1	0.10351	7	0.15	20.02
25	1216	2.32	6914	0.01415	1	0.09488	3	0.42	20.56
27	276	1.70	3188	0.01527	1	0.10208	11	0.11	20.63
29	1009	2.15	4770	0.01480	2	0.09885	3	0.50	20.64
30	223	1.25	2298	0.01428	1	0.09471	8	0.12	20.79
31	802	1.95	6632	0.01430	1	0.09230	3	0.32	21.36
32	1820	1.33	6120	0.01402	2	0.09808	4	0.41	19.71
33	180	1.27	1314	0.01457	1	0.09818	15	0.07	20.47
36	1346	2.15	12384	0.01411	1	0.09268	3	0.39	20.99
38	462	2.17	3918	0.01443	3	0.10188	7	0.39	19.54
39	2384	3.42	14366	0.01436	2	0.09723	3	0.51	20.37

Apparent ages (Ma)						
± (%)	206Pb* 238U*	± (Ma)	207Pb* 235U	± (Ma)	206Pb* 207Pb*	± (Ma)
2	98.5	1.0	97.8	2.1	80.1	47.1
2	95.0	1.0	98.8	2.2	190.1	48.0
10	97.7	1.5	95.5	8.9	39.7	232.1
12	92.8	0.9	85.8	10.0	-104.1	299.7
2	205.6	2.0	207.0	4.6	223.4	51.8
7	96.2	1.0	100.0	6.4	192.4	155.7
3	90.6	1.1	92.0	2.6	130.0	63.6
11	97.7	1.2	98.7	10.1	122.6	251.0
3	94.7	1.6	95.7	3.2	120.9	71.1
8	91.4	0.9	91.9	7.3	103.6	196.0
3	91.5	0.9	89.6	2.7	39.6	71.1
3	89.8	1.4	95.0	3.4	228.7	78.8
15	93.3	0.9	95.1	13.4	141.1	346.7
3	90.3	1.1	90.0	2.8	81.6	71.2
7	92.4	2.6	98.5	6.8	249.3	152.7
3	91.9	1.5	94.2	2.9	152.1	65.1

Table A.1 (cont.).

	Concentration					Isotope ratios			
	U (ppm)	U/Th	206Pb 204Pb	206Pb* 238U	± (%)	207Pb* 235U*	± (%)	error corr.	206Pb* 207Pb*
40	445	1.72	3482	0.01333	1	0.09152	12	0.10	20.08
01a	352	3.35	4719	0.01566	1	0.09855	5	0.16	21.91
02a	399	3.33	5175	0.01544	1	0.10818	6	0.10	19.68
04a	188	1.33	2754	0.01523	2	0.10242	14	0.14	20.50
07a	195	1.50	507	0.01704	2	0.11463	43	0.05	20.50
08a	218	1.70	2574	0.01585	1	0.11240	8	0.12	19.45
09a	568	2.49	4497	0.01677	1	0.11357	8	0.07	20.36
10a	218	1.28	2058	0.01543	1	0.10890	17	0.04	19.53
11a	314	1.45	3213	0.01535	1	0.10813	12	0.07	19.58
14a	536	4.35	6849	0.01523	1	0.10842	6	0.18	19.37
15a	807	7.74	19206	0.01623	1	0.10675	5	0.20	20.97
17a	446	4.82	11160	0.01533	1	0.10161	4	0.12	20.81
19a	209	1.46	2007	0.01553	2	0.09831	15	0.10	21.79
21a	350	1.18	4068	0.01537	1	0.10242	12	0.08	20.69
23a	127	2.82	2169	0.01475	2	0.09191	17	0.13	22.13
24a	274	1.99	4554	0.01566	1	0.10255	8	0.06	21.05
25a	314	1.41	4647	0.01544	1	0.09766	6	0.08	21.80
Sample 07-MC-067									
01	293	1.59	2924	0.01388	2	0.09654	12	0.20	19.83
02	187	1.82	1888	0.01442	2	0.09932	18	0.09	20.01
04	230	2.59	2328	0.01572	1	0.11271	10	0.10	19.23
05	157	2.36	1632	0.01417	3	0.09438	16	0.18	20.71
06	448	3.13	3604	0.01401	2	0.09549	6	0.26	20.23
07	152	1.43	1574	0.01478	2	0.09918	13	0.12	20.54
09	452	1.55	2214	0.01430	1	0.09541	8	0.13	20.66

Apparent ages (Ma)						
± (%)	206Pb* 238U*	± (Ma)	207Pb* 235U	± (Ma)	206Pb* 207Pb*	± (Ma)
12	85.3	1.1	88.9	10.6	185.9	289.5
5	100.2	0.8	95.4	4.7	-21.1	124.2
6	98.8	0.6	104.3	6.0	232.3	138.5
14	97.4	1.9	99.0	13.6	137.0	336.6
43	108.9	2.2	110.2	44.9	137.5	1051.4
8	101.4	1.0	108.2	8.6	260.0	191.4
8	107.2	0.5	109.2	7.9	153.5	179.1
17	98.7	0.7	105.0	16.6	249.6	386.0
12	98.2	0.8	104.3	11.8	244.2	273.7
6	97.4	1.1	104.5	6.2	269.1	141.7
5	103.8	1.0	103.0	5.0	83.9	118.4
4	98.1	0.5	98.3	3.8	102.0	94.2
15	99.4	1.6	95.2	13.8	-7.6	366.0
12	98.3	0.9	99.0	11.1	115.3	277.7
17	94.4	2.1	89.3	14.7	-45.1	417.6
8	100.1	0.5	99.1	7.7	74.8	193.7
6	98.8	0.5	94.6	5.4	-9.7	144.9
12	88.9	2.1	93.6	10.8	215.2	274.1
17	92.3	1.4	96.1	16.1	193.4	409.0
10	100.6	1.0	108.4	10.1	285.1	224.6
15	90.7	2.5	91.6	13.8	113.7	367.2
6	89.7	1.5	92.6	5.6	168.1	141.6
13	94.6	1.5	96.0	12.3	132.3	313.8
8	91.5	0.9	92.5	6.9	119.1	183.2

Table A.1 (cont.).

	Concentration					Isotope ratios			
	U (ppm)	U/Th	206Pb 204Pb	206Pb* 238U	± (%)	207Pb* 235U*	± (%)	error corr.	206Pb* 207Pb*
10	369	1.57	3370	0.01428	1	0.09416	9	0.13	20.91
13	308	1.21	3752	0.01414	2	0.08953	6	0.34	21.78
15	148	1.47	1236	0.01461	1	0.09958	14	0.09	20.23
17	785	2.98	4448	0.01502	2	0.10334	5	0.34	20.04
19	174	1.25	1530	0.01471	1	0.09595	11	0.11	21.14
22	203	1.78	2698	0.01510	1	0.10612	15	0.07	19.62
23	151	1.47	1260	0.01468	1	0.09434	28	0.04	21.46
25	266	2.03	3096	0.01448	2	0.10313	10	0.15	19.36
27	230	2.09	2650	0.01515	2	0.10368	12	0.16	20.15
28	421	2.26	3992	0.01504	1	0.10204	9	0.12	20.33
30	295	1.82	2024	0.01472	1	0.10371	10	0.10	19.57
31	209	1.88	1218	0.01443	1	0.10484	13	0.08	18.98
35	171	1.91	1944	0.01607	1	0.10129	14	0.07	21.88
37	949	2.80	6618	0.01504	1	0.11027	6	0.16	18.81
38	139	2.14	1912	0.01473	3	0.09837	14	0.19	20.65
39	345	1.29	6656	0.01495	2	0.09404	7	0.22	21.91
42	213	1.87	2276	0.01472	1	0.10649	13	0.08	19.06
43	395	2.34	3142	0.01575	1	0.10841	11	0.09	20.03
44	290	1.50	2962	0.01473	1	0.09390	4	0.27	21.62
01a	182	1.53	4608	0.01484	1	0.08888	11	0.07	23.02
02a	251	2.61	3436	0.01531	1	0.10787	11	0.04	19.57
04a	316	1.70	784	0.01496	2	0.08959	20	0.09	23.02
05a	157	1.48	4536	0.01495	1	0.09809	14	0.06	21.02
06a	133	1.92	3272	0.01462	1	0.08939	9	0.11	22.56

Apparent ages (Ma)						
± (%)	206Pb* 238U*	± (Ma)	207Pb* 235U	± (Ma)	206Pb* 207Pb*	± (Ma)
9	91.4	1.1	91.4	8.1	91.1	219.4
5	90.5	1.7	87.1	4.7	-6.9	127.9
14	93.5	1.2	96.4	12.7	168.5	322.2
4	96.1	1.5	99.9	4.4	189.7	102.1
11	94.1	1.1	93.0	9.8	64.5	260.3
15	96.6	1.0	102.4	14.6	238.9	345.4
28	94.0	1.0	91.5	24.6	28.5	684.6
10	92.7	1.4	99.7	9.8	270.0	234.8
11	97.0	1.8	100.2	11.1	177.4	267.4
9	96.3	1.0	98.7	8.2	156.9	202.1
10	94.2	0.9	100.2	9.8	245.0	235.4
13	92.4	0.9	101.2	12.3	315.8	290.6
14	102.8	1.0	98.0	13.3	-18.0	344.1
6	96.3	1.0	106.2	6.3	335.9	139.6
14	94.3	2.5	95.3	12.9	119.7	330.6
7	95.6	1.5	91.3	6.2	-21.8	168.7
13	94.2	1.0	102.7	13.0	305.7	303.1
11	100.8	1.0	104.5	10.7	191.2	249.3
4	94.2	0.9	91.1	3.2	10.7	85.7
11	95.0	0.7	86.5	9.1	-142.5	271.0
11	97.9	0.5	104.0	11.3	245.3	263.5
20	95.7	1.6	87.1	16.4	-142.5	489.5
14	95.7	0.8	95.0	12.6	78.1	330.4
9	93.6	0.9	86.9	7.4	-92.3	217.8

Table A.1 (cont.).

	Concentration		Isotope ratios								Apparent ages (Ma)					
	U (ppm)	U/Th	206Pb 204Pb	206Pb* 238U	± (%)	207Pb* 235U*	± (%)	error corr.	206Pb* 207Pb*	± (%)	206Pb* 238U*	± (Ma)	207Pb* 235U	± (Ma)	206Pb* 207Pb*	± (Ma)
07a	173	1.76	5732	0.01497	1	0.09210	12	0.05	22.41	12	95.8	0.5	89.5	10.1	-76.1	289.3
08a	363	1.72	5076	0.01495	1	0.10420	9	0.15	19.78	9	95.6	1.3	100.6	8.8	221.1	210.2
09a	229	1.26	4420	0.01488	1	0.09726	7	0.18	21.09	7	95.2	1.2	94.2	6.2	70.5	160.9
10a	221	1.75	5000	0.01443	2	0.09046	9	0.26	21.99	9	92.4	2.2	87.9	7.7	-30.4	213.8
11a	321	1.93	7960	0.01512	1	0.09570	6	0.20	21.79	6	96.8	1.1	92.8	5.2	-8.2	138.7
12a	228	2.70	5628	0.01522	2	0.09663	6	0.27	21.72	5	97.4	1.5	93.7	5.1	-0.1	131.7
13a	226	1.51	5432	0.01507	1	0.09640	8	0.16	21.56	7	96.4	1.2	93.4	6.8	17.9	179.8
14a	306	1.35	6664	0.01455	1	0.09146	6	0.21	21.94	6	93.1	1.2	88.9	5.4	-24.7	151.5
15a	290	2.72	6752	0.01510	1	0.10177	5	0.11	20.45	5	96.6	0.5	98.4	4.4	142.5	109.5
17a	256	1.01	4172	0.01460	1	0.09063	6	0.09	22.22	6	93.5	0.5	88.1	5.3	-55.1	152.2
19a	301	1.89	4860	0.01476	1	0.09721	5	0.13	20.93	5	94.4	0.5	94.2	4.1	88.1	107.2
20a	270	1.75	13764	0.03176	1	0.21865	3	0.16	20.03	3	201.6	1.0	200.8	5.6	191.6	70.7

APPENDIX B

RAW MAGNETIC SUSCEPTIBILITY DATA

Table B1. Raw magnetic susceptibility values for all stations

Station	Easting	Northing	Elev.	Rock type	MS1	MS2	MS3	MS4	MS5	MS6	MS7	MS8	MS9	St dev	MSavg
MC-010	346635	4137394	10278	HM	12.9	12.2	11.3	16	10.1	14.5	10.1	16.1	12.9	2.27	12.90
MC-095	346698	4137251	10421	HM	12.7	12.2	12.9	12.5	12.9	10.7	8.54	20.3	11.4	3.18	12.68
MC-093	346561	4137357	10407	HM	12.9	13.7	12.7	13.3	11.9	12.9	11.1	13.5	11.8	0.87	12.64
MC-069	347167	4134917	10083	HM	11.3	11.5	11.5	12.5	10.5	14.4	12.6	13.7	12.2	1.22	12.24
MC-026	346870	4138897	10757	HM	10.4	11.9	13.2	13.1	11.7	8.91	13.9	13	13.4	1.63	12.17
MC-094	346592	4137289	10423	HM	12.1	13	11	12.5	9.41	13.4	11.2	12	11.1	1.21	11.75
MC-012	346751	4137382	10218	HM	12.4	9.86	11.3	12.7	11.3	11.2	12.7	12.2	11.5	0.92	11.68
MC-139	346905	4135180	9944	HM	13.1	14.1	11.1	11.4	11.6	9.48	9.06	11.9	13.3	1.68	11.67
MC-098	346999	4137197	10042	HM	10.4	10.3	13.5	10.3	9.83	10.6	15	10.7	13.9	1.94	11.61
MC-132	347002	4135279	9997	IM	18	11.9	10.3	12.5	11.2	9.34	8.71	10.4	11.3	2.71	11.52
MC-061	348433	4135029	9556	IM	13.8	13.2	12.9	10	12.9	11.4	8.99	10.4	8.47	1.96	11.34
MC-096	346752	4137189	10329	HM	9.38	9.62	9.88	10.5	13.8	11.5	12.3	9.84	12.5	1.56	11.04
MC-060	348459	4135036	9483	IM	9.34	10.4	10.7	10.4	9.3	14.6	11.9	11.2	10.1	1.62	10.88
MC-008	346773	4138965	10669	HM	10.2	14.7	11.7	10.1	8.07	9.81	10.3	13.9	8.5	2.25	10.81
MC-078	346779	4139012	10817	HM	12.7	12.2	9.22	9.39	9.85	10.1	11.7	13.7	8.26	1.84	10.79
MC-133	347713	4137982	10511	HM	9.77	9.14	10.3	9.05	10.8	9.53	11.1	12.5	11.9	1.22	10.45
MC-128	347437	4135368	10092	IM	9.25	12.1	12.3	13.2	9.23	10.3	8.45	8.92	9.95	1.70	10.41
MC-030	346751	4138686	10847	HM	9.93	9.51	9.2	10	9.59	11.1	11.3	10.1	12.1	0.97	10.31
MC-013	346876	4137361	10213	HM	9.79	9.3	8.98	10.4	7.62	13.8	10.4	8.51	13.6	2.14	10.27
MC-130	347228	4135330	10165	IM	10.5	11.1	8.82	9.93	9.64	11.1	10	10	9.88	0.72	10.11
MC-077	346828	4137373	10194	HM	10.6	10.8	9.18	10.3	11.9	9.56	9.05	10.9	8.42	1.10	10.08
MC-034	346837	4138686	10763	HM	7.13	10	10.6	11.9	7.91	12.5	11	9.74	9.85	1.73	10.07
MC-038	346952	4138575	10788	HM	8.41	10.7	9.12	11.8	10.2	11	9.62	9.36	9.74	1.04	9.99

Table B1 (cont.).

MC-079	346842	4139021	10831	HM	11.3	9.59	10.1
MC-119	348234	4135395	9584	IM	9.46	10	14
MC-134	347712	4137847	10511	HM	10	9.4	11.4
MC-045	347373	4138254	10591	HM	10.2	11.1	9.52
MC-011-A	346671	4137378	10324	HM	8.89	12.5	9.11
MC-121	348143	4135424	9684	HM	10.8	10	10.7
MC-097	346856	4137178	10252	HM	9.23	10.6	8.12
MC-065	347833	4135019	10019	IM	9.98	10.2	8.97
MC-066	347677	4135050	10074	IM	9.7	9.58	12
MC-062	348293	4135011	9636	IM	9.54	9.87	8.35
MC-131	347142	4135318	10024	IM	10.7	9.09	7.67
MC-032	346802	4138673	10847	HM	8.73	8.7	9.13
MC-075	346931	4137365	10240	HM	10	10.9	8.87
MC-033	346830	4138649	10751	HM	9.94	10	10.4
MC-037	346931	4138626	10763	HM	9	10.3	9.69
MC-074	347010	4137368	10171	HM	9.43	8.04	8.25
MC-035	346863	4138662	10754	HM	8.99	8.36	9.84
MC-031	346751	4138728	10829	HM	8.99	8.79	10.3
MC-059	348581	4134997	9539	HM	9.54	10.2	9.39
MC-068	347431	4134993	10102	IM	9.14	8.01	10.7
MC-025	347086	4138752	10711	HM	8.88	9.58	9.34
MC-076	346924	4137324	10145	HM	9.25	10	9.73
MC-118	348331	4135435	9517	IM	8.65	7.77	8.79
MC-016-A	347720	4137262	9942	HM	8.58	10.7	10.1
MC-129	347338	4135343	10127	IM	8.22	9.74	8.52
MC-089	347847	4138003	10779	HM	8.82	9.14	10.4
MC-067	347540	4135025	10106	IM	9.42	9.16	8.14
MC-115	348458	4135537	9375	HM	8.09	9.75	7.67
MC-015	347873	4137366	10117	HM	8.27	8.62	7.86

10.2	8.34	12.1	9.4	8.57	10.3	1.20	9.99
11.2	11.1	9.11	7.52	8.84	8.66	1.90	9.99
9.77	10.5	8.93	10.4	10.4	8.26	0.94	9.90
9.61	10.1	10.9	8.5	10	8.56	0.90	9.83
9.47	8.43	9.87	9.92	10.9	8.76	1.27	9.76
9.39	9.01	8.88	9.89	9.58	9.34	0.68	9.73
9.88	8.69	9.03	9.47	10.6	11.4	1.05	9.67
10.7	10.4	9.77	8.87	9.21	8.48	0.77	9.62
7.77	9.44	9.18	9.73	8.61	10.5	1.18	9.61
9.54	8.82	10.2	9.82	10.1	10.2	0.64	9.60
10.7	8.26	11.6	10.6	9.43	8.35	1.36	9.60
9.55	10.4	8.67	9.89	9.26	11.5	0.94	9.54
8.18	9.89	9.19	10.2	8.95	9.43	0.82	9.51
9.51	9.99	7.31	8.82	9.52	10.1	0.94	9.51
10	9.28	8.99	10.1	8.47	9.18	0.61	9.45
10.6	8.67	8.85	9.32	12.1	9.66	1.26	9.44
9.1	9.67	10.2	10	9.15	9.53	0.58	9.43
9.69	10.5	9.4	9.43	9.05	8.62	0.65	9.42
9.11	8.4	8.01	8.77	10.5	10.7	0.93	9.40
9.84	8.96	9.78	10.6	7.91	9.29	0.99	9.36
10.3	8.74	8.88	9.29	10.1	8.99	0.56	9.34
7.8	9.63	7.42	9.01	10	10	0.97	9.20
9.99	7.94	8.71	9.04	8.62	11.6	1.16	9.01
7.11	8.97	8.61	8.57	8.5	7.75	1.09	8.77
9.45	8.69	7.61	7.38	8.85	8.98	0.78	8.60
8.15	6.55	8.45	7.97	8.24	8.16	1.03	8.43
7.6	8.05	9.74	8.69	7.88	7.07	0.89	8.42
7.97	5.29	10.3	9.7	8.51	7.2	1.54	8.28
6.49	8.64	8.81	8.28	8.25	9.2	0.77	8.27

Table B1 (cont.).

MC-039	347292	4137581	10270	IM	9.01	7.87	7.93
MC-099	347096	4137158	10016	IM	8.08	7.36	11.2
MC-122	348046	4135421	9763	LM	9.57	9.34	8.61
MC-017-A	347485	4137325	9850	IM	7.26	8.65	8.49
MC-057	348659	4135055	9409	IM	8.28	7.63	7.84
MC-103	347290	4137217	9765	IM	9.3	8.258	7.5
MC-102	347256	4137222	9836	IM	7.05	8.35	6.61
MC-040	347258	4137523	10273	HM	8.23	7.56	8
MC-042	347182	4137350	9978	HM	6.45	7.75	7.83
MC-117	348369	4135463	9472	IM	5.31	8.45	7.81
MC-063	348156	4135079	9684	IM	9.31	8.05	7.63
MC-058	348597	4135009	9510	IM	8.28	7.63	7.66
MC-127	347550	4135373	10076	LM	6.62	8.2	7.71
MC-044	347549	4137415	10111	IM	7.03	9.07	7.42
MC-014 A	347436	4137635	10215	IM	8.18	7.52	6.98
MC-090	347731		10678	HM	11.5	8.28	8.04
MC-064	347959	4135026	9896	LM	9.15	8.13	6.34
MC-135	347329	4138015	10273	IM	6.68	6.25	6.41
MC-073	347099	4137369	10049	IM	6.55	7.01	7.34
MC-125	347759	4135405	10020	LM	7.31	8.06	7.63
MC-126	347659	4135388	10094	LM	6.15	6.29	6.66
MC-114	348504	4135562	9290	HM	6.58	6.72	5.83
MC-123	347951	4135372	9852	LM	6.42	6.83	5.31
MC-071	347561	4139611	11598	HM	6.81	5.72	5.74
MC-124	347850	4135400	9907	LM	6.44	5.28	6.07
MC-116	348415	4135495	9402	HM	1.28	5.73	5.38
MC-113	348503	4135613	9252	HM	1.47	2.68	3.02
MC-112	348541	4135661	9216	HM	1.09	5.75	1.99
MC-088	347963	4139243	11490	HM	1.96	1.49	

8.33	7.27	8.51	9.32	8.25	7.75	0.64	8.25
8.15	9.64	7.27	7.89	7.04	7.45	1.35	8.23
6.87	8.08	6.44	6.91	9.58	8.66	1.22	8.23
7.58	8.52	8.65	7.82	7.18	9.18	0.71	8.15
5.82	9.02	8.53	8.61	8.67	8.42	0.95	8.09
7.21	7.53					0.84	7.96
8.97	7.85	9.09	7.12	7.81	8.77	0.90	7.96
7.43	6.71	7.49	7.95	8.54	8.68	0.62	7.84
8	8.44	8.44	7.25	9.06	6.86	0.83	7.79
9.04	8.54	7.18	9.54	7.05	6.76	1.31	7.74
7.02	6.44	7.71	6.05	9.05	8.38	1.10	7.74
7.67	8.29	7.67	7.04	9	6.27	0.78	7.72
7.87	7.36	7.18	8.35	7.48	7.65	0.53	7.60
9.04	8.04	7	6.94	6.15	7.52	0.98	7.58
6.92	7.77	6.73	7.55	7.45	7.65	0.46	7.42
9.45	6.67	7.7	5.14	3.85	5.77	2.32	7.38
7.69	6.49	5.13	8.07	7.86	7.5	1.20	7.37
6.28	6.58	8.47	6.59	9.04	9.43	1.29	7.30
6.23	7.93	6.91	7	8.04	8.43	0.73	7.27
7.03	6.49	7.08	6.44	6.73	7.2	0.53	7.11
6.87	6.3	7.62	6.98	7.88	7.03	0.60	6.86
7.44	5.01	10.9	4.99	6.17	4.21	1.95	6.43
7.2	5.93	5.74	6.79	5.92	5.69	0.63	6.20
5.74	6.8	5.94	6.44	5.59	6.15	0.47	6.18
4.5	4.24	6.24	6.05	4.59	5.72	0.83	5.46
3.83	7	8.6	4.86	3.75	5.67	2.08	5.12
1.69	1.43	2.33	5.12	3.97	4.68	1.38	2.93
1.56	0.636	1.22	0.935	2.8	2.4	1.56	2.04
						0.33	1.73

MC-055	348755	4135089		HM	2.68
MC-052	348832	4135133	9215	HM	1.37
MC-104	348915	4135401	8566	HM	0.148
MC-111	348635	4135718	9118	HM	0.249
MC-110	348673	4135743	9081	HM	0.132
MC-023	347928	4139687	11531	HM	0.406
MC-022CLVL	347926	4139024	11290	HM	0.307
MC-006	349055	4135244	8937	HM	0.444
MC-109	348726	4135764	8995	HM	0.044
MC-051	348917	4135173	9086	HM	0.176
MC-049	349022	4135222	8948	HM	0.175
MC-050	349005	4135219	8960	HM	0.145
MC-047	349104	4135289	8908	HM	0.03
MC-048	349078	4135248	8912	HM	0
MC-046	349268	4135263	8686	HM	-0.025

Table B1 (cont.).

2.53	1.78	3.73	0.912	0.24	0.802	0.266	2.48	1.22	1.71
4.83	2.4	0.404	1.06	1.2	0.988	1.25		1.39	1.69
1.45	0.114	0.33	4.07	0.393	0.754	1.1	0.484	1.24	0.98
0.211	0.446	0.245	0.324	0.439	0.22	0.323	3.3	1.00	0.64
1.46	0.238	0.47	0.057	0.08	0.491	0.502	1.82	0.63	0.58
0.234	0.298	0.897	0.52	1.27	0.249	0.353	0.471	0.35	0.52
0.503	0.398	0.188	0.363	0.385	0.312	0.627	0.615	0.15	0.41
0.319	0.187							0.13	0.32
0.168	0.112	1.44	0.105	0.47	0.107	0.206	0.064	0.45	0.30
0.325	0.182							0.08	0.23
0.186								0.01	0.18
0.126								0.01	0.14
									0.03
									0.00
-0.077	-0.105	-3.15	-0.011	0.113	-0.037			1.18	-0.47